

MAJOR PROJECT REPORT
ON
“STUDY AND ANALYSIS OF HIGH LIFT DEVICES AND
HIGH LIFT DEVICES MORPHING FOR MULTI FLIGHT
REGIME”

Submitted by:

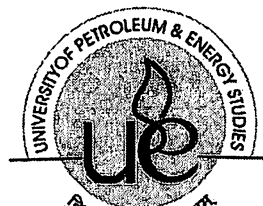
Aakanksha Tiwari [R290209001]

Abhilasha Shah [R290209005]

Deepali Joshi [R290209021]

FOR PARTIAL FULFILMENT
Of
BACHELOR OF TECHNOLOGY
In
AEROSPACE ENGINEERING

Under the Supervision of Prof. Karthik Sundarraj



Harnessing Energy through Knowledge

DEPARTMENT OF AEROSPACE ENGINEERING
COLLEGE OF ENGINEERING STUDIES (COES)
UNIVERSITY OF PETROLEUM & ENERGY STUDIES
DEHRADUN- 248007, INDIA

APRIL/MAY 2013

THESIS CERTIFICATE

I hereby certify that the work which is being presented in the project report entitled “**Study and Analysis of High Lift Devices and High Lift Devices Morphing for Multi Flight Regime**” in partial fulfilment of the requirements for the satisfactory performance for B.Tech Aerospace Engineering, Major Project submitted in the Department of Aerospace Engineering, University of Petroleum and Energy Studies, Dehradun is an authentic record of my own work carried out during a period from July 2012 to April 2013.

SUBMITTED BY:

Aakanksha Tiwari [R290209001]

Abhilasha Shah R290209005]

Deepali Joshi [R290209021]

This is to certify that the above statement made by the candidate is correct to the best of our knowledge.


Prof. Karthik Sundarraj

Guide

Date: 29/04/13

Panel Members:

Prof. Linsu Sibestian

Prof. Sudhir Chaturvedi

Prof. Karthik Sundarraj

Dr. Om Prakash

Head of Department
Aerospace

ABSTRACT

In contemporary scenario, the competition between the aviation giants is largely driven by the pre-production as well as post-production cost of the airplane. Pre-production cost includes the designing of aircraft for maximum payload carrying capability, short take-off and landing distances and less complexity of the installed mechanism. Post-production cost includes the maintenance, reliability, safety and economics of flight. The prime concern of aerodynamicists is to maintain the economic viability of flight. One of the way to achieve it is the use of high lift devices i.e.- Multi element aerofoil. The problems with the current high lift devices are that they use actuator mechanism having high level of complexity and thus use more engine power. Plus they are heavy and estimated to have cost about 6-11% of the total cost of the plane. In addition, there are gaps and overlap in conventional high lift system which generates the eddies in the flow and thus the drag. All the above listed problems can be solved by the using morphing concept.

An iterative method would be used in which a five element airfoil would be analysed using FLUENT and the separation point will be observed at different angle of attack. Based on the flow separation location, different elements will be associated and disassociated simultaneously and different possibility of delaying the separation point would be covered.

The use of various lift enhancing devices like flaps, slats, slots etc. to increase the C_{lmax} during take-off and landing is being presented in this report. The numerical analysis of simple aerofoil, 3-element aerofoil and 5-element aerofoil is being studied using ANSYS ICEM CFD and FLUENT software. Finally the concept of morphing wing, its advantages over conventional high lift system and its implementation as lift enhancing technique is being studied.

DECLARATION

We hereby declare that the project report entitled "STUDY AND ANALYSIS OF HIGH LIFT DEVICES AND HIGH LIFT DEVICES MORPHING FOR MULTI FLIGHT REGIME" has been carried out under the supervision of Professor Karthik Sundarraj, "University of Petroleum and Energy Studies" as a guide. This report or any part of this work has not been submitted elsewhere for any other degree or diploma.

Aakanksha

Aakanksha Tiwari (R290209001)

Abhilasha Shah (R290209005)

Deepali Joshi (R290209021)

Place: Dehradun

Date:

ACKNOWLEDGEMENT

It is with a sense of great satisfaction and pride that we are sitting down to pen out our major project thesis report. First and foremost we sincerely salute our esteemed Institution **University of Petroleum & Energy Studies, Dehradun** for giving this golden opportunity for fulfilling our warm dreams of becoming a bachelor.

The first and foremost person we would like to express our deep sense of gratitude and profound thanks to our guide **Prof. Karthik Sundarraj**, Department of Aerospace Engineering, UPES Dehradun for his valuable advice, suggestions, insurmountable guidance which played a vital role in carrying out our project work successfully. Our thanks to **Prof. (Dr.) Om Prakash**, Head, Department of Aerospace Engineering, UPES, Dehradun for his valuable guidance towards our project.

We would like to thank all faculty, staff, and students of Department of Aerospace Engineering and for rendering help during various stages of the project work.

Aakanksha Tiwari [R290209001]

Abhilasha Shah [R290209005]

Deepali Joshi [R290209021]

TABLE OF CONTENTS

<i>THESIS CERTIFICATE</i>	ii
<i>ABSTRACT</i>	iii
<i>DECLARATION</i>	iv
<i>ACKNOWLEDGEMENT</i>	v
<i>LIST OF FIGURES</i>	viii
<i>LIST OF TABLES</i>	x
<i>LIST OF GRAPHS</i>	xi
<i>NOMENCLATURE</i>	xii
<i>ABBREVIATIONS</i>	xiii
<i>PROJECT PLAN</i>	xiv
<i>TIME PLAN</i>	xvi
<i>APPENDIX</i>	xvii
1. INTRODUCTION	1
1.1 MULTI-ELEMENT AIRFOIL	1
1.2 COMPUTATIONAL FLUID DYNAMICS	1
2. PROJECT OBJECTIVES	4
2.1 AIMS AND OBJECTIVES	4
2.2 METHODOLOGY	4
3. LITERATURE REVIEW	5
3.1 AIRFOIL GEOMETRY AND NOMENCLATURE	5
3.2 AERODYNAMIC FORCES ON AEROFOIL	5
3.3 KUTTA CONDITION	9
3.4 BOUNDARY LAYER FLOW	11
3.4.1 PROPERTIES OF THE BOUNDARY LAYER FLOW	12
3.4.2 THE BOUNDARY LAYER EQUATIONS	13
3.4.3 DISPLACEMENT THICKNESS	16
3.4.4 MOMENTUM THICKNESS	17
3.4.5 LAMINAR BOUNDARY LAYER	18
3.4.6 TURBULENT BOUNDARY LAYER	18
3.4.7 FACTORS EFFECTING INSTABILITY AND TRANSITION	18
3.5 HIGH LIFT DEVICES	21
3.6 TURBULENCE MODELS	29
3.6.1 CLASSIFICATION OF TURBULENCE MODEL	29
3.7 DISCRETIZATION	32

3.7.1 REASON FOR DISCRETIZATION	33
3.7.2 FINITE DIFFERENCE METHOD	34
3.7.3 EXPLICIT FORMULATION	36
3.7.4 IMPLICIT APPROACH	37
3.7.5 COMPARISON OF EXPLICIT AND IMPLICIT SCHEMES	38
3.7.6 FINITE ELEMENT METHOD	38
3.7.7 FINITE VOLUME METHOD	39
3.8 GRID DEPENDENCE STUDY	39
3.9 MORPHING CONCEPT	41
4. NUMERICAL ANALYSIS	43
4.1 GEOMETRY CREATION	43
4.2 GRID GENERATION	45
4.3 BOUNDARY CONDITION	48
5. RESULTS AND DISCUSSION	50
5.1 CONFIGURATION 1: BASIC AIRFOIL	50
5.2 CONFIGURATION 2: THREE ELEMENT AIRFOIL	53
5.3 CONFIGURATION 3: FIVE ELEMENT AIRFOIL	56
5.4 COMPARISON	60
6. FUTURE CONSIDERATIONS	63
6.1 CASE 1: 5 ELEMENT AIRFOIL AT 5 DEGREE ANGLE OF ATTACK	63
6.2 CASE 2: 5 ELEMENT AIRFOIL AT 15 DEGREE ANGLE OF ATTACK	64
7. REFERENCES	65

LIST OF FIGURES

FIGURE 1. AEROFOIL GEOMETRY	5
FIGURE 2. PRESSURE AND SHEAR POINT	6
FIGURE 3. AERODYNAMIC FORCE AND MOMENT	6
FIGURE 4. AERODYNAMIC FORCES	7
FIGURE 5. PRESSURE AND SHEAR STRESS DISTRIBUTION	7
FIGURE 6. PRESSURE AND SHEAR FORCES	8
FIGURE 7. NO CIRCULATION	9
FIGURE 8. LOW CIRCULATION	10
FIGURE 9. HIGH CIRCULATION	10
FIGURE 10. CIRCULATION SUCH THAT KUTTA CONDITION IS SATISFIED	10
FIGURE 11. BOUNDARY LAYER	11
FIGURE 12. PROPERTIES OF BOUNDARY LAYER	12
FIGURE 13. PRESSURE AND SHEAR FORCES	13
FIGURE 14. FLUID ELEMENT	15
FIGURE 15. BOUNDARY LAYER	17
FIGURE 16. EFFECTIVE BODY	17
FIGURE 17. LAMINAR BOUNDARY LAYER	18
FIGURE 18. BOUNDARY LAYER FLUCTUATIONS	19
FIGURE 19. CENTRIFUGAL INSTABILITY	20
FIGURE 20. TYPICAL HIGH LIFT SYSTEM AND ITS EFFECT ON AIRPLANE LIFT	21
FIGURE 21. SPLIT FLAP	22
FIGURE 22. PLANE FLAP	22
FIGURE 23. SINGLE SLOTTED FOWLER FLAP	23
FIGURE 24. SIMPLE SLOTTED FLAP	23
FIGURE 25. FIXED VANE/MAIN DOUBLE SLOTTED FLAP	24
FIGURE 26. ARTICULATING VANE/MAIN DOUBLE SLOTTED FLAP	24
FIGURE 27. MAIN/AFT DOBLE SLOTTED FLAP	25
FIGURE 28. TRIPLE SLOTTED FLAP	25
FIGURE 29. FIXED SLOT	26
FIGURE 30. SIMPLE KRUEGER FLAP	26
FIGURE 31. FOLDING, BULL NOSE KRUEGER FLAP	27
FIGURE 32. TWO POSITION SLAT	27
FIGURE 33. C_l Vs. AOA FOR DIFFERENT FLAP CONFIGURATION	28
FIGURE 34. GRID	32
FIGURE 35. EXPLICIT APPROACH	37
FIGURE 36. IMPLICIT APPROACH	37
FIGURE 37. WAKE REGION	41
FIGURE 38. MORPHING CONCEPT	42
FIGURE 39. FIVE ELEMENT AEROFOIL	44
FIGURE 40. THREE ELEMENT AEROFOIL	44
FIGURE 41. BASIC AEROFOIL	44
FIGURE 42. BOUNDARY DEPICTION	45
FIGURE 43. STRUCTURED MESH-BASIC AEROFOIL	47
FIGURE 44. STRUCTURED MESH-THREE ELEMENT AEROFOIL	47
FIGURE 45. STRUCTURED MESH-FIVE ELMENT AEROFOIL	48

FIGURE 46. VELOCITY VECTOR AT 0 & 5 DEG AOA RESP.	51
FIGURE 47. VELOCITY VECTOR AT 10 & 15 DEG AOA RESP.	51
FIGURE 48. VELOCITY VECTOR AT 20 DEG AOA	51
FIGURE 49. BOUNDARY LAYER AT 20 DEG AOA	52
FIGURE 50. VELOCITY VECTOR AT 5 and 10 DEG AOA RESP	53
FIGURE 51. VELOCITY VECTOR AT 15 & 20 DEG AOA RESP.	54
FIGURE 52. VELOCITY VECTOR AT 25 & 30 DEG AOA RESP.	54
FIGURE 53. BOUNDARY LAYER AT 30 DEG AOA	54
FIGURE 54. RECIRCULATION AT 25 DEG AOA	55
FIGURE 55. COUNTER CIRCULATION AT 30 DEG AOA	56
FIGURE 56. BOUNDARY LAYER AT 15 DEG AOA	57
FIGURE 57. VELOCIT VECTOR AT 0 & 5 DEG AOA FOR FIVE ELEMENT AEROFOIL RESP.	57
FIGURE 58. VELOCITY VECTOR AT 10 & 15 DEG AOA FOR FIVE ELEMENT AEROFOIL RESP.	58
FIGURE 59. VELOCITY VECTOR AT 20 DEG AOA FOR FIVE ELEMENT AEROFOIL	58
FIGURE 60. CIRCULATION AT 10 DEG AOA	58
FIGURE 61. COUNTER-CIRCULATION AT 15 DEG AOA	59
FIGURE 62. SLAT EFFECT OF 5 ELEMENT AEROFOIL	59
FIGURE 63. COEFFICIENT OF PRESSURE AT 0 DEG AoA	60
FIGURE 64. COEFFICIENT OF PRESSURE AT 0 DEG AoA	60
FIGURE 65. STREAMLINE AT 5 DEG AOA FOR 5 ELEMENT AEROFOIL	63
FIGURE 66. STREAMLINE AT 15DEG AOA FOR FIVE ELEMENT AEROFOIL	64

LIST OF TABLES

TABLE 1. VARIOUS GEOMETRIES	44
TABLE 2. BASIC AEROFOIL GRID INDEPENDENCE STUDY	46
TABLE 3. THREE ELEMENT GRID INDEPENDENCE STUDY	46
TABLE 4. FIVE ELEMENT GRID INDEPENDENCE STUDY	46
TABLE 5. BOUNDARY CONDITIONS	48
TABLE 6. EPSILON VALUES OF VARIOUS CONFIGURATIONS	49

LIST OF GRAPHS

GRAPH 1. C_l Vs. AOA- BASIC AEROFOIL	50
GRAPH 2. C_l Vs. AOA CURVE FOR THREE ELEMENT AEROFOIL	53
GRAPH 3. C_l Vs. AOA FOR FIVE LEMENT AEROFOIL	56
GRAPH 4. COMPARISON BETWEEN VARIOUS LIFT COEFFICIENT CURVE	60

NOMENCLATURES

L	Airplane lift	lbs
g	Acceleration due to gravity	ft/s ²
T	Thrust	lbs
V	Velocity	ft/s
α	Angle of attack	deg
ρ_{∞}	Ambient density	slug/ft ³
W	Gross weight of aircraft	lb
$C_{L\alpha}$	Wing lift slope	rad ⁻¹
C_{L0}	Zero lift coefficient	~
C_{Lmax}	Maximum wing lift coefficient	~

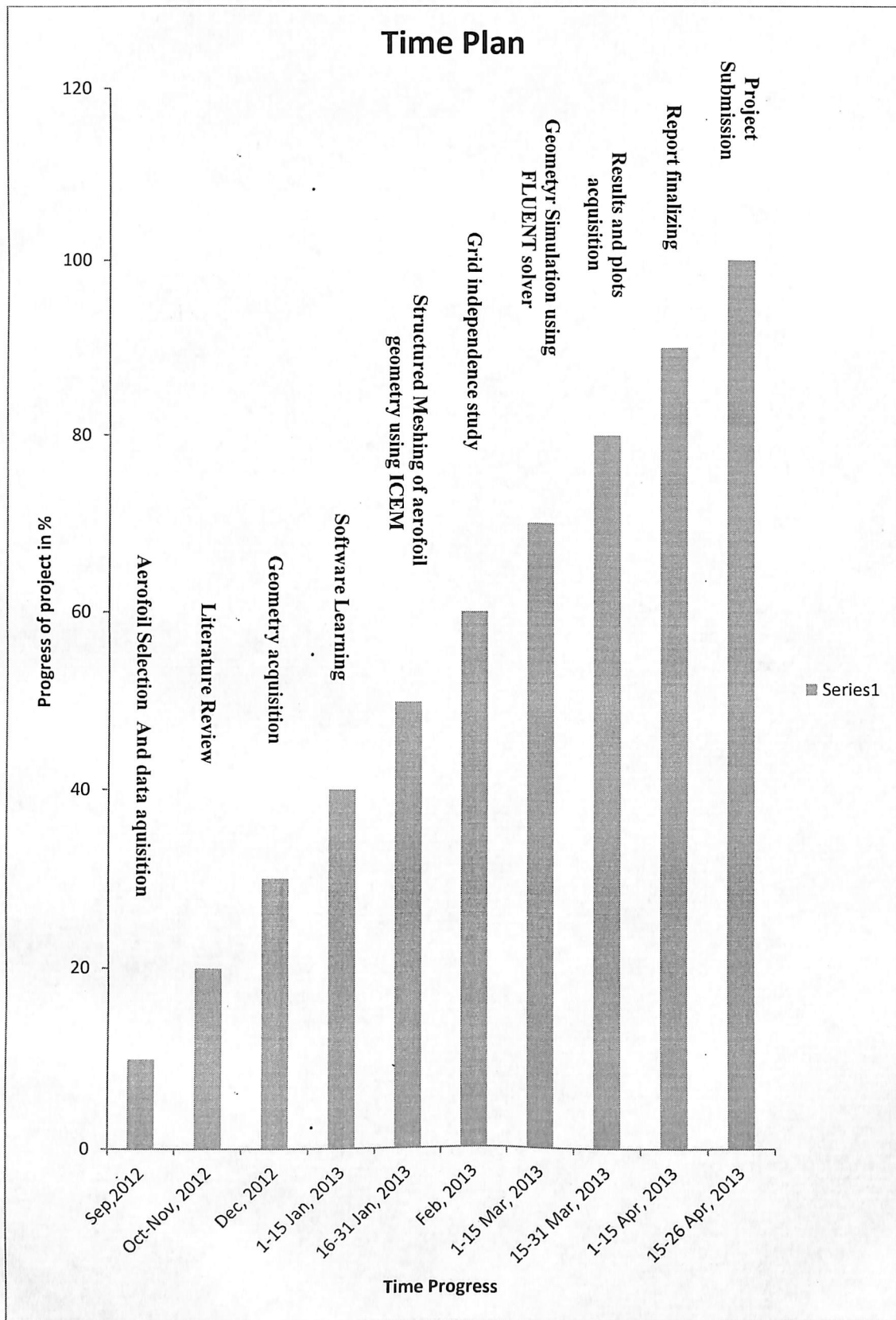
ABBREVIATIONS

A.C	Aerodynamic Centre
B.L	Boundary Layer
AoA	Angle of Attack
L.E	Leading Edge
T.E	Trailing Edge

PROJECT PLAN

<i>ABSTRACT</i>	ABHILASHA SHAH(AS)
<i>DECLARATION</i>	DEEPALI JOSHI(DJ)
<i>ACKNOWLEDGEMENT</i>	DEEPALI JOSHI(DJ)
<i>LIST OF FIGURES</i>	AAKANKSHA TIWARI
<i>LIST OF TABLES</i>	AAKANKSHA TIWARI
<i>NOMENCLATURE</i>	AAKANKSHA TIWARI
<i>ABBREVIATIONS</i>	AAKANKSHA TIWARI
<i>PROJECT PLAN</i>	ABHILASHA SHAH(AS)
1. INTRODUCTION	
1.1 MULTI-ELEMENT AIRFOIL	DEEPALI JOSHI(DJ)
1.2 COMPUTATIONAL FLUID DYNAMICS	
2. PROJECT OBJECTIVES	
2.1 AIMS AND OBJECTIVES	ABHILASHA SHAH(AS)
2.2 METHODOLOGY	
3. LITERATURE REVIEW	
3.1 AIRFOIL GEOMETRY AND NOMENCLATURE	DEEPALI JOSHI(DJ)
3.2 AERODYNAMIC FORCES ON AEROFOIL	
3.3 KUTTA CONDITION	
3.4 BOUNDARY LAYER FLOW	
3.4.1 PROPERTIES OF THE BOUNDARY LAYER FLOW	
3.4.2 THE BOUNDARY LAYER EQUATIONS	
3.4.3 DISPLACEMENT THICKNESS	
3.4.4 MOMENTUM THICKNESS	AAKANKSHA TIWARI
3.4.5 LAMINAR BOUNDARY LAYER	
3.4.6 TURBULENT BOUNDARY LAYER	
3.4.7 FACTORS EFFECTING INSTABILITY AND	
TRANSITION	
3.5 HIGH LIFT DEVICES	
3.6 TURBULENCE MODELS	
3.6.1 CLASSIFICATION OF TURBULENCE MODEL	
3.7 DISCRETIZATION	
3.7.1 REASON FOR DISCRETIZATION	
3.7.2 FINITE DIFFERENCE METHOD	
3.7.3 EXPLICIT FORMULATION	
3.7.4 IMPLICIT APPROACH	
3.7.5 COMPARISON OF EXPLICIT AND IMPLICIT	ABHILASHA SHAH(AS)
SCHEMES	
3.7.6 FINITE ELEMENT METHOD	
3.7.7 FINITE VOLUME METHOD	
3.8 GRID DEPENDENCE STUDY	

3.9 MORPHING CONCEPT.	
4. NUMERICAL ANALYSIS	ABHILASHA SHAH(AS)
4.1 GEOMETRY CREATION	DEEPALI JOSHI(DJ)
4.2 GRID GENERATION	AAKANKSHA TIWARI
4.3 BOUNDARY CONDITION	
5. RESULTS AND DISCUSSION	
5.1 CONFIGURATION 1: BASIC AIRFOIL	ABHILASHA SHAH(AS)
5.2 CONFIGURATION 2: THREE ELEMENT AIRFOIL	DEEPALI JOSHI(DJ)
5.3 CONFIGURATION 3: FIVE ELEMENT AIRFOIL	AAKANKSHA TIWARI
5.4 COMPARISON	
6. FUTURE CONSIDERATIONS	
6.1 CASE 1: 5 ELEMENT AIRFOIL AT 5 DEGREE ANGLE OF ATTACK	ABHILASHA SHAH(AS)
6.2 CASE 2: 5 ELEMENT AIRFOIL AT 15 DEGREE ANGLE OF ATTACK	
7. REFERENCES	



CHAPTER 1

INTRODUCTION

1.1 Multi-element airfoil^{[2][13]}

The use of high lift multi element airfoil has been increasing rapidly for better take-off and landing performance of the aircraft. During landing or taking off of an aircraft, especially high values of lift coefficient is required in order to maintain the flight at desired low speed. The maximum lift coefficient for many conventional low speed aircraft would be only about 1.3 or 1.4 corresponding to a value for the stalling speed. To have lower stalling speeds, higher values for the maximum lift coefficient are required. Studies have shown that an increase in 1% in cl_{max} value during fixed approach speed landing may increase the payload carrying capability of the airplane by 4400lbs which is equivalent to 22 passengers. Increase in L/D by 1% during take-off can increase the payload carrying capability by 2800lbs which is equivalent to 14 passengers. Other benefits of increased cl includes short take-off and landing, low stall speeds and it ensures the economic viability of flight. Thus it can be seen that by increasing the aerodynamic coefficient by just a small value, large benefits can be attained.

The maximum lift coefficient can be increased simply by increasing the camber of the airfoil. But this would also increase the drag not only at high incidence angle but also at low angle of attack. Giving too much camber to the airfoil would mean that the separation point would be much forward of the trailing edge and thus large pressure drag would be introduced by the formation of a region of dead air known as wake. Another disadvantage of increasing camber is that it would lead to the increase of leading edge radius. Thus the formed dynamic stall vortex would be of much larger strength and it would reduce the maximum angle of attack of the airfoil. This problem can be overcome by incorporating such devices which increases maximum lift coefficient at low speeds and rendered ineffective at high speeds. Such devices are known as high lift devices. They fall under two broad categories:-

- One that alters the geometry of aircraft by increasing the wing camber and effective chord length such as flaps
- Other which controls the behaviour of boundary layer over the wing such as slot

1.2 Computational fluid dynamics^{[1][3]}

In the beginning of 1960s, the researchers came across computational methods to solve their flow problems around complex geometries. This provided them with a powerful tool of computational fluid dynamics to analyse the flow within or outside the body. Computational fluid dynamics provides a third approach in the philosophical study & development of the entire discipline of fluid mechanics. Throughout most of the twentieth century the use of pure theory and pure experiment was involved in the practice of fluid mechanics. However the

advent of high speed digital computer combined with the development of accurate numerical algorithms for solving physical problems on these computers has revolutionised the way we study and practise fluid dynamics.

However to keep things in perspective, computational fluid dynamics provides a third approach to physical problems and nothing more than that. We have to still rely on experiment and theory to validate our results. The future ascent of fluid dynamics will rest on the proper equilibrium of all the three approaches, with computational fluid dynamics helping to interpret and understand the result of theory and experiment and vice versa.

The three general governing equations applicable to CFD are: -

- Continuity equation- This states that the net outflow of mass from a control volume is equal to the time rate of decrement of mass inside the control volume. Mathematically it can be written as follows: -

$$\frac{\partial}{\partial t} \iiint_V \rho dV + \int_S \rho V \cdot dS = 0$$

The physical meaning of this equation is that mass cannot be created and nor be destroyed. The above equation is known as integral form of continuity equation. No assumption was made during deriving this equation except the fact that flow is continuum. Thus above equation is applicable to steady, unsteady, incompressible, compressible and any other type of flow.

- Momentum equation- The net force on a particle is equal to the time rate of change of linear momentum in an inertial reference frame. The momentum equation in x, y and z direction can be written as: -

$$\frac{\partial(\rho u)}{\partial t} + \nabla \cdot (\rho u V) = -\frac{\partial p}{\partial x} + \frac{\partial \tau_{xx}}{\partial x} + \frac{\partial \tau_{yx}}{\partial y} + \frac{\partial \tau_{zx}}{\partial z} + \rho f_x$$

$$\frac{\partial(\rho v)}{\partial t} + \nabla \cdot (\rho v V) = -\frac{\partial p}{\partial y} + \frac{\partial \tau_{xy}}{\partial x} + \frac{\partial \tau_{yy}}{\partial y} + \frac{\partial \tau_{zy}}{\partial z} + \rho f_y$$

$$\frac{\partial(\rho w)}{\partial t} + \nabla \cdot (\rho w V) = -\frac{\partial p}{\partial z} + \frac{\partial \tau_{xz}}{\partial x} + \frac{\partial \tau_{yz}}{\partial y} + \frac{\partial \tau_{zz}}{\partial z} + \rho f_z$$

- Energy equation- Rate of change of fluid inside the element is equal to the net flux of heat into the element and the amount of work done on the element due to body and surface forces.

$$\rho \frac{D}{Dt} \left(e + \frac{V^2}{2} \right) = \rho q + \frac{\partial}{\partial x} \left(k \frac{\partial T}{\partial x} \right) + \frac{\partial}{\partial y} \left(k \frac{\partial T}{\partial y} \right) + \frac{\partial}{\partial z} \left(k \frac{\partial T}{\partial z} \right) - \frac{\partial (u\tau)}{\partial x} - \frac{\partial (v\tau)}{\partial y} - \frac{\partial (w\tau)}{\partial z} + \frac{\partial \tau_{xx}}{\partial x} + \frac{\partial \tau_{yx}}{\partial y} + \frac{\partial \tau_{zx}}{\partial z} + \frac{\partial \tau_{xy}}{\partial x} + \frac{\partial \tau_{yy}}{\partial y} + \frac{\partial \tau_{zy}}{\partial z} + \frac{\partial \tau_{xz}}{\partial x} + \frac{\partial \tau_{yz}}{\partial y} + \frac{\partial \tau_{zz}}{\partial z} + \rho f \cdot V$$

The steps involved in the computational fluid dynamics are as follows: -

- Pre-processor
- Solver
- Post-processor

The pre-processor involves the following steps -

- Geometry acquisition/Geometry making- This is the first step in simulating any flow problem in CFD. The geometry on which the simulation has to be done is either to be made or acquired from other source.
- Discretization- This step involves the division of fluid domain and the geometry into small elements or volumes with the help of meshes. The mesh can be structured as well as unstructured.
- Boundary condition- This step involves the dividing of whole fluid domain into different physical phases like inlet, outlet, wall, symmetry etc.

Solver: -

The discretization process is being done in pre-processor using meshing tools. The actual flow simulation is done using the solver tools. The solver like fluent provide us with the varieties of the flow simulation which includes viscous or non-viscous, compressible or incompressible, whether heat transfer based solution is required or not etc. The boundaries to the problem are given in pre-processing but the actual initial conditions are given in the solvers. If suppose a velocity inlet is given to a face in meshing tools then the value of the velocity flowing through that face is given in solver and so on.

Post-processor: -

Post-processor is used to visualize to results after a simulation has taken place. The post-processor allows us to visualize the results which we get through the solver. The post-processor tools give us the contours of pressure, velocity, streamline etc. over the body. The visualization of the results helps us to infer the physical phenomenon which is taking place and hence help us to make better planes.

CHAPTER 2

PROJECT OBJECTIVES

2.1. Aims and Objectives:

The aim of the project is to study the high lift system for civil aircraft and numerically analyse the flow field around the airfoil and what are the impact of incorporating flaps and slats on the airfoil geometry. Finally the use of morphing leading and trailing edge to overcome the disadvantages of conventional system is studied and the literature will be verified using ANSYS ICEM CFD and FLUENT software.

Total of four geometries will be studied which includes:-

- A simple airfoil with no flaps and slats
- Three element airfoil incorporating one slat and single slotted fowler flap
- Five element airfoil incorporating one slat and triple slotted fowler flap
- A morphed airfoil geometry

The objective of the project is: -

- To study the aerodynamic characteristics of the high lift devices.
- To conduct an ICEM CFD and FLUENT analyses over the above mentioned geometries
- To study the grid dependence behaviour of the flow over the geometries.
- To morph the five-element geometry covering different gaps using various combinations.

2.2 Methodology:

A structured method is used to accomplish the objectives stated above.

- Numerical analysis was conducted using Ansys ICEM CFD software for the multi element airfoil
- A BAC 3-11/RES/30/21 airfoil was taken into consideration and three different geometries with the use of slats and flaps was meshed and analysed.
- Structured meshing was done keeping accuracy in mind using ICEM CFD.
- All the three geometries were given the same boundary conditions and the comparison of the results was done using coefficient of lift graph.
- The coefficient of lift was calculated at different angle of attacks for all the three geometries using FLUENT and the graphs and contours were plotted for the same.

CHAPTER 3

LITERATURE REVIEW

3.1 Airfoil Geometry and Nomenclature^[9]

Airfoil: It is defines as a section of the wing. It affects the take off & landing distance, cruise speed, stall speed and handling qualities during different phases of flight.

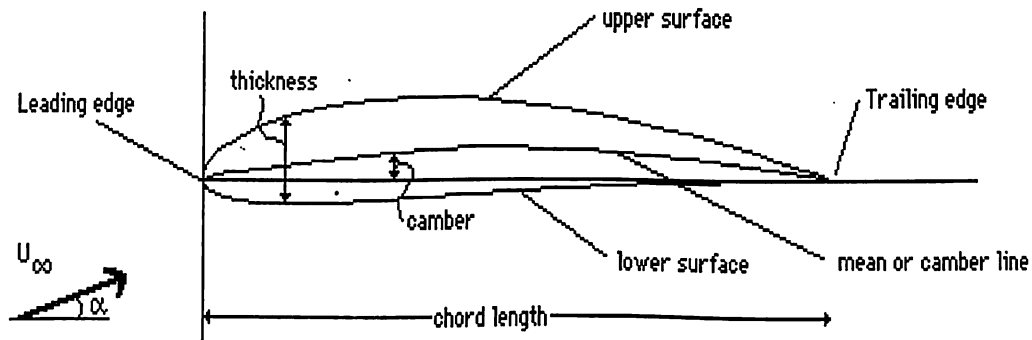


Figure 1: airfoil geometry^[11]

Camber: The curvature characteristics of an aerofoil are determined by its camber. The equidistant line from the upper surface and the lower surface is known as the mean camber line.

Chord: It is defined as the straight line joining the leading and the trailing edge of an airfoil.

Thickness: It is measured as the perpendicular distance to the “mean camber line” of the airfoil from the upper to the lower surface.

Leading edge: The part of an airfoil which comes in contact with the air flow first is known as the leading edge. It can be straight or curved.

Trailing edge: It is the rear edge of an airfoil. All the control surfaces are attached at this end and the flow separated by the L.E is again attached here.

3.2.1. Aerodynamic Forces on Airfoil^[10]

Irrespective of the complexity of the body, the sources of aerodynamic forces and moments on the body are pressure distribution over the body and shear stress distribution over the body. The only way by which fluid exerts force on the body is through pressure and shear stress. The pressure is the normal force acting on a point on the aerofoil whereas shear stress acts tangentially to the surface. The shear stress is generated due to the friction between the

fluid and the solid boundary. The point of application of pressure and shear stress is shown in the following figure: -



Figure 2: pressure and shear point^[10]

It is the integration of these two forces over the complete surface which gives a net aerodynamic force R and the moment M.

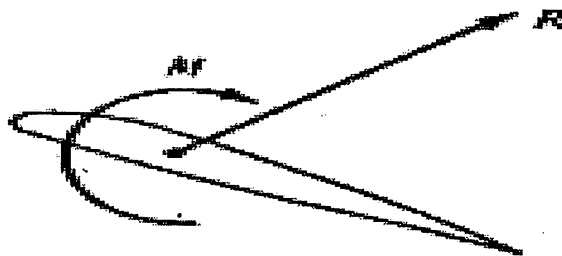


Figure 3: Aerodynamic force and moment^[10]

Consider one such aerofoil which is inclined at an angle α to the relative wind V. The term V is called the free stream velocity as it is the velocity of the wind far ahead of the body. The aerodynamic force R can be resolved into two components viz. one parallel to the free stream direction known as drag and denoted by D and other perpendicular to the free stream known as lift which is denoted by L.

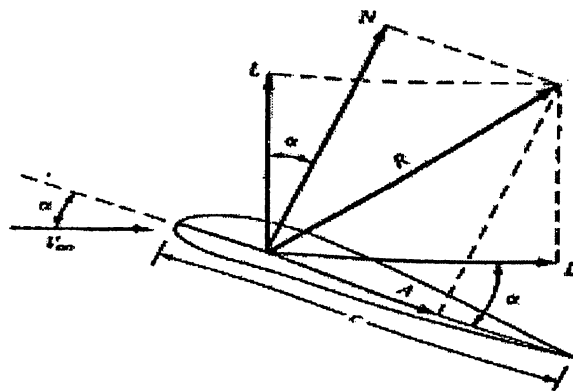


Figure 4: aerodynamic forces^[20]

Apart from this, the aerodynamic force R can be resolved perpendicular and parallel to the chord line as well, known as normal force (N) and axial force (A) respectively. The angle α is the angle between the chord line of the aerofoil and the free stream direction and is known as angle of attack. The lift and drag are related to normal and axial force by the following relation: -

$$L = N \cos \alpha - A \sin \alpha$$

$$D = N \sin \alpha + A \cos \alpha$$

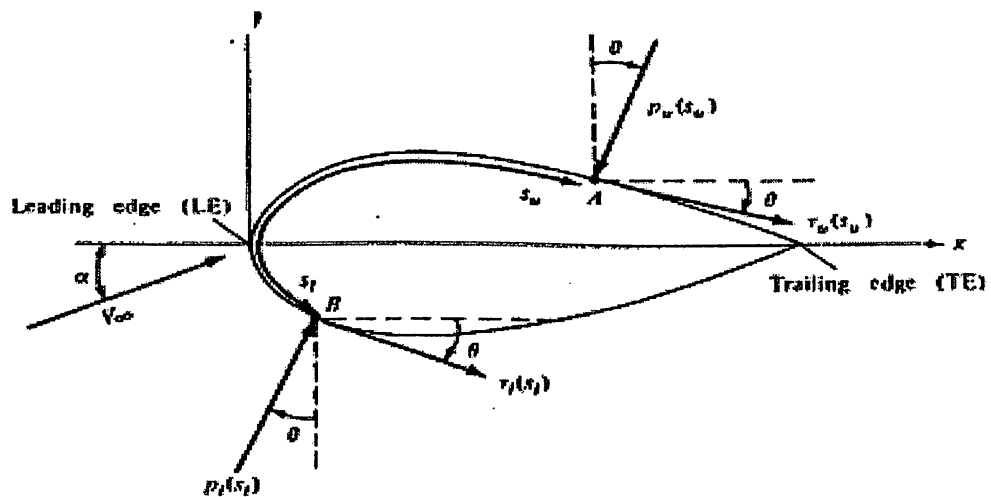


Figure 5: pressure and shear stress distribution^[10]

Now let us consider the figure shown above which highlights the pressure and shear stress distribution over an aerofoil whose integration will provide us with the aerodynamic force and moment over this aerofoil. The chord line of the aerofoil is horizontal and the relative free stream wind is inclined at an angle of α to the chord line. The point A is situated at the upper surface of the aerofoil at a distance S_u from the leading edge measured along the curvature of the aerofoil. Similarly point B is located at the lower surface of the aerofoil at a distance S_l measured along the curvature. The pressure and the shear force on the upper surface are denoted by p_u and τ_u respectively both being functions of S_u . Similarly the lower surface quantities are denoted by p_l and τ_l and both are functions of S_l . The pressure and the shear stress at the given point are inclined by an angle θ to the vertical and horizontal respectively, θ being positive when measured in clockwise direction from the vertical to the p direction and from the horizontal to the τ direction. Consider a cylinder of infinitely long span as shown in figure below. The shaded region in the figure shows the elemental strip of area ds . N' and A' represents the normal and axial force per unit span resp. Thus the force on the upper surface on the elemental strip is given by: -

$$dN'_u = -p_u ds_u \cos \theta - \tau_u ds_u \sin \theta$$

$$dA'_u = -p_u ds_u \sin \theta + \tau_u ds_u \cos \theta$$

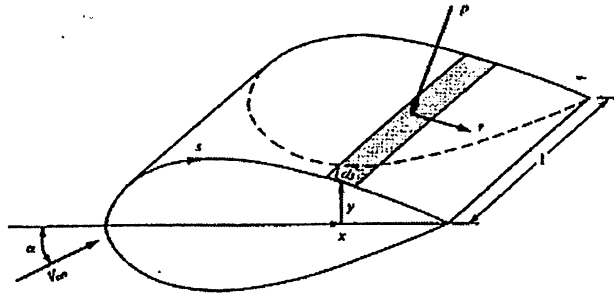


Figure6. Pressure and shear forces^[10]

And that on the lower surface is given by: -

$$dN'_l = p_l ds_l \cos \theta - \tau_l ds_l \sin \theta$$

$$dA'_l = p_l ds_l \sin \theta + \tau_l ds_l \cos \theta$$

The total normal and axial force can be written as follows after integrating the above equations: -

$$N' = - \int_{LE}^{TE} (p_u \cos \theta + \tau_u \sin \theta) ds_u + \int_{LE}^{TE} (p_l \cos \theta - \tau_l \sin \theta) ds_l$$

$$A' = \int_{LE}^{TE} (-p_u \sin \theta + \tau_u \cos \theta) ds_u + \int_{LE}^{TE} (p_l \sin \theta + \tau_l \cos \theta) ds_l$$

3.3 Kutta Condition^{[2][10]}

When a symmetric smooth body moves with zero AoA through a fluid no lift is generated. There are two points on an airfoil called the stagnation points where the local velocity of air flow is zero on the body, one at the front of the body while the other at the rear. If the cylinder moves with some AoA the number of stagnation points still remains two, one under the cylinder while the other on the top of it. Despite of the positive AoA there is no circulation around the smooth cylinder and hence no lift is generated.

If an airfoil has some AoA then the two stagnation points will lie on the lower surface near the L.E and on the upper surface near the T.E. Due to the sharp trailing edge of an airfoil in a real flow, the velocity at the corner is very large. As a result of this, viscous stresses are created due to large velocity gradients despite of very small viscosity coefficient of air. Hence the air flow does not follow the airfoil contour and forms a vortex. The vortex formed

thus induces a downward flow on upper surface of the airfoil hence providing a circulation effect. It moves the stagnation point downwards. The stagnation point keeps moving rearwards as the vortex persists as long as the zero local velocity point (stagnation point) is forward to the T.E.

As the airfoil moves through the air, the stagnation point is at the trailing edge. The flow on the topside adapts itself to the airfoil's upper surface. The flow over the upper and lower surfaces of an airfoil meet at the T.E and leaves the airfoil moving parallel to each another. This is termed as Kutta condition.

The Kutta condition tells us why the airfoils are always sharp at the T.E, even though it is not desired from manufacturing and structural point of view. An airplane with a smoothly rounded wing at the trailing edge would generate no lift or very little lift.

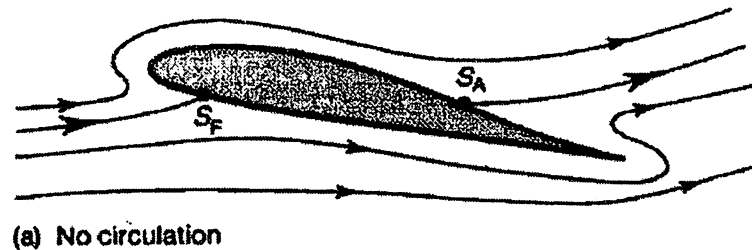


Figure 7: no circulation^[12]

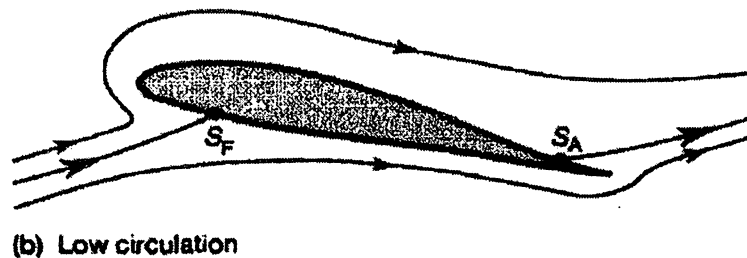
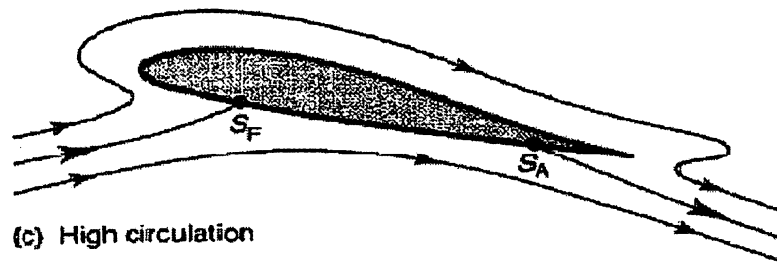
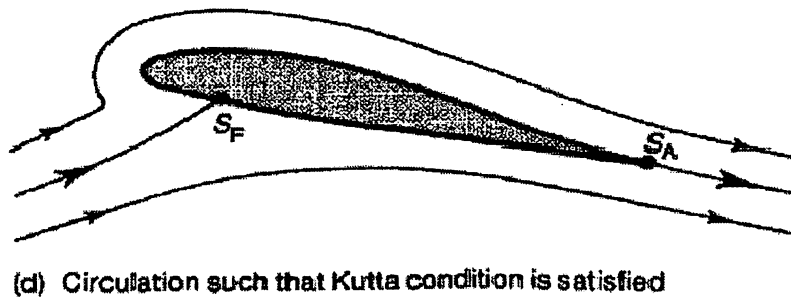


Figure 8: low circulation^[12]

Figure 9: high circulation^[12]Figure 10: circulation such that kutta condition is satisfied^[12]

3.4 Boundary Layer Flow^[10]

The boundary layer and its study are one of the main traits of aerodynamics. Practically friction is present throughout every point in the flow but is of little importance except in the boundary layer. According to Ludwig Prandtl, "A very satisfactory explanation of the physical process in the boundary layer between a fluid and the solid body can be obtained by hypothesis of the adhesion of the fluid to the walls, that is, by the hypothesis of the zero relative velocity between fluid and wall. If the viscosity was very small and the fluid path along the wall not too long, the fluid velocity ought to assume its normal value at a very short distance from the wall. In the thin transition layer however, the sharp changes of velocity, even with small coefficient of friction, produced marked results."

In a simple language, the above statement can be understood as follows. Consider a real viscous fluid flow past a solid boundary or object. The particles of the fluid tend to adhere to the body due to force of adhesion between the solid wall and the fluid. Thus the velocity of the fluid particles adjacent to the wall will be same as that of the wall. If the wall is at rest, then the fluid particles will also be stationary. This is known as 'no-slip condition.' The velocity of fluid at the wall will be zero and goes on increasing as we move farther away from the wall. As the distance from the wall increases, a point is reached when the velocity of the fluid will be closed to the free-stream velocity. Thus the region where the velocity varies

from the 0 to 99% of free-stream velocity is called boundary layer and its thickness is known as boundary layer thickness. The boundary layer thickness goes on increasing along the chord of the aerofoil ranging from fraction of the mm at the leading edge to the few per cent of chord at the trailing edge as shown below. In addition to the velocity boundary layer, there also exists thermal boundary layer. The surface temperature is denoted by T_w which is also called wall temperature while the thermal boundary layer thickness is represented by δ_t .

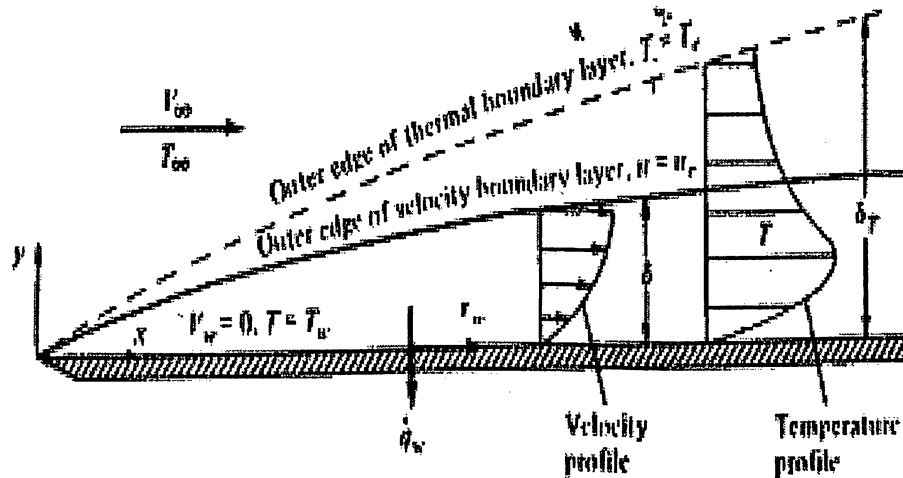


Figure 11: boundary layer^[10]

In this particular region the velocity gradient is present and thus shear stress. The layer of the fluid close to the wall retards the layer just above it due to viscosity. The value of this shear stress is given by Newton as: -

$$\tau = \mu \frac{\partial u}{\partial y}$$

The shear stress is basically the rate of transfer of molecular momentum in the lateral direction of the flow. The molecules carry out a momentum transfer between the fast and slow moving layers of the fluid thus creating a stress. The shear stress varies from τ at the wall to zero at $y = \delta$.

3.4.1. Properties of the boundary layer flow

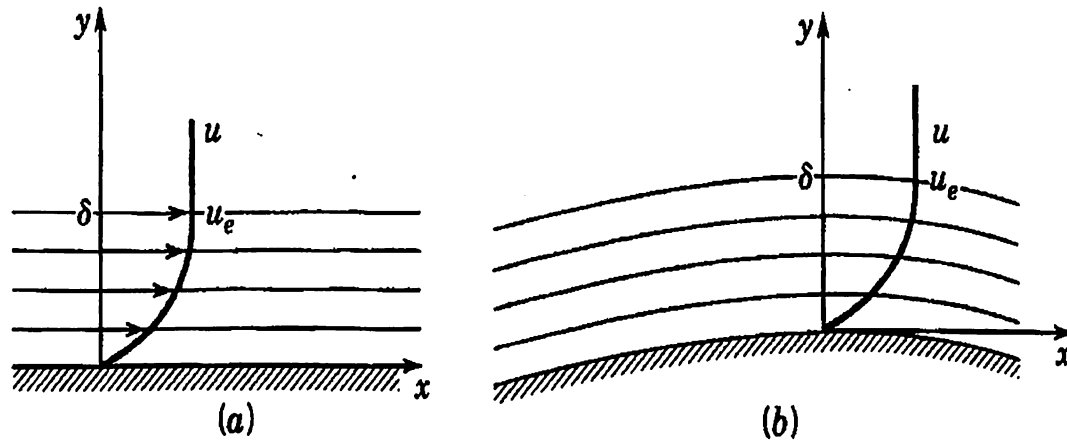


Figure 12: properties of the B.L.^[10]

Boundary layer flow is characterized by high viscous stress and velocity gradient as discussed earlier. In addition to above, one more important feature of boundary layer flow is that pressure change across the boundary layer is practically zero, i.e. there is no pressure change as we move across the boundary layer from $y=0$ to $y=\delta$. This can be deduce from the following explanation; as the value of δ is quite small hence the value of $d\delta/dx$ is also small everywhere. This implies that the streamlines gets curved with a large radius of curvature. The equation of the variation of pressure across the boundary layer is given by: -

$$\frac{\partial p}{\partial y} = \frac{\rho u^2}{R}$$

Since the value of R is large hence we can conclude that dp/dy is practically zero at each location.

Another fact about boundary layer is that the flow is rotational inside the boundary layer. The value of curl for a two dimensional flow is given by: -

$$\text{curl}_z \mathbf{V} = \frac{\partial v}{\partial x} - \frac{\partial u}{\partial y}$$

Since the value of thickness δ is very small hence the first term on right hand side of above equation is very small and hence can be neglected. Thus the curl has a finite non-zero value and we can deduce that the flow is rotational everywhere inside the boundary layer.

3.4.2. The boundary layer equations: -

The equations applicable to the boundary layer can be derived using Newton's laws of motion. Consider a fluid element of dimensions $\Delta x \Delta y \Delta z$ having density ρ . According to the newton's second law the equation for this elemental volume can be written as: -

$$\rho \Delta x \Delta y \Delta z \frac{\mathcal{D}\mathbf{V}}{\mathcal{D}t} = \mathbf{F}$$

Consider the forces that the fluid element is subjected to. Only x momentum equation of the flow is being written here.

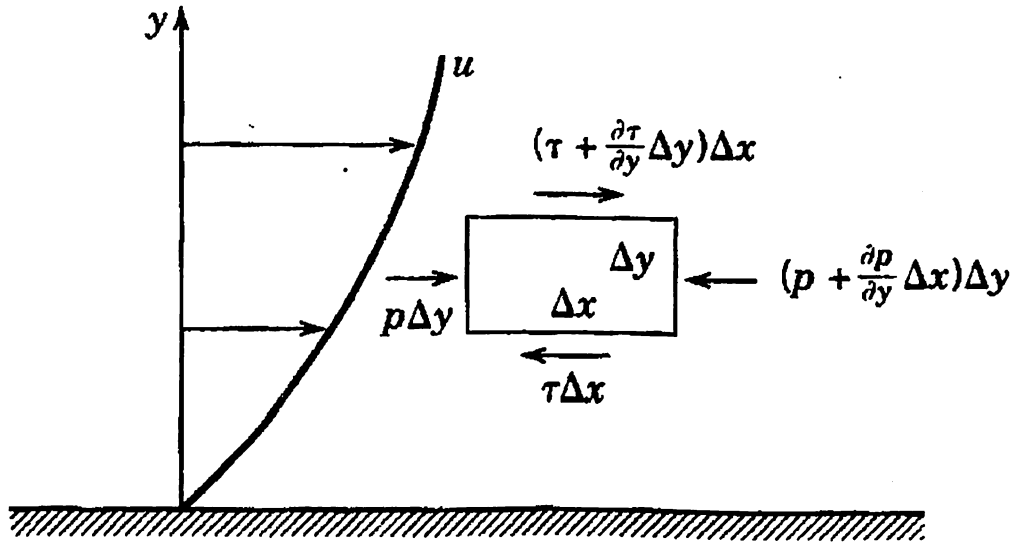


Figure 13: pressure and shear forces^[10]

Taking the unit thickness in z direction, the two dimensional pressure and shear forces which constitute the right hand side of the equation can be written as: -

$$\left(-\frac{\partial p}{\partial x} + \frac{\partial \tau}{\partial y} \right) \Delta x \Delta y$$

The complete equation in x direction can be written as: -

$$\rho \Delta x \Delta y \frac{\mathcal{D}u}{\mathcal{D}t} = \left(-\frac{\partial p}{\partial x} + \frac{\partial \tau}{\partial y} \right) \Delta x \Delta y$$

Dividing the above equation by $\Delta x \Delta y$, expanding the left hand side of the equation and putting the value of τ from above equations, we get the equation of motion of the boundary layer as: -

$$\rho \left(\frac{\partial u}{\partial t} + u \frac{\partial u}{\partial x} + v \frac{\partial u}{\partial y} \right) = - \frac{\partial p}{\partial x} + \frac{\partial}{\partial y} \left(\mu \frac{\partial u}{\partial y} \right)$$

In addition to the above equation, the momentum equation is also applied to the boundary flow which can be expressed as: -

$$\frac{\partial}{\partial x}(\rho u) + \frac{\partial}{\partial y}(\rho v) = 0$$

The above two equations has three unknowns namely u , v and p but only has two equations. The third variable can be solved by considering momentum equation in y direction. From our previous discussions we can write the y momentum equation as: -

$$\frac{\partial p}{\partial y} = 0$$

This implies that the pressure changes only in the x direction and not across the boundary. Hence the pressure at the outer edge of the boundary layer is directly transferred to the surface. The pressure, thus throughout the boundary layer is $p = p(x)$.

For compressible flows, energy equation has to be added to the boundary layer flow to completely determine the flow properties. Consider the fluid element as shown below.

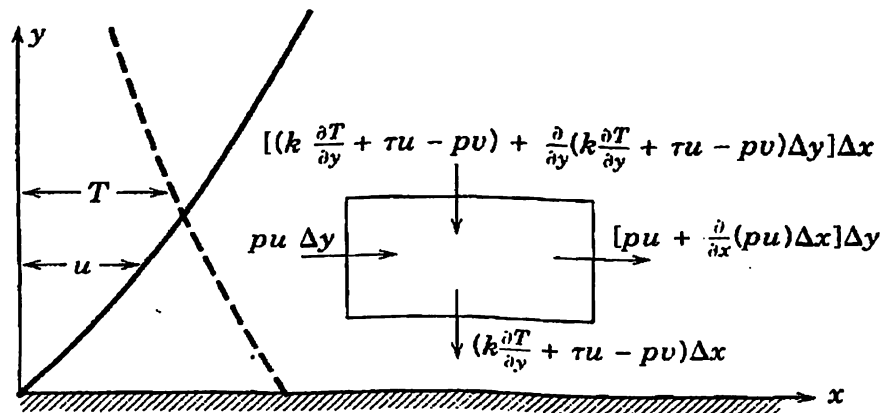


Figure 14: Fluid Element^[10]

From the conservation of the energy principle, the equation for two dimensional elements can be written as: -

$$\rho \Delta x \Delta y \frac{de}{dt} = \frac{\delta}{\delta t} \iint_{\hat{S}_1} \rho (q - w) d\hat{S}_1$$

Here q and w represent the heat and work transfer across the fluid element having surface DS_1 which is bounded by Δx and Δy . The specific internal energy e , of the system moving with velocity u can be written as: -

$$e = c_v T + \frac{1}{2}u^2 + \text{constant}$$

While deriving this equation it is further assumed that $\frac{\delta T}{\delta Y} \gg \frac{\delta T}{\delta X}$ and hence we can deduce that the heat transfer can only take place from top and bottom surface and not from the left and right surface of the fluid element. Applying previous assumptions of $Dp/Dy=0$ and $Du/Dy \gg Du/Dx$, the heat flux entering from the bottom face of the fluid element can be written as: -

$$-k(\partial T/\partial y) \Delta x$$

While that from the top face can be written as: -

$$\left[-k \frac{\partial T}{\partial y} + \frac{\partial}{\partial y} \left(-k \frac{\partial T}{\partial y} \right) \Delta y \right] \Delta x$$

The net heat flux entering to the fluid element can be obtained by above two equations as: -

$$\frac{\partial}{\partial y} \left(k \frac{\partial T}{\partial y} \right) \Delta x \Delta y$$

The work done across the fluid element is transferred from the vertical and horizontal sides by the pressure and the shear stresses as shown in the figure above. The resultant of the work done is given by: -

$$\left[\frac{\partial}{\partial y} (\tau u) - \frac{\partial}{\partial x} (p u) - \frac{\partial}{\partial y} (p v) \right] \Delta x \Delta y$$

Putting the value of work done and the heat flux in the energy conservation equation, we get:-

$$\rho \frac{d}{dt} \left(c_v T + \frac{u^2}{2} \right) = \frac{\partial}{\partial y} \left(k \frac{\partial T}{\partial y} \right) + \frac{\partial}{\partial y} (\tau u) - \frac{\partial}{\partial x} (p u) - \frac{\partial}{\partial y} (p v)$$

The physical significance of the above equation is that it states that the rate of change of total energy inside the fluid element is the sum total of energy due to heat flux and the work done

by pressure and stress on the element. The left hand side of the equation can be written in the form of C_p as: -

$$\begin{aligned} \rho \frac{d}{dt} \left(c_p T + \frac{u^2}{2} \right) &= \rho \frac{d}{dt} \left(c_p T - \frac{p}{\rho} + \frac{u^2}{2} \right) \\ &= \rho \frac{d}{dt} \left(c_p T + \frac{u^2}{2} \right) - \frac{dp}{dt} + \frac{p}{\rho} \frac{d\rho}{dt} \end{aligned}$$

Applying Euler's equation and newton's law of viscosity, the above equation can be written in its final form as: -

$$\rho \frac{d}{dt} \left(c_p T + \frac{u^2}{2} \right) = \frac{\partial}{\partial y} \left(k \frac{\partial T}{\partial y} \right) + u \frac{\partial}{\partial y} \left(\mu \frac{\partial u}{\partial y} \right) + \mu \left(\frac{\partial u}{\partial y} \right)^2$$

3.4.3. Displacement thickness: -

Denoted by δ^* , displacement thickness is defined as the distance by which the boundary layer has to be displaced perpendicular to the flow to compensate for the reduction of the mass flow due to presence of the boundary layer.

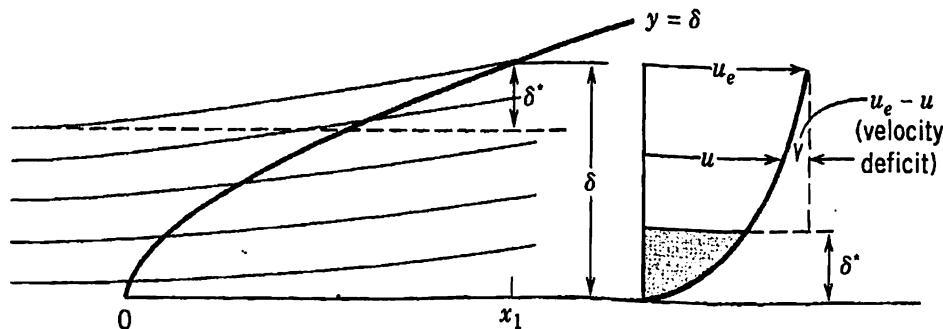
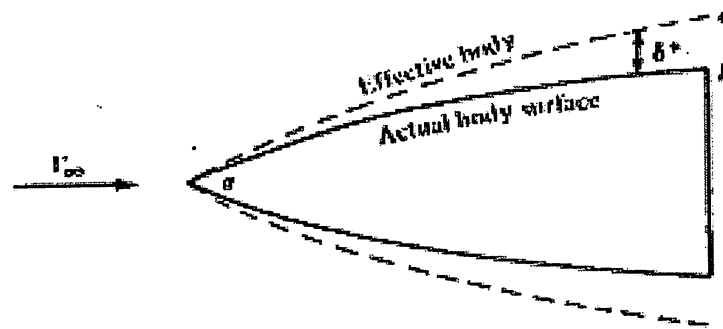


Figure 15: boundary layer^[10]

The expression for the displacement thickness can be written as: -

$$\delta^* = \int_0^{\infty} \left(1 - \frac{u}{u_e} \right) dy$$

Another importance of displacement thickness is that due to presence of the boundary layer, the flow retards and thus the streamlines are deflected outwards by a distance δ^* . This gives rise to the concept of effective body. Due to presence of this effect the actual shape of the body seen by the free stream is enlarged and thus the required manipulation needs to be done.

Figure16. Effective Body^[10]

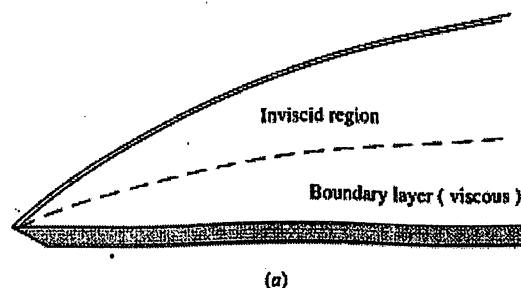
3.4.4. Momentum Thickness: -

Denoted by θ , momentum thickness is defined as the distance by which the boundary layer has to be displaced perpendicular to the flow to compensate for the reduction in the momentum of the flow due to presence of the boundary layer. The expression for momentum thickness is given by: -

$$\theta = \int_0^{\delta} \frac{u}{u_e} \left(1 - \frac{u}{u_e} \right) dy$$

3.4.5. Laminar Boundary Layer: -

To define the laminar (or turbulent) boundary layer considers the viscous flow of velocity U over the flat plate as shown below.

Figure 17: laminar B.L^[10]

Since the plate is stationary, the flow is retarded due to the formation of the boundary layer which starts from the leading edge of the plate. The distance from the leading edge up to which the thickness of the boundary layer is 12 – 14% of the chord is called laminar region. The Reynolds number in this region is below 5×10^5 .

3.4.6. Turbulent Boundary layer: -

As the distance from the leading edge increases, the flow becomes unstable and the transition of the flow from laminar to turbulent takes place. In turbulent region the thickness of the boundary layer is quite large and the flow is characterized by eddies and momentum transfer.

3.4.7. Factors effecting instability and transition: -

1. Pressure gradient: -

The favourable pressure gradient has a stabilizing effect on the boundary layer whereas an adverse pressure gradient has a destabilizing effect. The favourable pressure gradient allows the flow to smoothly pass over the surface thus having a laminar nature whereas an unfavourable pressure gradient causes the flow to separate from the surface due to back flow. Thus the boundary layer destabilizes and the transition takes place from laminar to turbulent. This phenomenon is verified by Schubauer and Skramstad with the help of oscilloscope. A curved plate was used in this experiment having favourable pressure gradient at the leading edge while adverse pressure gradient towards the trailing edge. The results of the experiment are as shown below: -

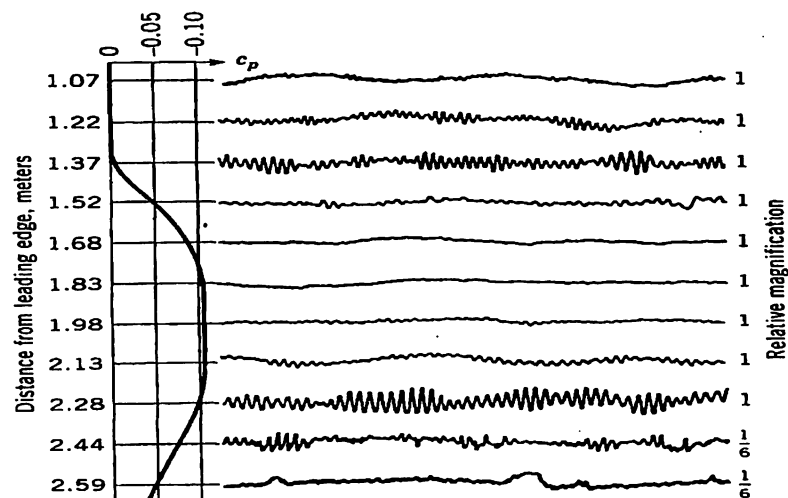


Figure 18: B.L Fluctuation^[10]

The above figure clearly explains that the fluctuations in the flow towards the leading edge are dampened out due to favourable pressure gradient while that towards the trailing edge amplifies due adverse pressure gradient.

2. Suction: -

It is well known fact that suction on any surface decreases the width of the boundary layer and causes the velocity profile to deviate from the inflection point and hence instability. This can be explained as following; as the suction pressure increases, the velocity over that surface will also increase. The increased velocity will act as highly energised flow which is capable of delaying separation and hence transition.

3. Heat: -

The viscosity of air is directly proportional to the temperature. This is due to the fact that at elevated temperatures, the molecular momentum transfer supersedes the inter-molecular attraction. Thus the viscosity of air increases with the temperature and vice versa. It has been shown earlier that as we move across the boundary layer perpendicular to the direction of flow, there exists a temperature gradient. Since the temperature directly effects viscosity and viscosity inversely affects the Reynolds number, the boundary layer is thus affected.

4. Compressibility: -

The air flow above Mach .3 is considered as compressible since the compressibility is more than 5 %. At high speeds, the flow compresses as it move along the body and hence the density of the flow increases. Since the Reynolds number is directly proportional to the density of the fluid hence increased density has direct effect on the Reynolds number. As the Reynolds number increases the flow becomes unstable and thus transits from laminar to turbulent.

5. Roughness: -

The presence of roughness on the surface of the wall increases the instability in the flow and thus the transition from laminar to turbulent boundary layer takes place.

6. Centrifugal instability: -

The instability in the flow caused by the curvature of the streamline as it passes through the body is called centrifugal instability. Consider the case of streamlines as shown below: -

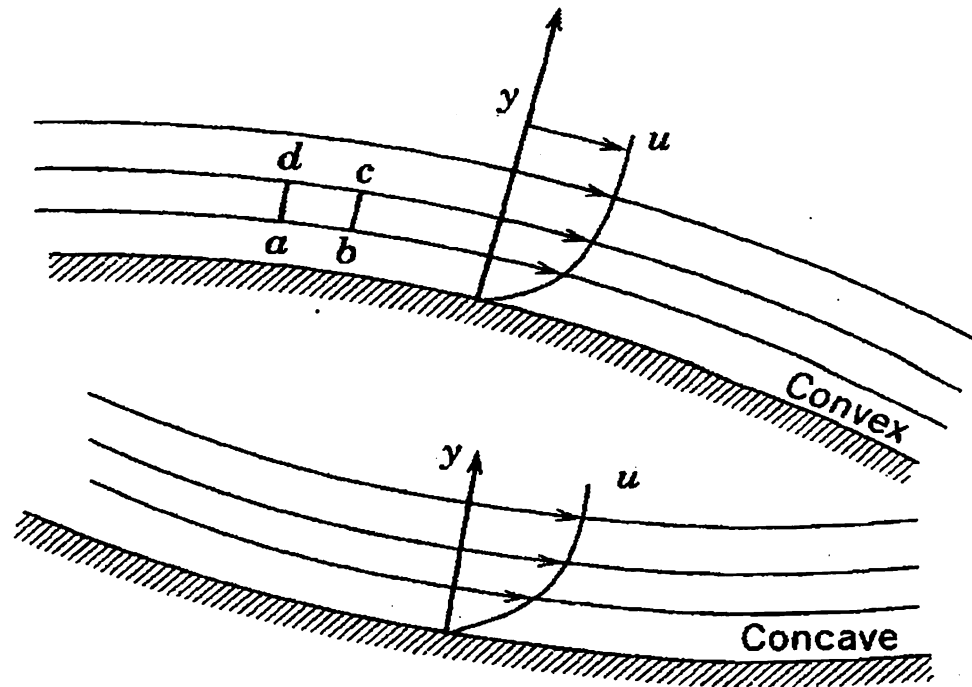


Figure 19: centrifugal instability^[10]

The above figure represents the boundary layer profile over a convex and concave surface. Let us consider the fluid element abcd as shown in figure. The local curvature radius is r whereas the local velocity is u . According to Euler's equation, the local pressure gradient in polar co-ordinates is given by: -

$$\frac{\partial p}{\partial r} = \frac{\rho u^2}{r}$$

The above equation signifies that the resultant pressure on the fluid element is exerted towards the centre of curvature and its magnitude is equal to the centrifugal force in equilibrium. Thus for the above cases, the pressure force is directed towards the surface in case of convex shape and away from it in case of concave shape.

If the fluid is disturbed due to roughness present on the wall, then the convex surface will try to bring back the layer of fluid to its original location thus stabilizing the flow whereas in case of concave shape, vice versa happens and the flow destabilizes.

3.5 High Lift Devices^{[2][15]}

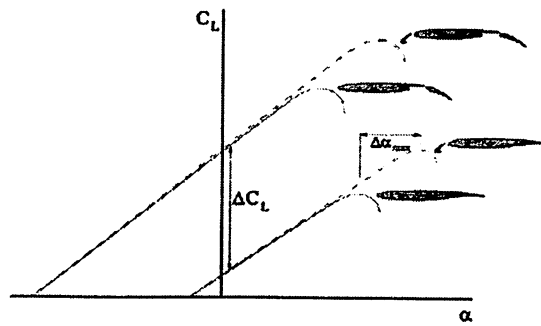


Figure 20: Typical high lift system and its effect on airplane lift^[21]

The high lift devices fall mainly into two categories:

The most common type of auxiliary device in the first classification are trailing edge devices known as flaps. Most common trailing edge devices are:-

- Split flap
- Plain flap
- Single-slotted fowler flap
- Simple slotted flap
- Fixed vane/main double-slotted flap
- Articulating vane/main double-slotted flap
- Main/aft double-slotted flap
- Triple slotted flap

1. Split flap: - In case of split flap only the lower part of the trailing edge is deflected. Since the upper surface remains unchanged thus there are marked reduction separation effects. This kind of flap adversely effects the operation at low speeds due to formation of wake behind the flap.

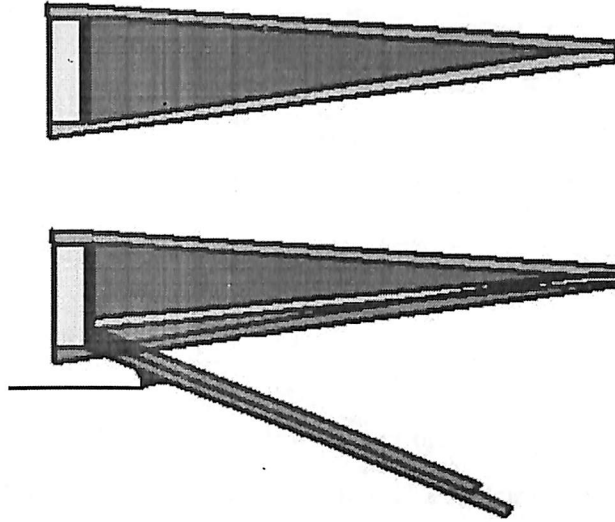


Figure 21: Split Flap^[22]

2. Plain flap: - A plain flap is one which is deflected downward from the trailing edge without producing any gap. Its deflection is restricted to 20 degrees due to constraint of over camberness.

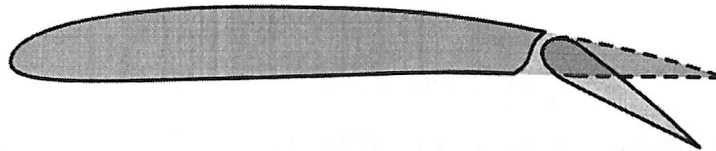


Figure 22: plain flap

3. Single slotted fowler flap: - When extended, single slotted fowler flap creates gap between the flap and the upper edge or cove of the aerofoil. This is the most weight and cost effective flap as compared to other fowler flaps. It can be extended maximum up to 40 degrees.

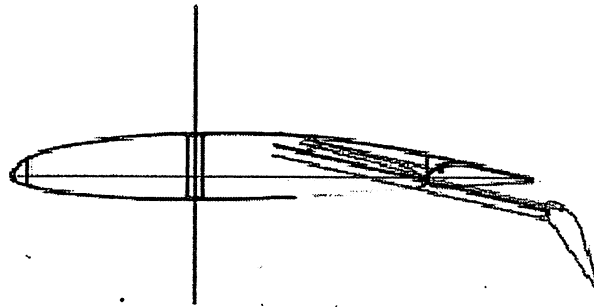


Figure 23: Single slotted fowler flap^[24]

4. Simple slotted flap: - It act as a fowler flap but with very little gap. It has round cavity and it does not move far away from its wing fixed railing edge. It can be deflected maximum to 35 degrees.

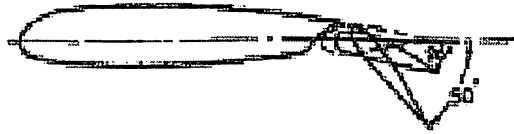


Figure 24: Simple slotted flap^[13]

5. Fixed vane/main double-slotted flap: - It has a vane which is attached rigidly to the main flap thus producing a double slotted fowler flap. Its maximum deflection is 55 degrees. It has got a complex mechanism for actuation and provides only a small increment in lift than single slotted fowler flap.

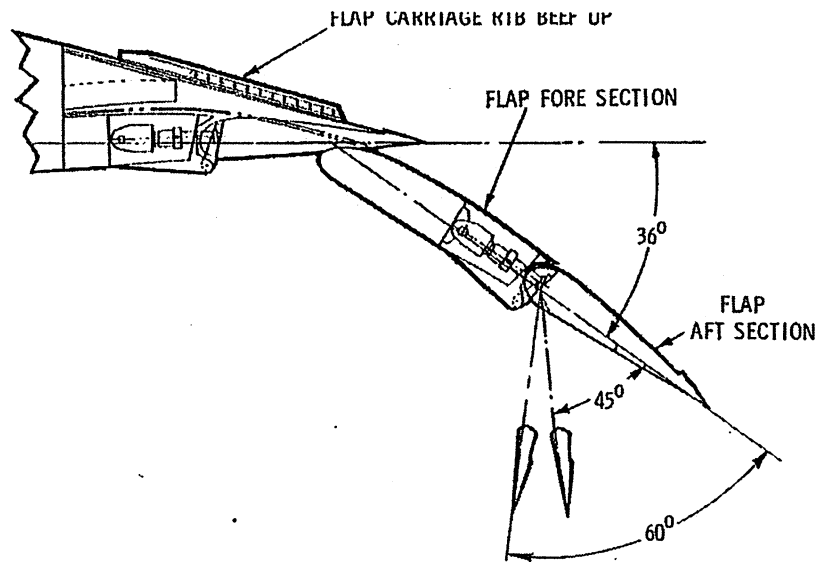


Figure 25: Fixed vane/main double slotted flap^[26]

6. **Articulating vane/main double-slotted flap:** - In this the vane is also extended from its cove increasing the fowler deflection. The main advantage of such kind is that, for the flap deflection of 5 to 15 degrees they remain single slotted for the optimum L/D ratio.

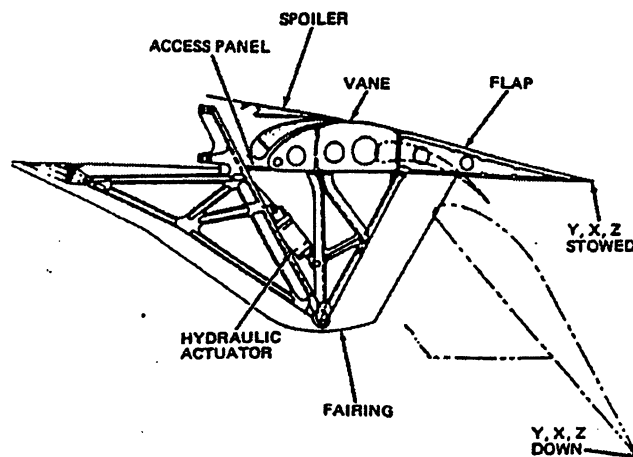


Figure 26: Articulating vane/Main double slotted flap^[4]

7. **Main/aft double-slotted flap:** - This type of flap is more complex than the articulating type. The main flap is the larger element and the aft one is the smaller. The main flap overlaps the wing and the smaller flap overlaps the main flap. This configuration facilitates the deflection of main flap of about 35 degrees and that of small vane of about 28 degrees. Thus the total flap deflection adds up to be 62-65 degrees.

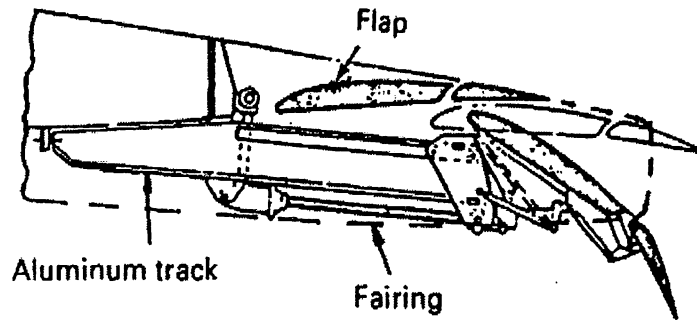


Figure 27: Main/Aft double slotted flap^[4]

8. Triple-slotted flap: - The triple slotted flap is like articulating type with an additional aft small flap element. The total deflection of such kind of flap is about 80 degrees. They provide higher lift coefficient than any other flap configuration but the edge losses are high.

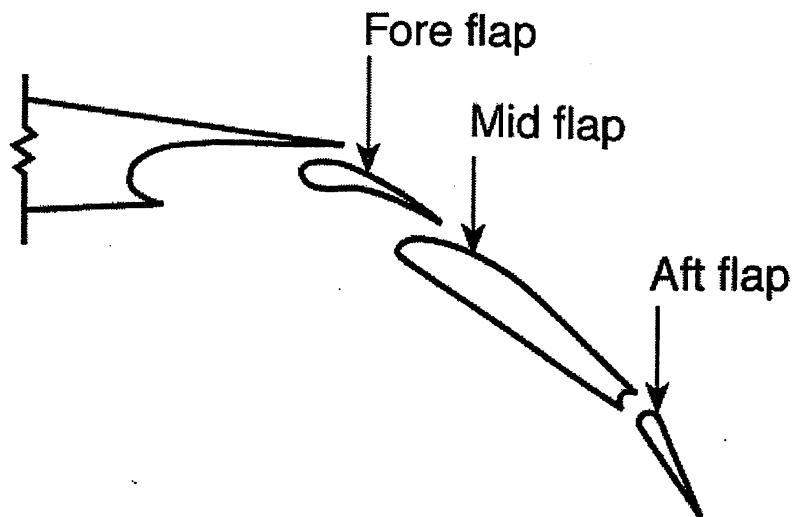


Figure 28: Triple Slotted flap^[27]

Various leading edge devices with brief information about each are as follows: -

- Fixed slot
- Simple Krueger flap
- Folding, bull nose Krueger flap
- Two position slat

1. Fixed slot: - A fixed slot type leading edge device is being illustrated below. It is efficient at low speeds but its drag penalty is unacceptable at high speeds.

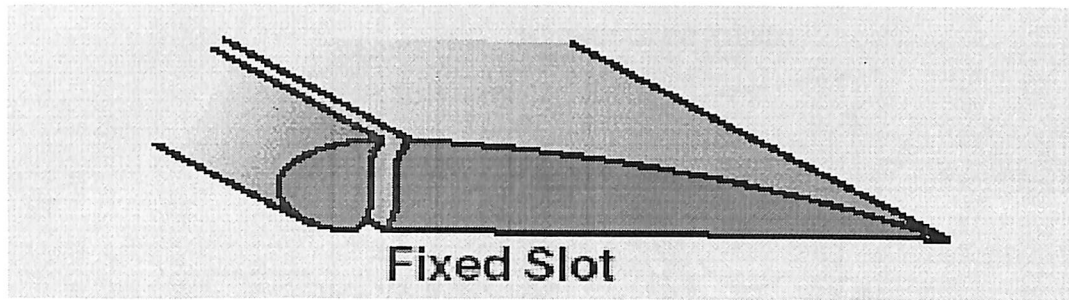


Figure 29: Fixed slot^[11]

2. Simple Krueger flap: - It consists of a panel at the lower edge. First the flap is being rotated about a hinge line and then it is protruded forward so that its upper edge seals with the lower edge of wing. The maximum deflection of such kind is 60 to 80 degrees.

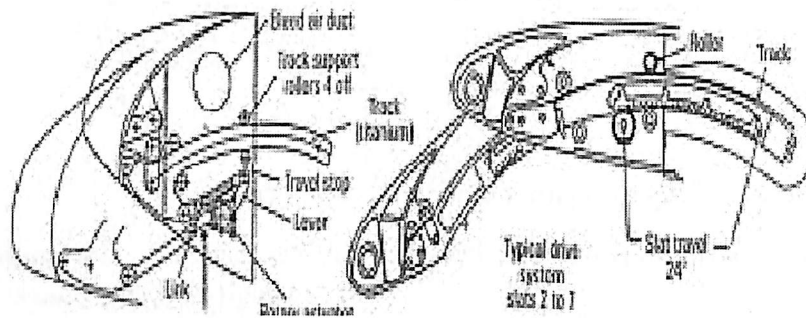


Figure 30: Simple Krueger flap^[28]

3. Folding, bull nose Krueger flap: - This type of flap is similar to simple Krueger flap but it incorporates a retractable D shaped nose at the end of the flap. The advantage of such kind is that it is more tolerant to the change in angle of attack. It uses more complex mechanism.

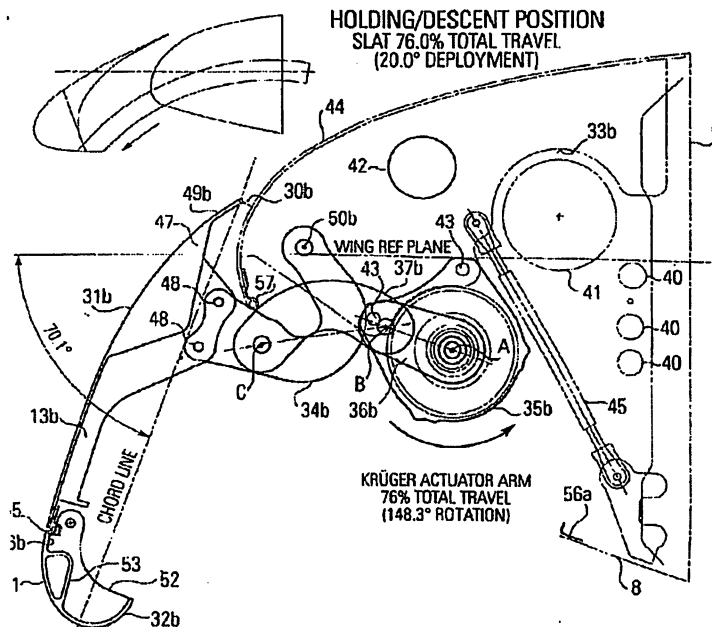


Figure 31: Folding, Bull nose Krueger flap^[29]

4. Two position slat: - It has two position slats one in deployed and other in stowed condition. It is used mainly in fighter aircrafts.

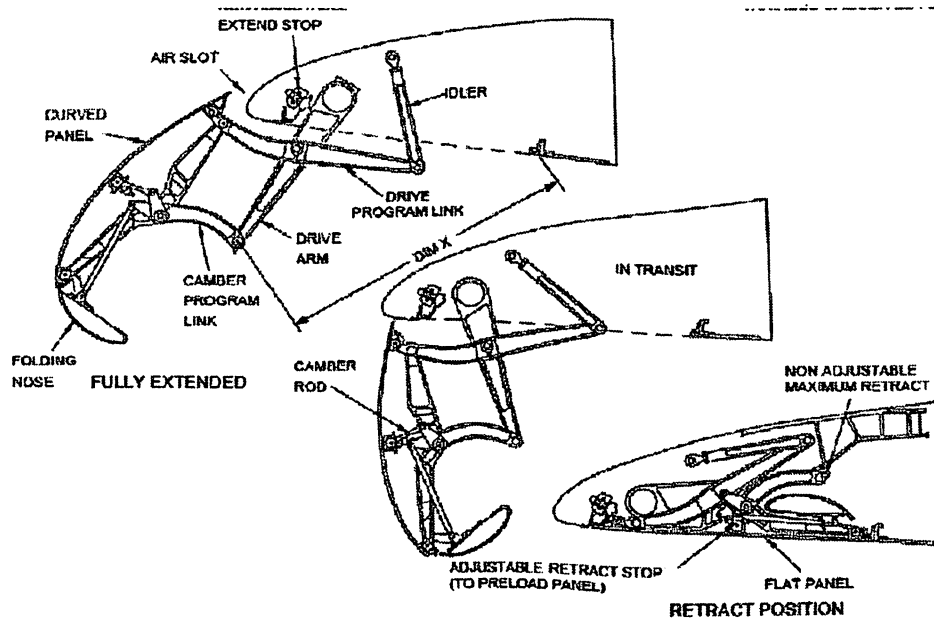


Figure 32: Two position slat^[30]

Discussed above are different types of high lift devices which are used in civil transport aircraft. These devices can be used separately as well as the combination of two of them i.e. a leading edge device in combination with a trailing edge device can be used. In the report

basic airfoil, three element airfoil (single fixed slot with single slotted fowler flap) and 5-element airfoil (single fixed slot with triple slotted fowler flap) is being analysed numerically with the help of CFD software ANSYS ICEM and FLUENT.

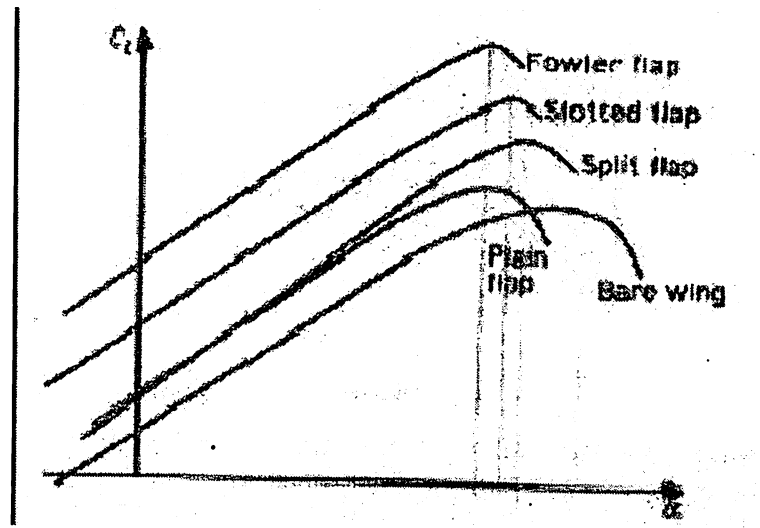


Figure 33: C_l vs. AoA curve for different flap configuration^[2]

The disadvantage of such type of high lift geometry is that they are heavy, uses complex mechanism for their actuation and thus uses more of engine power, has high production as well as maintenance cost and have exposed edges. The gaps and overlaps resulting from the extension of these devices lead to the availability of sharp and bare edges. These sharp edges create vortices and eddy. These eddies compel the boundary layer to transit from laminar to turbulent and thus increasing skin friction drag. Moreover the separation, resulting from high camber, occurs at low angle of attack and thus limiting the maximum stall angle. The wakes thus produced due to separation add to the pressure drag.

Due to the above mentioned reasons concept of morphing leading edge is being studied numerically to overcome the disadvantages of conventional high lift devices. Morphing means "Smooth transition from one shape to another". Morphing concept has less components thus increases reliability, has no exposed edges thus increases stealth and aerodynamics of body and it has capability to operate at wide range of speeds and temperatures. The response time of actuator is very less and it provides excellent strain resistance to repetitive actuations.

3.6 Turbulence Models^{[9][10]}

"Turbulent fluid motion is an irregular condition of flow in which the various quantities show a random variation with time and space coordinates, so that statistically distinct average value can be observed" - Hinze

The key problem in CFD simulations is selecting the correct turbulence model. Virtually all engineering applications are turbulent in nature and hence a turbulent model is required.

3.6.1 Classification of turbulence models:

1. RANS-based models

- Linear eddy-viscosity models
 - Algebraic models
 - One equation models
 - Two equation models
- Non-linear eddy viscosity models and algebraic models
- Reynolds stress transport models
 - Large eddy simulations
 - Detached eddy simulations and other hybrid models
 - Direct numerical simulations

The turbulence models considered for the project are as follows:

- **Spalart-Allmaras model:** It is a one equation model for the turbulent viscosity. The model solves the transport equation for a viscosity like variable.
- **K-epsilon model:** The k-epsilon is a two equation model which uses two extra transport equations to depict the turbulent properties of the flow. It is one of the most commonly used models though it does not show good results in cases of adverse pressure gradients.

The two transported variables used in this model are turbulent kinetic energy, k which determines the energy in turbulence, and turbulent dissipation, ϵ which determines the scale of turbulence.

The different k-epsilon models are:

- Standard k-epsilon model : Transport equations for standard k-epsilon model-

For turbulent kinetic energy k ,

$$\frac{\partial}{\partial t}(\rho k) + \frac{\partial}{\partial x_i}(\rho k u_i) = \frac{\partial}{\partial x_j} \left[\left(\mu + \frac{\mu_t}{\sigma_k} \right) \frac{\partial k}{\partial x_j} \right] + P_k + P_b - \rho \epsilon - Y_M + S_k$$

For dissipation ϵ ,

$$\frac{\partial}{\partial t}(\rho \epsilon) + \frac{\partial}{\partial x_i}(\rho \epsilon u_i) = \frac{\partial}{\partial x_j} \left[\left(\mu + \frac{\mu_t}{\sigma_\epsilon} \right) \frac{\partial \epsilon}{\partial x_j} \right] + C_{1\epsilon} \frac{\epsilon}{k} (P_k + C_{3\epsilon} P_b) - C_{2\epsilon} \rho \frac{\epsilon^2}{k} + S_\epsilon$$

Turbulent viscosity is given as,

$$\mu_t = \rho C_\mu \frac{k^2}{\epsilon}$$

- Realisable k-epsilon model: Transport equations for this model is-

For turbulent kinetic energy k ,

$$\frac{\partial}{\partial t}(\rho k) + \frac{\partial}{\partial x_j}(\rho k u_j) = \frac{\partial}{\partial x_j} \left[\left(\mu + \frac{\mu_t}{\sigma_k} \right) \frac{\partial k}{\partial x_j} \right] + P_k + P_b - \rho \epsilon - Y_M + S_k$$

For dissipation ϵ ,

$$\frac{\partial}{\partial t}(\rho \epsilon) + \frac{\partial}{\partial x_j}(\rho \epsilon u_j) = \frac{\partial}{\partial x_j} \left[\left(\mu + \frac{\mu_t}{\sigma_\epsilon} \right) \frac{\partial \epsilon}{\partial x_j} \right] + \rho C_1 S \epsilon - \rho C_2 \frac{\epsilon^2}{k + \sqrt{\nu \epsilon}} + C_{1\epsilon} \frac{\epsilon}{k} C_{3\epsilon} P_b + S_\epsilon$$

Where

$$C_1 = \max \left[0.43, \frac{\eta}{\eta + 5} \right], \quad \eta = S \frac{k}{\epsilon}, \quad S = \sqrt{2 S_{ij} S_{ij}}$$

In the above equations, P_k depicts the turbulence kinetic energy generation because of the mean velocity gradient and P_b represents turbulence kinetic energy generation cause of buoyancy.

Turbulent viscosity is given as,

$$\mu_t = \rho C_\mu \frac{k^2}{\epsilon}$$

Where

$$C_\mu = \frac{1}{A_0 + A_s \frac{k U^*}{\epsilon}}$$

$$U^* \equiv \sqrt{S_{ij} S_{ij} + \tilde{\Omega}_{ij} \tilde{\Omega}_{ij}}$$

$$\tilde{\Omega}_{ij} = \Omega_{ij} - 2 \epsilon_{ijk} \omega_k$$

$$\Omega_{ij} = \overline{\tilde{\Omega}_{ij}} - \epsilon_{ijk} \omega_k$$

Here $\overline{\tilde{\Omega}_{ij}}$ represents the mean rate of rotation tensor with angular velocity ω_k .
The constants A_0 & A_s are given as:

$$A_0 = 4.04, \quad A_s = \sqrt{6} \cos \phi$$

$$\phi = \frac{1}{3} \cos^{-1}(\sqrt{6}W), \quad W = \frac{S_{ij}S_{jk}S_{ki}}{\tilde{S}^3}, \quad \tilde{S} = \sqrt{S_{ij}S_{ij}}, \quad S_{ij} = \frac{1}{2} \left(\frac{\partial u_j}{\partial x_i} + \frac{\partial u_i}{\partial x_j} \right)$$

Constants

$$C_{1\epsilon} = 1.44, \quad C_2 = 1.9, \quad \sigma_k = 1.0, \quad \sigma_\epsilon = 1.2$$

- **RNG k-epsilon model:** This model was developed to take into consideration the effects of smaller scales of motion. Transport equations of this model are-

For turbulent kinetic energy k,

$$\frac{\partial}{\partial t}(\rho k) + \frac{\partial}{\partial x_i}(\rho k u_i) = \frac{\partial}{\partial x_j} \left[\left(\mu + \frac{\mu_t}{\sigma_k} \right) \frac{\partial k}{\partial x_j} \right] + P_k - \rho \epsilon$$

For dissipation ϵ ,

$$\frac{\partial}{\partial t}(\rho \epsilon) + \frac{\partial}{\partial x_i}(\rho \epsilon u_i) = \frac{\partial}{\partial x_j} \left[\left(\mu + \frac{\mu_t}{\sigma_\epsilon} \right) \frac{\partial \epsilon}{\partial x_j} \right] + C_{1\epsilon} \frac{\epsilon}{k} P_k - C_{2\epsilon}^* \rho \frac{\epsilon^2}{k}$$

Where

$$C_{2\epsilon}^* = C_{2\epsilon} + \frac{C_\mu \eta^3 (1 - \eta/\eta_0)}{1 + \beta \eta^3} \quad \eta = Sk/\epsilon$$

$$S = (2S_{ij}S_{ij})^{1/2}$$

The turbulent viscosity is calculated in the similar manner as of standard k-epsilon.

Model constants,

$$C_\mu = 0.0845_{(0.09)}$$

$$\sigma_k = 0.7194_{(1.0)}$$

$$\sigma_\epsilon = 0.7194_{(1.30)}$$

$$C_{\epsilon 1} = 1.42_{(1.44)}$$

$$C_{\epsilon 2} = 1.68_{(1.92)}$$

$$\eta_0 = 4.38$$

$$\beta = 0.012_{(\text{derived from experiment})}$$

- **Selection of turbulence model:** The realizable k- ϵ turbulence model was selected keeping in mind the effect of circulation and eddies formation. In this model a eddy

viscosity is calculated from a single turbulence scale length. It is easy to implement and computationally cheap.

3.7 Discretization^{[7][3]}

The dictionary meaning of word discretization is to put something separately or distinctly or to divide something in parts. In the context of CFD, the word discretization has much more of the technical meaning although the zest of the word remains the same. The discretization is defined as a process in which a closed form mathematical expression which comprises of function, differential or integral terms and has infinite continuum values over a defined boundary can be approximated by using different expressions which define these values at finite number of points over the given region. The point might refer to a node, element or cell which are either randomly located in the domain (unstructured grid) or are arranged in a sequential order (structured grid).

The close form or the analytical solution of the mathematical equations gives the continuous values of properties over the complete domain while numerical methods provide the solutions at defined points (discrete points) also known as grid points. To make it clearer, consider the grid points in xy plane as shown in figure below. The grids are spaced equally in x direction with width of each grid as Δx and similarly in y direction as Δy .

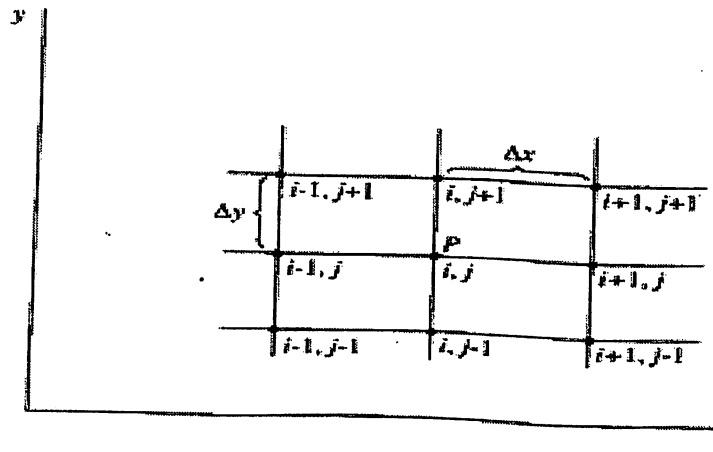


Figure 34: grids^[3]

In general, though the spacing between the grids in x and y direction need not to be uniform and the user has a choice of using grids of unequal spacing if it satisfies the problem definition but still an equal spaced grid is chosen because it is easier to program, reduces computation costs and results in an higher accuracy. The location of a point in a grid is represented by index (i, j) where the i describes the location in x direction and j in y direction. Thus if the point p in the figure has value (i, j) then the point just above it will have value (i, j+1). Similarly the values of points at the right, left and bottom of the point p can be written as (i+1, j), (i-1, j) and (i, j-1) respectively. The above method of discretization is called finite difference method. The other two methods are finite element method and finite volume method which will be discussed later.

3.7.1 Reason for Discretization: -

As being discussed earlier, the analytic solution of the equations give exact values at infinite points of the flow domain but difficulty arises when these equation are to be used for complex geometries like the complete aircraft, gas turbine engine etc. or for complex flow fields like shock wave and boundary layer interaction, flow in a boundary layer with heat conduction etc. Thus there exists a need to simplify these problems by dividing the fluid domain into smaller finite points at which the flow properties can be calculated by approximation methods.

The governing equations of continuity, momentum and energy in the form of differential equations can be written as follows: -

Continuity Equation: -

$$\frac{\partial \rho}{\partial t} + \nabla \cdot (\rho \mathbf{V}) = 0$$

X-Momentum equation: -

$$\frac{\partial(\rho u)}{\partial t} + \nabla \cdot (\rho u \mathbf{V}) = -\frac{\partial p}{\partial x} + \frac{\partial \tau_{xx}}{\partial x} + \frac{\partial \tau_{yx}}{\partial y} + \frac{\partial \tau_{zx}}{\partial z} + \rho f_x$$

Y-Momentum equation: -

$$\frac{\partial(\rho v)}{\partial t} + \nabla \cdot (\rho v \mathbf{V}) = -\frac{\partial p}{\partial y} + \frac{\partial \tau_{xy}}{\partial x} + \frac{\partial \tau_{yy}}{\partial y} + \frac{\partial \tau_{zy}}{\partial z} + \rho f_y$$

Z-Momentum equation: -

$$\frac{\partial(\rho w)}{\partial t} + \nabla \cdot (\rho w \mathbf{V}) = -\frac{\partial p}{\partial z} + \frac{\partial \tau_{xz}}{\partial x} + \frac{\partial \tau_{yz}}{\partial y} + \frac{\partial \tau_{zz}}{\partial z} + \rho f_z$$

Energy equation: -

$$\begin{aligned} \frac{\partial}{\partial t} \left[\rho \left(e + \frac{V^2}{2} \right) \right] + \nabla \cdot \left[\rho \left(e + \frac{V^2}{2} \right) \mathbf{V} \right] &= \rho \dot{q} + \frac{\partial}{\partial x} \left(k \frac{\partial T}{\partial x} \right) + \frac{\partial}{\partial y} \left(k \frac{\partial T}{\partial y} \right) \\ &+ \frac{\partial}{\partial z} \left(k \frac{\partial T}{\partial z} \right) - \frac{\partial(u p)}{\partial x} - \frac{\partial(v p)}{\partial y} - \frac{\partial(w p)}{\partial z} + \frac{\partial(u \tau_{xx})}{\partial x} \\ &+ \frac{\partial(u \tau_{yx})}{\partial y} + \frac{\partial(u \tau_{zx})}{\partial z} + \frac{\partial(v \tau_{xy})}{\partial x} + \frac{\partial(v \tau_{yy})}{\partial y} \\ &+ \frac{\partial(v \tau_{zy})}{\partial z} + \frac{\partial(w \tau_{xz})}{\partial x} + \frac{\partial(w \tau_{yz})}{\partial y} + \frac{\partial(w \tau_{zz})}{\partial z} + \rho \mathbf{f} \cdot \mathbf{V} \end{aligned}$$

Where: -

$$\nabla \equiv \mathbf{i} \frac{\partial}{\partial x} + \mathbf{j} \frac{\partial}{\partial y} + \mathbf{k} \frac{\partial}{\partial z}$$

The above equations are in differential forms having unknowns' u , v , w , ρ and T . These equations can be solved but rigorous mathematical tools will be implemented. To make the solution easy, the above differential equations can be approximated by using Taylor's expansion theorem to change the differential form in the algebraic form.

$$\left(\frac{\partial u}{\partial x} \right)_{i,j} = \frac{u_{i+1,j} - u_{i-1,j}}{2\Delta x} + O(\Delta x)^2$$

The above method of discretization is called Finite difference method (FDM) which will be elaborated in the subsequent paragraphs. Another two methods Finite element method (FEM) and finite volume method (FVM) will also be discussed in detail.

3.7.2 Finite Difference Method: -

The partial derivatives in the governing equation are replaced by the approximate algebraic terms in this method. The most common process of transformation is the Taylor's series expansion. Reviewing our previous discussion on the two dimensional grid, if U_i represents the velocity at the (i, j) th point then the velocity U_{i+1} at $(i+1, j)$ th can be written using Taylor series as: -

$$u_{i+1} = u_i + \Delta x \left(\frac{\partial u}{\partial x} \right)_i + \frac{\Delta x^2}{2} \left(\frac{\partial^2 u}{\partial x^2} \right)_i + \frac{\Delta x^3}{3!} \left(\frac{\partial^3 u}{\partial x^3} \right)_i + \frac{\Delta x^4}{4!} \left(\frac{\partial^4 u}{\partial x^4} \right)_i + \dots$$

Similarly the velocity at location $(i-1, j)$ can be written as: -

$$u_{i-1} = u_i - \Delta x \left(\frac{\partial u}{\partial x} \right)_i + \frac{\Delta x^2}{2} \left(\frac{\partial^2 u}{\partial x^2} \right)_i - \frac{\Delta x^3}{3!} \left(\frac{\partial^3 u}{\partial x^3} \right)_i + \frac{\Delta x^4}{4!} \left(\frac{\partial^4 u}{\partial x^4} \right)_i + \dots$$

The above two expressions are exact expression for differential terms if either the series contains infinite terms which eventually converge or $\Delta x \rightarrow 0$. Solving the first of the two equations for $(Du/Dx)_i$ we get the expression as: -

$$\left(\frac{\partial u}{\partial x}\right)_{i,j} = \underbrace{\frac{u_{i+1,j} - u_{i,j}}{\Delta x}}_{\text{Finite-difference representation}} - \underbrace{\left(\frac{\partial^2 u}{\partial x^2}\right)_{i,j} \frac{\Delta x}{2} - \left(\frac{\partial^3 u}{\partial x^3}\right)_{i,j} \frac{(\Delta x)^2}{6} + \dots}_{\text{Truncation error}}$$

The first term on right hand side is called finite difference representation while the second term as truncation error. The truncation error in the above equation can be collectively written as $O(\Delta x)$ which means other terms containing order of Δx .

$$\left(\frac{\partial u}{\partial x}\right)_i = \frac{u_{i+1} - u_i}{\Delta x} + O(\Delta x)$$

The above equation is known as forward difference equation since the information is taken from the right side of the point i.e. $i+1$ and not from the left hand side. Moreover the above equation is first order accurate since the error terms in the equation contains first degree of Δx . Similarly the first order accurate backward difference equation can be written as: -

$$\left(\frac{\partial u}{\partial x}\right)_i = \frac{u_i - u_{i-1}}{\Delta x} + O(\Delta x)$$

And the second order accurate central difference terms can be written as: -

$$\left(\frac{\partial u}{\partial x}\right)_i = \frac{u_{i+1} - u_{i-1}}{2\Delta x} + O(\Delta x^2)$$

The above mentioned algebraic approximations are sufficient for inviscid flow which has only first order partial differential terms in their governing equations but viscous flow also contains second order partial differential terms as well in their governing equation. Thus the second order terms can be approximated as follows: -

$$\left(\frac{\partial^2 u}{\partial x^2}\right)_i = \frac{u_{i+1} - 2u_i + u_{i-1}}{\Delta x^2} + O(\Delta x^2)$$

The expressions of y terms are almost same in above equations. The only change that needs to be done is to replace x by y and i by j.

3.7.3 Explicit formulation: -

The way by which any problem would be solved comes under CFD technique. Generally all CFD techniques comes under two divisions namely Explicit and implicit. The former one is being explained here. To simplify the explanation let us consider a one dimensional parabolic heat transfer equation given by: -

$$\frac{\partial T}{\partial t} = \alpha \frac{\partial^2 T}{\partial x^2}$$

Let us apply the Taylor's expansion theorem to the above equation writing DT/Dt in forward difference form and D^2T/Dx^2 in central difference terms. The transformed algebraic equation is given by: -

$$\frac{T_i^{n+1} - T_i^n}{\Delta t} = \frac{\alpha(T_{i+1}^n - 2T_i^n + T_{i-1}^n)}{(\Delta x)^2}$$

We know that parabolic equations have time marching solutions. Thus the above equation infers that temperature T at all grid points are known at time step n and the temperature at time step $n+1$ is desired. Thus writing above equation taking known and unknown variables at different sides, we can write: -

$$T_i^{n+1} = T_i^n + \alpha \frac{\Delta t}{(\Delta x)^2} (T_{i+1}^n - 2T_i^n + T_{i-1}^n)$$

When the values at $n+1$ is known then the value are calculated at $n+2$ thus the solution marches through time. The above scheme is called explicit scheme because it contains only one unknown and thus can be explicitly solved. The grid representing such scheme is shown below. The points 1 and 7 represents boundaries thus the values at these points are known at each time step

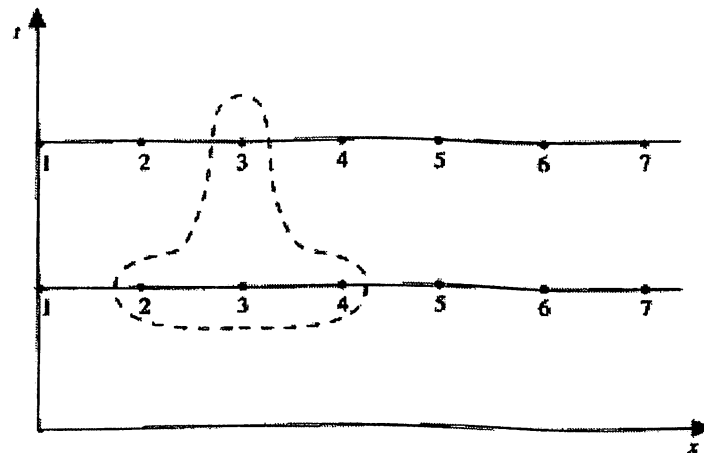


Figure 35: explicit approach^[3]

3.7.4 Implicit Approach: -

In this type of approach, more than one unknown value needs to be calculated. In our previous example of one dimensional heat flow, the term D^2T/Dx^2 is also written at time step $n+1$. The equation thus results can be written as: -

$$\frac{\alpha \Delta t}{2(\Delta x)^2} T_{i-1}^{n+1} - \left[1 + \frac{\alpha \Delta t}{(\Delta x)^2} \right] T_i^{n+1} + \frac{\alpha \Delta t}{2(\Delta x)^2} T_{i+1}^{n+1} = -T_i^n - \frac{\alpha \Delta t}{2(\Delta x)^2} (T_{i+1}^n - 2T_i^n + T_{i-1}^n)$$

The above equation has three unknowns which can be solved simultaneously and thus called implicit schemes. The seven point grid governing this equation is shown below: -

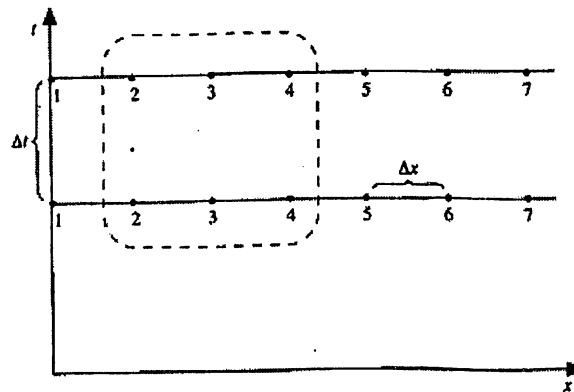


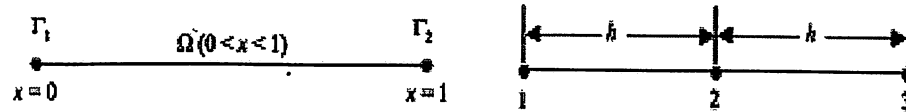
Figure 36: implicit approach^[3]

3.7.5 Comparison of explicit and implicit schemes: -

- The explicit schemes are relatively simple and easy to program but there exists the problem of stability. The time step in explicit schemes should be kept as small as possible to get a stable solution. A term known as Courant number(C) is directly proportional to the time step Δt . Thus if $C \geq 1$, the solution is stable while is unstable at all other values of C. The computation time is increased and so does the cost of computing.
- The main advantage of implicit scheme is that the solution remains stable over a wide range of Courant number. Thus larger time steps can be used to get the results faster. However, the complexity involved in such equations are much more and thus difficult to program. The solution uses matrix method and hence needs much memory for storing the results.

3.7.6 Finite Element Method: -

Abbreviated as FEM, finite element method is used basically for structural analysis. Finite element form of discretization is a complex one thus the explanation of the same is given for one dimensional case only. Consider a one dimensional domain which is subdivided into two subdomains given by e_1 and e_2 . The end point of each element is called node.



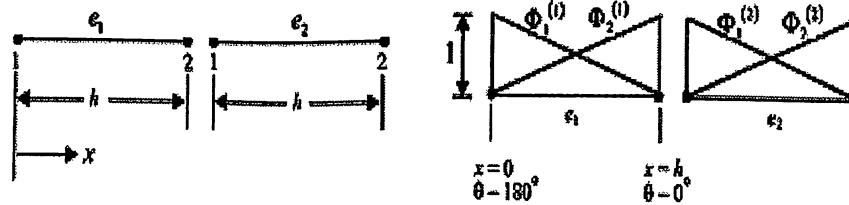
Let us assume a variable $u^{(e)}(x)$ which is linear in terms of x . Thus the variable can be written as: -

$$u^{(e)}(x) = \alpha_1 + \alpha_2 x$$

From the above equation we can write two equations for each node given by $x=0$ and $x=h$. The values at nodes are depicted by $u_1^{(e)}$ and $u_2^{(e)}$. Solving for α_1 and α_2 the final value of variable $u^{(e)}(x)$ is calculated as: -

$$u^{(e)}(x) = \left(1 - \frac{x}{h}\right)u_1^{(e)} + \left(\frac{x}{h}\right)u_2^{(e)} = \Phi_N^{(e)}(x)u_N^{(e)} \quad (N = 1, 2)$$

Where $U_N^{(e)}$ represents the value at node N for element e and $\Phi_N^{(e)}(x)$ represents the values of variable at nodes. These values are called shape functions and attain the value of one at a node under consideration and zero at the other node linearly varying in between.



$$\Phi_1^{(e)}(x) = 1 - \frac{x}{h}, \quad \Phi_2^{(e)}(x) = \frac{x}{h}$$

$$0 \leq \Phi_N^{(e)}(x) \leq 1$$

These one dimensional problems can be solved by Galerkin's Method.

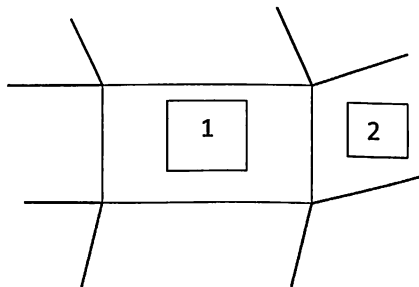
$$(\Phi_N^{(e)}(x), R^{(e)}) = \int_0^h \Phi_N^{(e)}(x) \left(\frac{d^2 u^{(e)}(x)}{dx^2} - 2 \right) dx = 0$$

3.7.7 Finite Volume Method: -

In this method, a cell to cell solution is provided to approximate the partial differential terms. The FVM deals with integral form of governing equations rather than their differential form. One of the methods of discretizing using FVM is Gauss divergence theorem which states that, "The surface integral of normal component of vector function F taken around a closed surface S is equal to the integral of divergence of F taken over the volume V enclosed by surface S ." Mathematically it can be written as: -

$$\iint \cdot F \cdot n ds = \iiint \text{div } F dv$$

Consider a cell as shown below: -



3.8 Grid Dependence Study^[5]

The flow characteristics while doing a CFD analysis is largely dependent on the Grid generated. As the number of nodes and cells change, the flow properties and thus the results tends to change. The CFD is based on numerical method. The governing equations of continuity, momentum, energy etc. are in the form of differential equation of different order. The following are the governing equations in the differential conservative form: -

Continuity Equation: -

$$\frac{\partial \rho}{\partial t} + \nabla \cdot (\rho \mathbf{V}) = 0$$

X-Momentum equation: -

$$\frac{\partial(\rho u)}{\partial t} + \nabla \cdot (\rho u \mathbf{V}) = -\frac{\partial p}{\partial x} + \frac{\partial \tau_{xx}}{\partial x} + \frac{\partial \tau_{yx}}{\partial y} + \frac{\partial \tau_{zx}}{\partial z} + \rho f_x$$

Y-Momentum equation: -

$$\frac{\partial(\rho v)}{\partial t} + \nabla \cdot (\rho v \mathbf{V}) = -\frac{\partial p}{\partial y} + \frac{\partial \tau_{xy}}{\partial x} + \frac{\partial \tau_{yy}}{\partial y} + \frac{\partial \tau_{zy}}{\partial z} + \rho f_y$$

Z-Momentum equation: -

$$\frac{\partial(\rho w)}{\partial t} + \nabla \cdot (\rho w \mathbf{V}) = -\frac{\partial p}{\partial z} + \frac{\partial \tau_{xz}}{\partial x} + \frac{\partial \tau_{yz}}{\partial y} + \frac{\partial \tau_{zz}}{\partial z} + \rho f_z$$

Where: -

$$\nabla \equiv \mathbf{i} \frac{\partial}{\partial x} + \mathbf{j} \frac{\partial}{\partial y} + \mathbf{k} \frac{\partial}{\partial z}$$

The differential terms in the above equations can be approximated using Taylor's expansion theorem. The differential terms using the above mentioned can be written in second order accuracy as: -

$$\left(\frac{\partial u}{\partial x} \right)_{i,j} = \frac{u_{i+1,j} - u_{i-1,j}}{2\Delta x} + O(\Delta x)^2$$

Where Δx is the cell width or distance between the nodes. As the number of nodes changes, the value of Δx changes and thus the governing equations gets altered. The above method is called the discretization. Thus to get values which are independent of the grids a grid dependence study is performed so that appropriate number of cells can be chosen and the results can be obtained with minimum error.

3.9 Morphing Concept^[6]

The high lift systems available at present can be used to achieve the desired increment in the value of cl during landing and take-off but has low efficiency. Apart from providing circulation and thus delayed separation point, the gaps and overlaps present in the high lift systems also produces drag. A fully deflected flap configuration act as a thick aerofoil and produces a considerable amount of pressure drag.

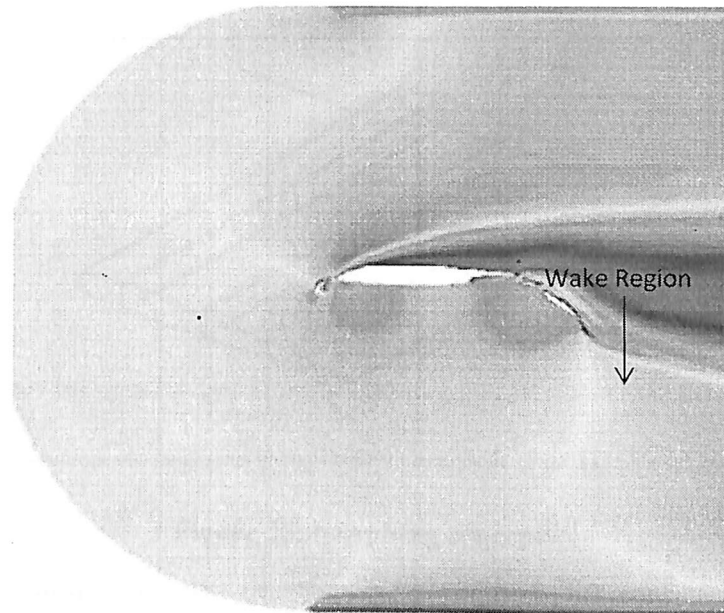


Figure 37: wake region

Thus to increase the efficiency of such high lift systems, the aerodynamicists are working on the concept of morphing. A morphing structure can be defined as one which is capable of altering its geometric configuration and tune its properties (stiffness and damping) based on the mission requirement and the loading during flight. The definition of morphing in context of 'NASA's Morphing Project' is, "*Efficient multipoint adaptability that may include micro, macro, structural and fluidic approaches.*" Generally it can be described a method in which a structure can change its interaction with the environment by modifying its shape and geometry.

Though the morphing concept can be applied to any structure of an aircraft, the main focus is on the wing. The wing is the main structure of an aircraft which is designed to bear main loads during flight. The main idea behind morphing is using SMA (shape memory alloys) to design such structure which is not only capable of withstanding prescribed loads but also capable of changing its shape to withstand the different ones. Shape memory alloys are an alloy of titanium which when heated gets soft and deflects while on cooling regains its original shape with maximum efficiency. The combination of different mechanisms of actuators, motors and links are used for this purpose.

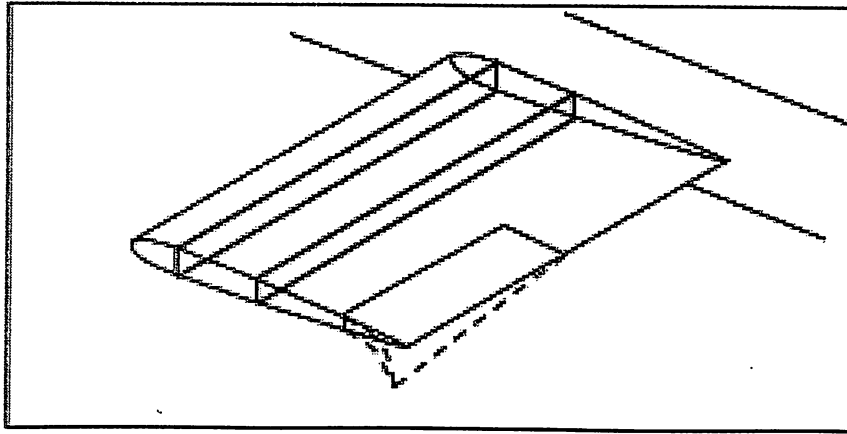


Figure 38: morphing concept^[11]

The morphing concept can also be incorporated in high lift configuration. The above mentioned difficulty with the high lift devices can be overcome if same camber can be achieved without gaps and flaps. The structure can be deployed at particular angle to give the desired lift without producing the drag. The structure need to be deployed at minimum thus the effective thickness of the total structure is less than that of fully deployed flaps.

CHAPTER 4

NUMERICAL ANALYSIS

The use of numerical approximation in the study of algorithms is known as numerical analysis. It aims at giving approximate, but accurate solutions to arduous problems. A systematic order is used to conduct the numerical analysis and it is as follows-

- Geometry creation
- Mesh generation
- Boundary conditions

Geometry creation includes, processing of points, formatting, representing the geometry in forms of points, lines and surfaces to give the geometry a physical definition.

Grid generation is one of the most important and repetitive process before the flow can be numerically analysed over an object. There are two techniques of mesh generation namely, structured and unstructured. The accuracy and quality of the result depends on the quality of the mesh.

Boundary condition defines the flow parameters for a particular geometry. It includes the selection of different models along with the number of iterations. All the geometries are solved for different angle of attacks.

4.1. Geometry Creation^[4]

The geometry of all the three namely, basic airfoil, three element airfoil and five element airfoil was made available. The geometry used for the analysis is BAC 3-11/RES/30/21 airfoil whose thickness and nose radius is 11% and r/c of 0.0137 respectively. The above mentioned airfoil is used in three conditions-

- BAC 3-11/RES/30/21 with no elements
- BAC 3-11/RES/30/21 with two elements – slats deployed at 25° (thickness at 12.5%) and a single slotted flap deployed at 20%
- BAC 3-11/RES/30/21 with four elements – slats deployed at 25% and triple slotted flap deployed at 7.5°, 40°, 20°

The figures below show the geometry of all the three airfoils created in ICEM CFD.

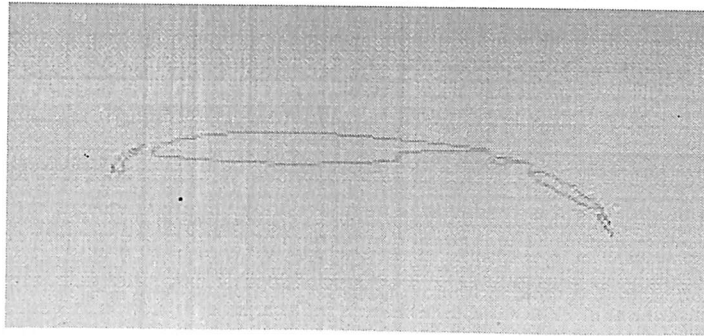


Figure 39: five element airfoil

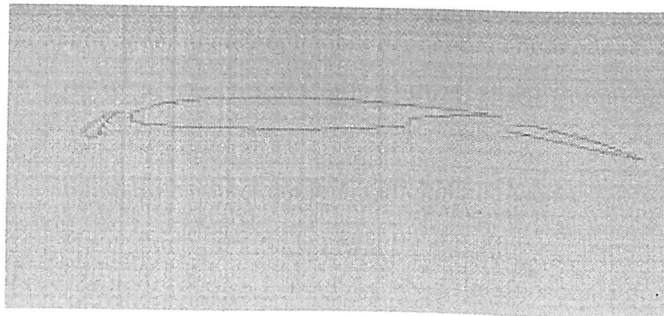


Figure 40: three element airfoil

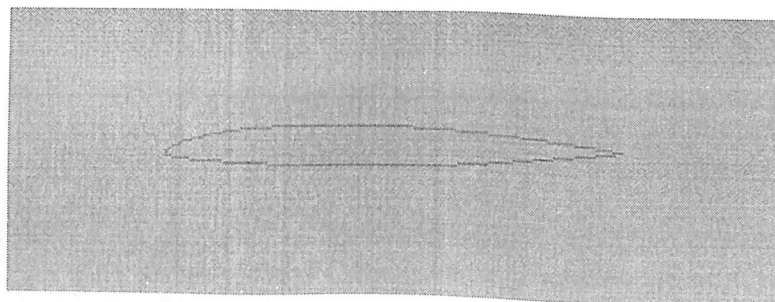


Figure 41: basic airfoil

Parameters	Basic aerofoil	Three-element aerofoil	Five-element aerofoil
Wing section	BAC 11/RES/30/21 3-	BAC 11/RES/30/21 3-	BAC 11/RES/30/21 3-
Overall length (m)	0.669	0.9201	0.956259
Slats	No	Yes, deployed at 25°	Yes, deployed at 25°
Flaps	No	1 slot, deployed at 20°	3 slots, deployed at 7.5°, 40°, 20°

Table 1: various geometries

4.2. Grid generation^[4]

To generate a grid enclosing the geometry, a boundary was created. The flow problems were analysed around the geometry and the enclosed boundary behaved as the test section. All the three geometries, boundaries were constructed and meshed. The figure below depicts the boundary constructed for a geometry section.

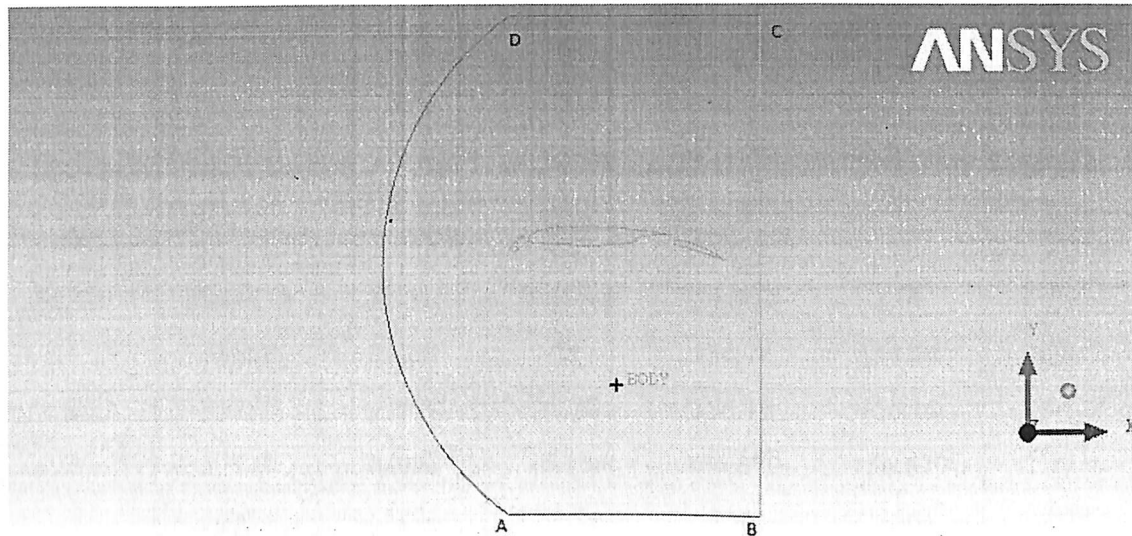


Figure 42: boundary depiction

In the figure above, AD represents the test section inlet, AB is the bottom, BC is the test section outlet and CD is the top. The similar boundary is constructed for the basic and five element airfoil.

Two types of mesh were generated using the test section, structured and unstructured mesh. Accuracy was the main parameter kept in focus while generating the two grids. The value of lift in CFD analysis is affected by many factors, one such factor is the type of grid. To minimize the error due to grids a complete grid independence study is done.

After running the analyses on progressively finer grids to attain the value of lift at some angle of attack the grid is fine enough and the solution will not change (or change less than a tolerance) so that the solution is 'grid independent'.

In this report all the three geometries were solved for 0° AoA and 67m/s free stream velocity and the results are tabulated below

SI No.	Elements	Nodes	X Force	Y Force	Lift	C_L
1	8087	5156	6.17	-1.615	-1.615	0.01698
2	10700	6884	5.8313	-1.712	-1.712	0.01799
3	12992	8396	5.7799	-1.8184	-1.8184	0.01917
4	14627	9476	5.759	-1.816	-1.816	0.01909
5	16916	10988	5.81	-1.878	-1.878	0.01974

Table 2: basic airfoil grid independence study

From the above table it is concluded that on increasing the grid elements lift also increases. But after a limit of 13000 elements it reduces and increases again with a fine change. Therefore 12992 elements were selected for basic airfoil analysis.

SI No.	Elements	Nodes	X Force	Y Force	Lift	C_L
1	33568	21724	25	154.74	154.74	2.0342
2	35350	22908	25.08	156.19	156.19	2.0532
3	37132	24092	25.186	156.579	156.579	2.0736
4	38914	25276	25.21	156	156	2.0507
5	42478	27644	25.399	154.94	154.94	2.0367

Table 3: three element airfoil grid independence study

SI No.	Elements	Nodes	X Force	Y Force	Lift	C_L
1	29945	19336	78.29	509.51	509.51	3.3574
2	32330	20920	78.55	510.34	510.34	3.3647
3	36305	23560	78.78	514.47	514.47	3.3929
4	37100	24088	79.31	509.103	509.103	3.3556
5	39485	25672	79.29	508.612	508.612	3.3533

Table 4: five element airfoil grid independence study

Applying the same approach for three and five element aerofoils it was concluded that set number three will be used for both cases.

The values selected after conducting the grid independence study were used for analysing the flow through all angle of attack for all the cases. This will help keep the errors minimum and will give better accuracy on the lift value. Grids were created using the same values.

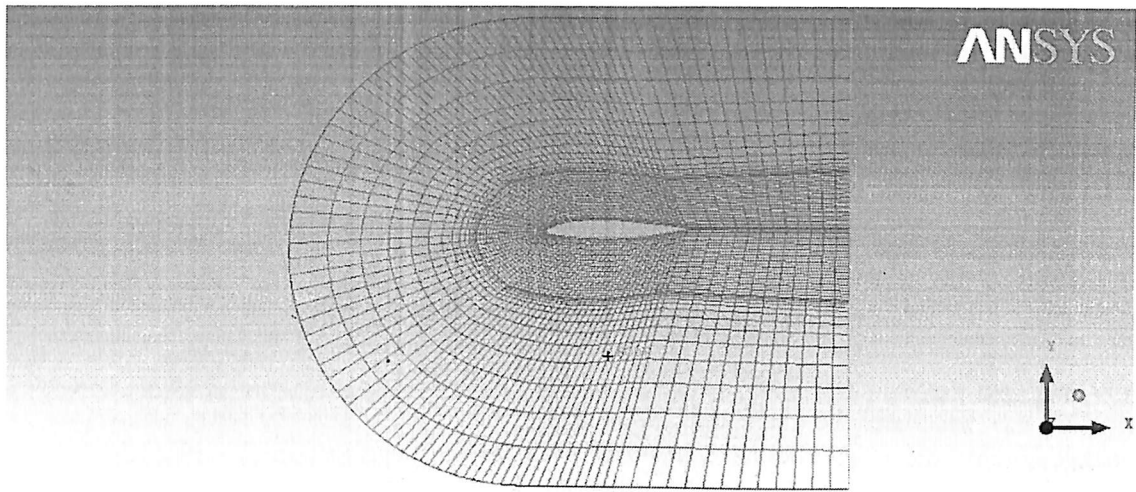


Figure 43: structured mesh - basic airfoil

The above picture shows a structured mesh of a basic aerofoil with no elements. A C type grid method was used to mesh the aerofoil. This method is mainly used for analysing an airfoil as it increases the accuracy in computing fluid parameters especially at the leading edge. From the above shown geometry it is vivid that the mesh gets finer near the geometry, this is done to save the computing time.

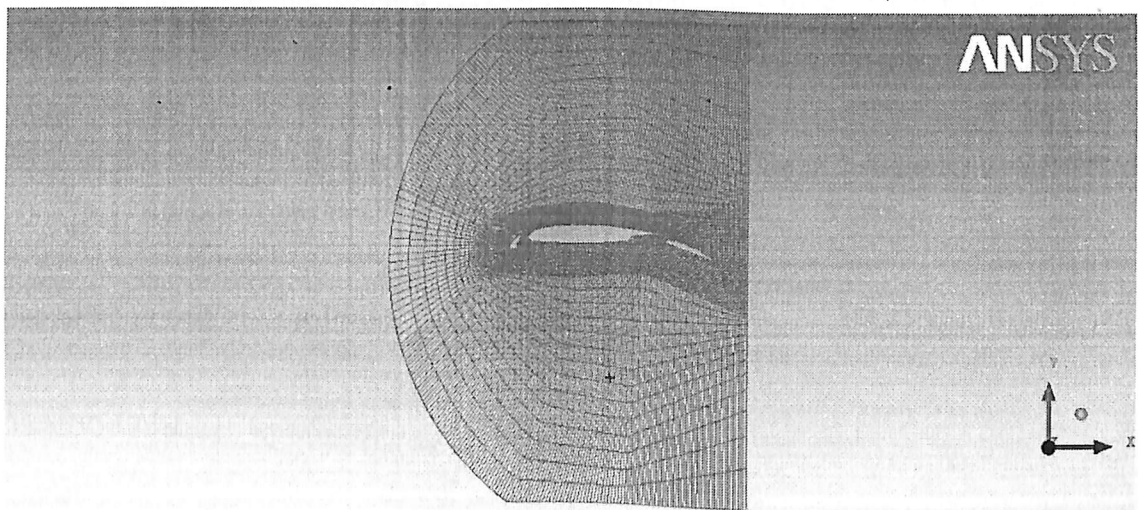


Figure 44: structured mesh - three element airfoil

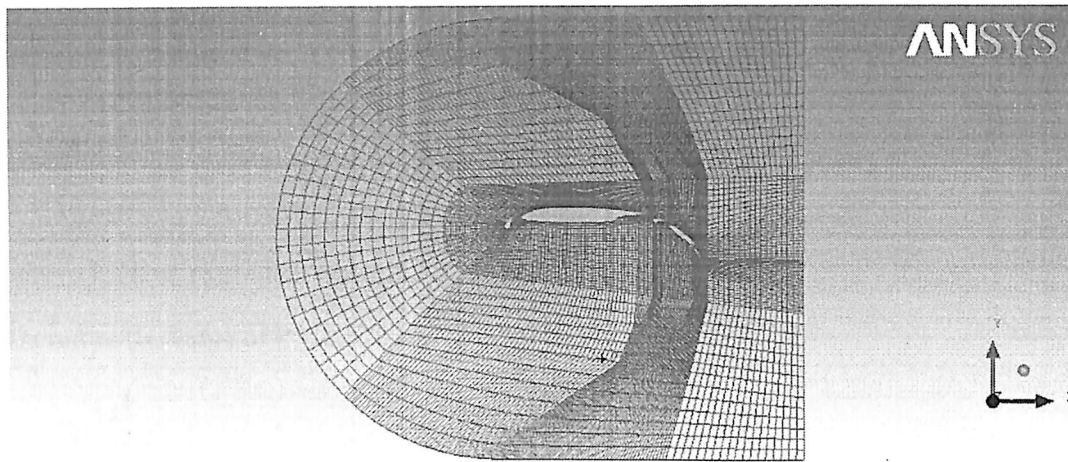


Figure 45: structured mesh - five element airfoil

The above two pictures show the mesh generated for three and five element airfoil respectively. A multi blocking technique was used to block the multi element airfoil where the test section is cut into various small blocks and meshed. Similar C type grid method is used to increase the accuracy of the results.

4.3. Boundary conditions^[4]

Boundary conditions are defined as the conditions given to control volume to excel the effects of flow near the geometry. FLUENT software was used to solve the boundary conditions and the results were obtained along with the flow data.

The boundary conditions given to the control volume were common to all the three geometries and are as shown in the table below:

Boundary parameters	Value
Basic Navier-Stokes equation in combination with viscous forces	To the control volume
Standard k-ε turbulence model	For eddies and turbulence viscosity
Velocity (m/s)	67 at the inlet
Outlet	Outlet vent
Airfoil	Wall- no slip condition
Bottom and top	Wall
Side walls	Symmetry

Table 5: boundary conditions

The parameters mentioned in the above table are common to all the three configurations. The velocity is resolved in its appropriate components as the AoA is changed. The values obtained are then given to the software and hence solved.

The following equations are used to find the turbulent kinetic energy and dissipation –

$$k = \left(\frac{3}{2}\right) (Iu)^2$$

where $I = 0.01$ (turbulent intensity) and $u = 67$ m/s

Therefore the value of $k = 0.67\text{m}^2/\text{s}^2$

$$\varepsilon = C\mu^{\frac{3}{4}} \frac{k^{\frac{3}{2}}}{l_t}$$

Where $C\mu = 0.09$ and $l_t = 0.07L$, where L is the characteristic length of the geometry.

Therefore values of epsilon(ε) are –

Geometry	ε value
Basic airfoil with no elements	1.92
Three element aerofoil	1.3989
Five element aerofoil	1.34

Table 6: epsilon values of various configurations

The inlet of the geometry is given velocity inlet and the geometry under the test is given the condition wall with no slip, this is done to clearly understand the boundary layer effect on every element and its influence on the elements near it. The outlet is represented as outlet vent where the flow saturates to the atmosphere. The flow is pressure based, where the input & output difference is considered in the test section. The bottom and top are taken as wall of the test section.

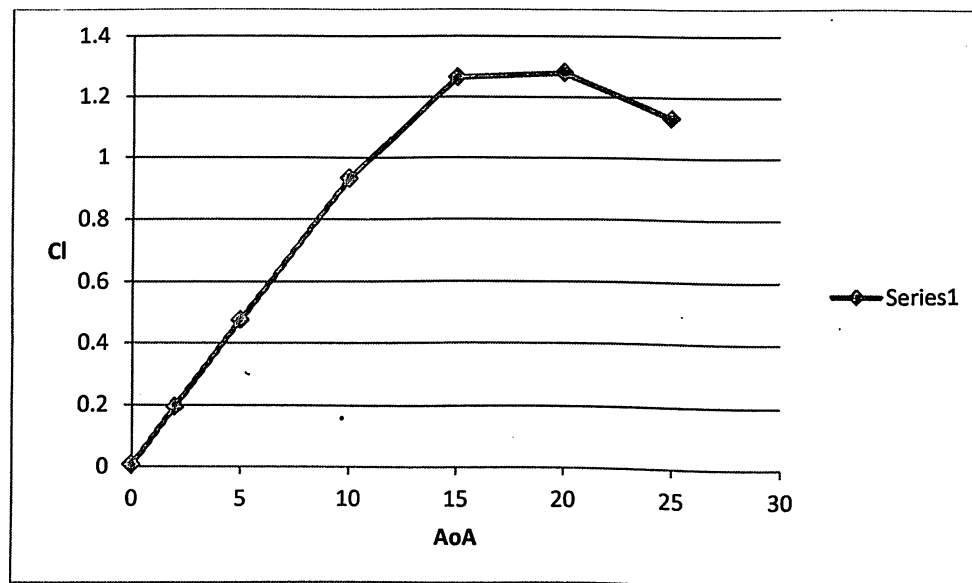
The side walls are taken as symmetry to get a 2D flow effect. This was done cause the actual 2-D model was prone to errors. The inlet, symmetry and outlet had problems being exported in ICEM CFD. To counter this effect an small area was given in z direction and a symmetric condition was given to both side walls.

CHAPTER 5

Results and Discussions

5.1.Configuration 1: Basic airfoil:

The basic airfoil was analysed using FLUENT by giving the boundary conditions and the following graph was obtained between coefficient of lift (C_l) and AoA.



Graph 1: Cl vs AoA- basic airfoil

From the figure above it is concluded that the airfoil stalls at an angle of 20° , where the airfoil experiences stall with a maximum C_l of 1.28.

The Fluent software was used to obtain the lift curve by using force data. The X & Y coordinates of force data for all angle of attack was calculated. Lift was calculated by the following equation -

$$L = Y \cos \alpha - X \sin \alpha$$

Further coefficient of lift was calculated using the above equation as shown-

$$Cl = \frac{2L}{\rho v^2 S}$$

The streamline flow around the airfoil at 0°, 5°, 10°, 15° & 20° AoA are depicted below:

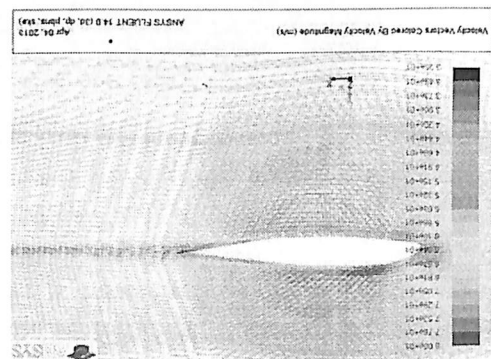
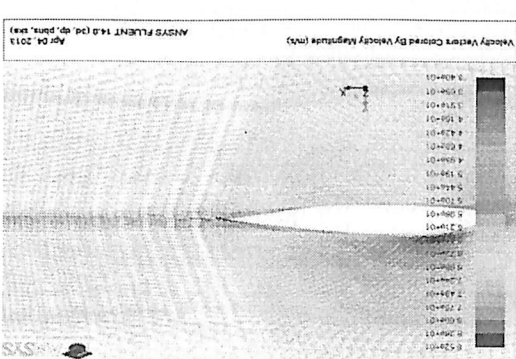


Figure 46: velocity vector at 0 & 5 deg AoA respectively

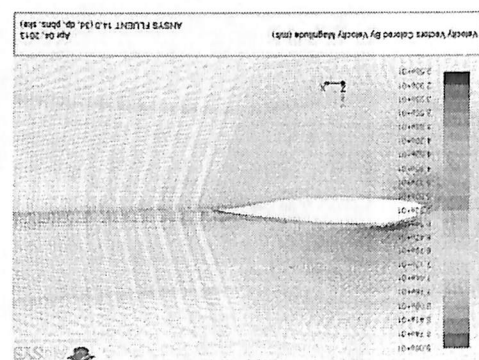
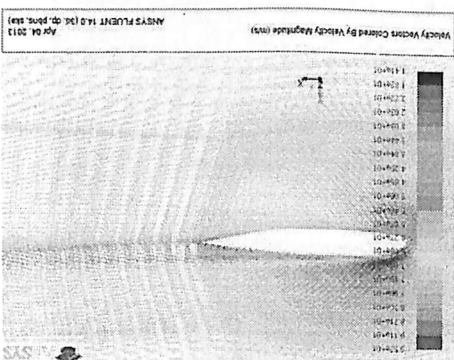


Figure 47: velocity vector at 10 & 15 deg AoA respectively

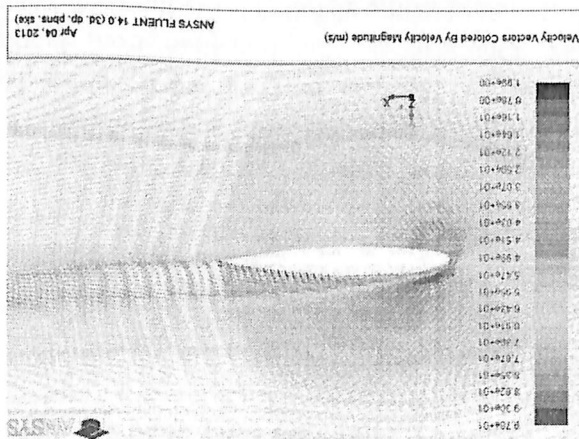


Figure 48: velocity vector at 20 deg AoA

The figures above show the gradual transition of steady and smooth flow to separation of flow. At 0 & 5 deg AoA the flow satisfies the Kutta condition and leaves the trailing edge relatively smoothly. This is because the flow above and below the airfoil is smooth.

As the angle of attack increases the streamlines start curling near the leading edge as seen from the image of velocity vector at 10 deg. At this AoA, the flow starts to separate at the trailing edge and moves upstream as shown in the figure:26 at 20 deg AoA, the flow stalls at the T.E. The separation of flow can be resolved by using high lift devices such as slats and flaps. The presence of high lift devices tend to energize the flow due to the effect of circulation and hence prevent the flow separation.

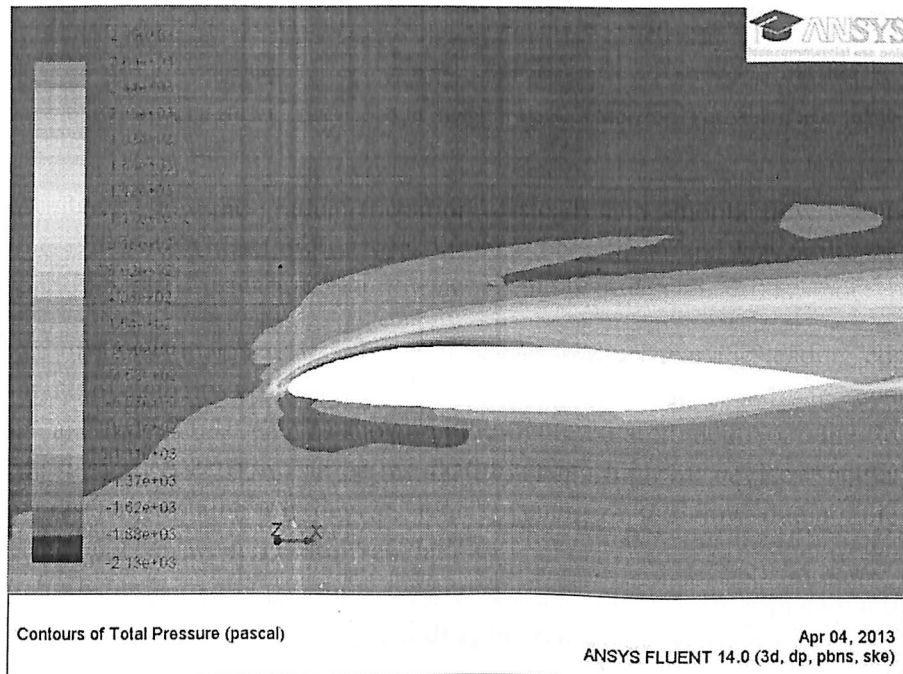


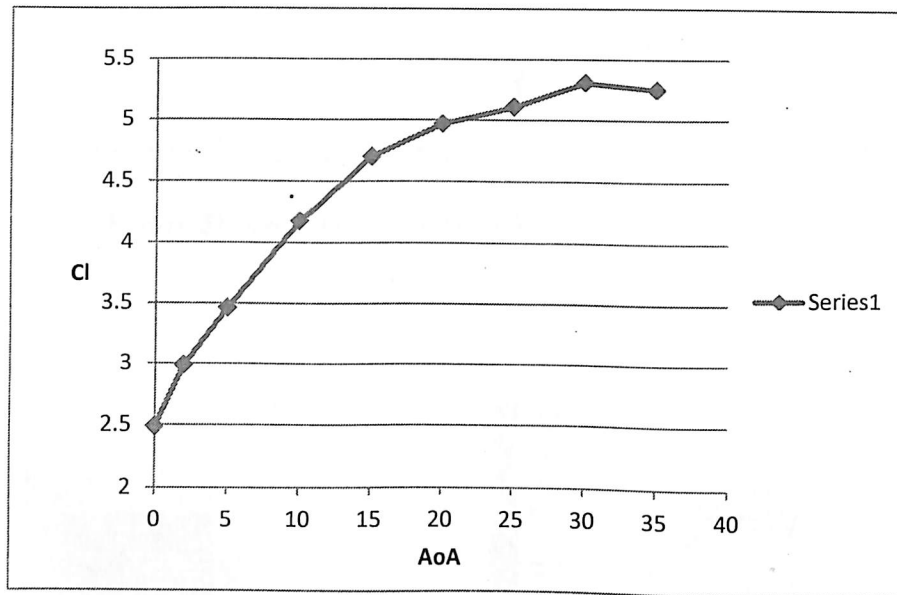
Figure 49: boundary layer at 20 deg AoA

From the velocity vector it is clear that as the angle of attack increases the boundary layer also increases gradually in thickness. After a certain AoA where the value of C_l is maximum, stall occurs and the BL from the upper surface is washed off.

The BL thickness in fig 44 shows that the boundary layer starts at leading edge, moving downstream the BL is washed off and joins with the free stream. The region forms the wake and considers viscous effects, this can be observed by either reducing the pressure or increasing the velocity. One can see the transition from laminar to turbulent BL at approximately the quarter chord of the airfoil. This is the point where the thickness starts to increase.

5.2.Configuration 2: three element airfoil:

The same conditions as the basic airfoil were fed to the software for the 3 element airfoil. The resulting coefficient of lift vs angle of attack is shown below.



Graph 2: Cl Vs AoA curve for three element airfoil

The maximum coefficient of lift for 3 element airfoil is 5.306 at 30 deg AoA. In comparison to the basic airfoil where the maximum Cl was 1.28 at 20 deg AoA, by application of high lift devices the maximum coefficient of lift as well as the stall angle is increased.

The images of streamline flow at 5, 10, 15, 20, 25 & 30 deg AoA are shown below-

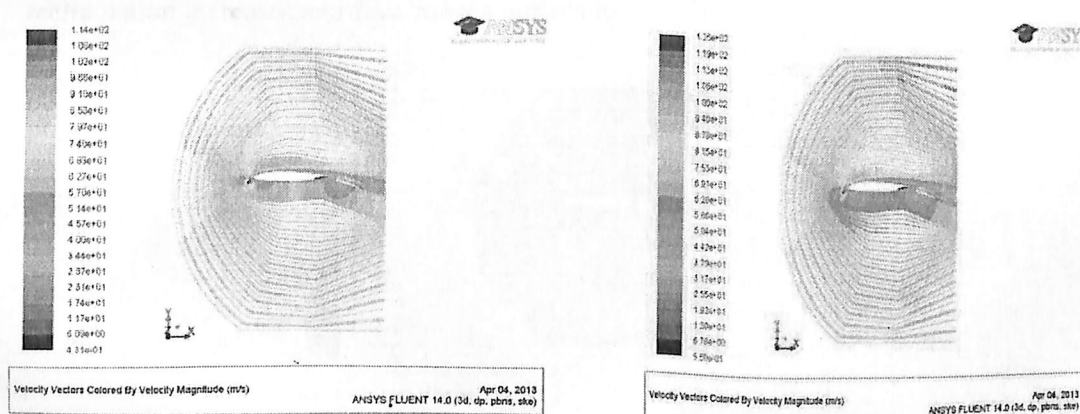


Figure 50: velocity vector at 5 & 10 deg AoA respectively

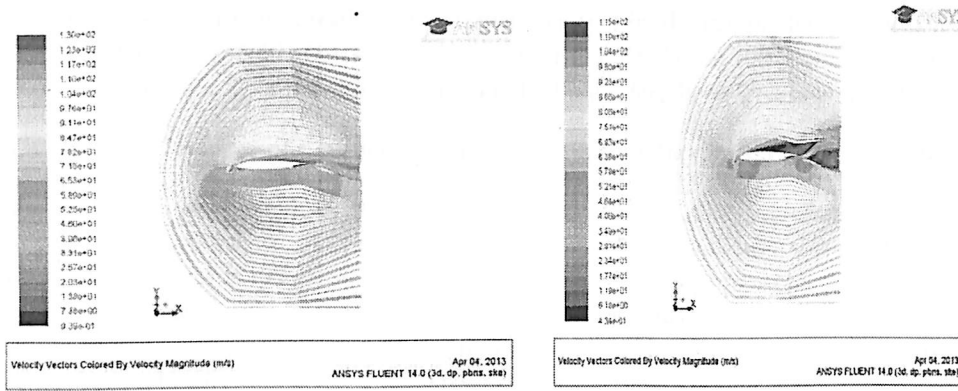


Figure 51: velocity vector at 15 & 20 deg AoA respectively

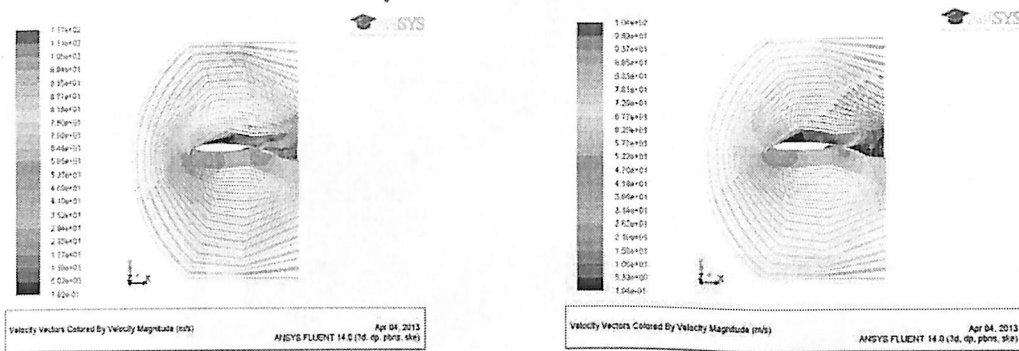


Figure 52: velocity vector at 25 & 30 deg AoA respectively

As the angle of attack increases, the flow separation begins at the trailing edge. The flow starts separating at 20 deg AoA at the trailing edge. As the AoA further increases the flow recirculation increases and flow moves upstream.

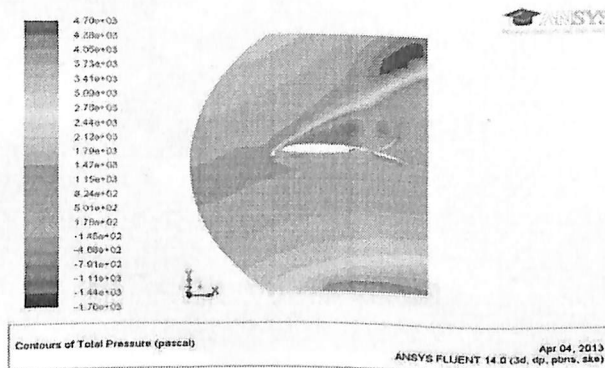


Figure 53: boundary layer at 30 deg AoA

The boundary layer is re-energized by the circulation effect by the use of slats throughout the airfoil at the upper surface. Figure-49 shows the conversion of laminar BL to turbulent and eventually washes off at the leading edge. This transition is countered by boundary layer as shown in figure-49.

This is due to the presence of slats which reenergizes the boundary layer and prevents flow separation.

As the angle of attack increases the re-circulation of air flow also increases and the flow moves upstream. Figure 46 below shows increasing strength of recirculation that will eventually move upstream and stall. As the angle of attack reaches 30 deg a counter recirculation takes place, due the flaps circulatory effect which is at the trailing edge of the airfoil. The velocity of recirculation is alleviated by the counter circulation of the flaps and hence the flow cannot be attached back to the airfoil surface and stalls.

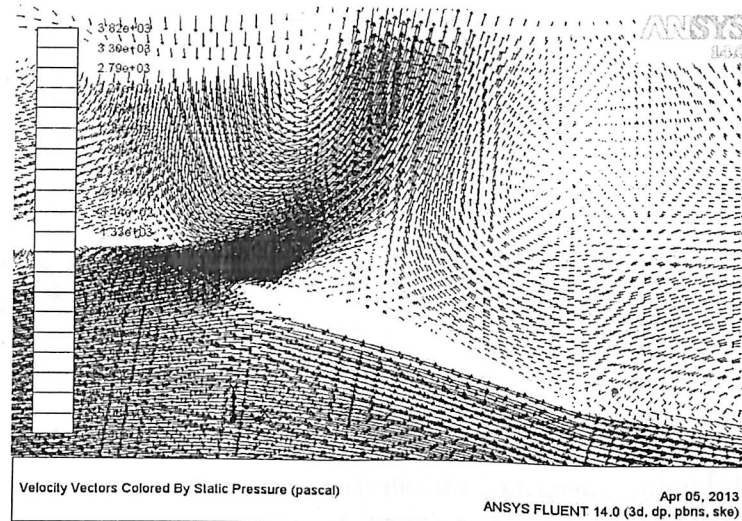


Figure 54: recirculation at 25 deg

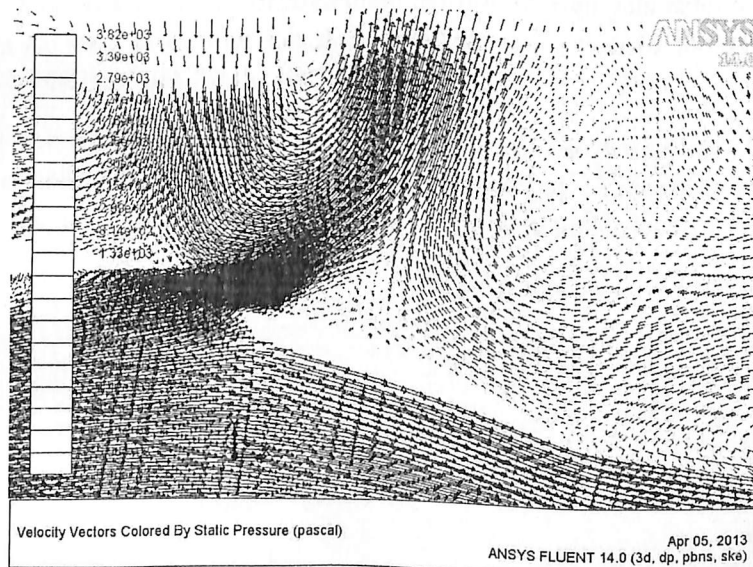
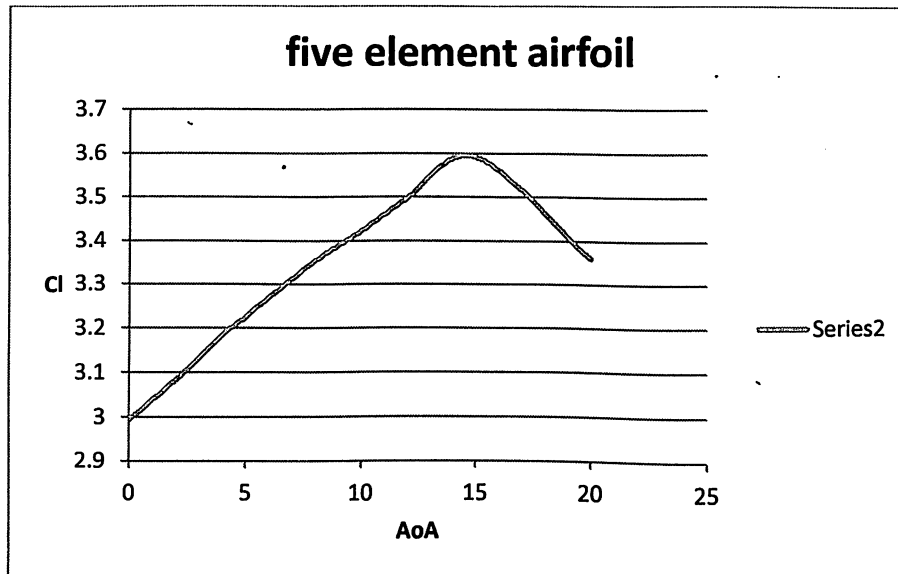


Figure 55: counter circulation at 30 deg

5.3. Configuration 3: Five element Aerofoil^[12]

The boundary conditions for the 5-element aerofoil were assigned same as that of other two configurations. The results and data for the Cl were calculated for 13 different angle of attacks taking both positive as well as negative values. The results show that the 5 element aerofoil gets stalled at 15 degrees giving the maximum lift coefficient of 3.59. The graph of lift coefficient vs. angle of attack is shown below.



Graph 3: Cl vs AoA for five element airfoil

The gradual change in lift coefficient suggests that the 5 element aerofoil behaves as the thick aerofoil. Moreover the value of maximum lift coefficient for 5-element is less than that of 3-element. This is due to the presence of large wake behind the 5-element aerofoil which adds up in the total drag. The elements of 5-element aerofoil though gets extended to increase the plan-form area as well as camber but the downward deflection of the same increases the thickness which compensates for the increase in lift.

Looking at the velocity contours and the total pressure contour we can say that the boundary layer gets separated near the leading edge of the aerofoil at 15 degrees angle of attack and thus it can be concluded that the aerofoil stall is categorized under leading edge stall.

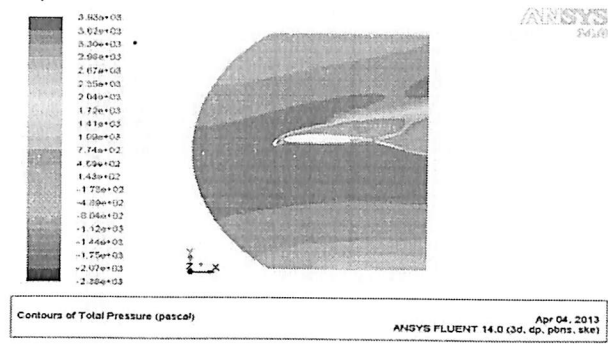


Figure 56: boundary layer at 15 deg AoA

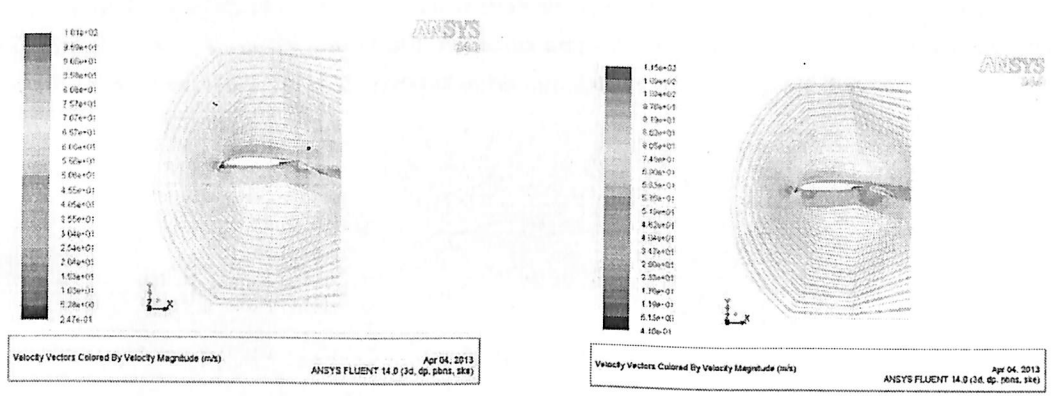


Figure 57: velocity vector at 0 & 5 deg AoA for five element airfoil

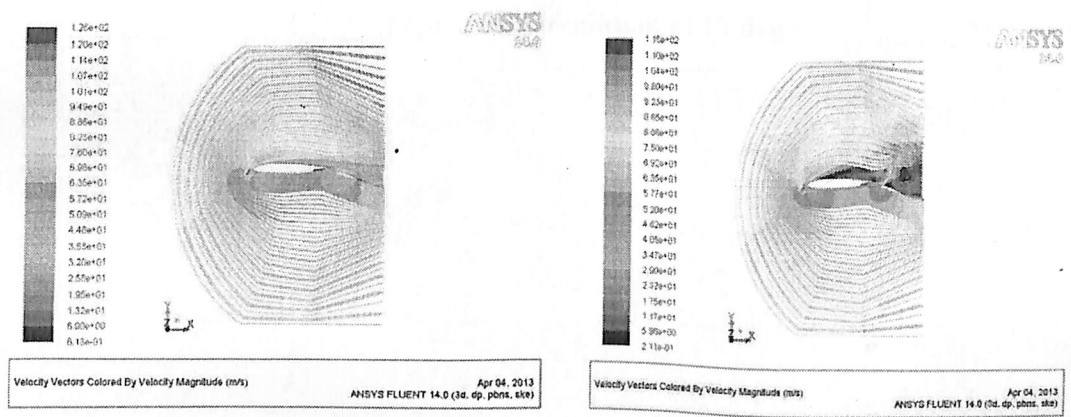


Figure 58: velocity vector at 10 & 15 deg AoA for five element airfoil

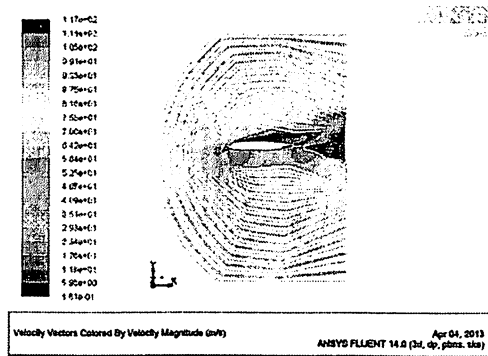


Figure 59: velocity vector at 20 deg AoA for five element airfoil

Stall for five element occurs at 20 deg and is less than the three element airfoil since after extending the flaps and slats for this airfoil the chord increases and hence it behaves like a thick airfoil. The figure below shows circulation at 10 deg and counter circulation at 15 deg were it stalls .

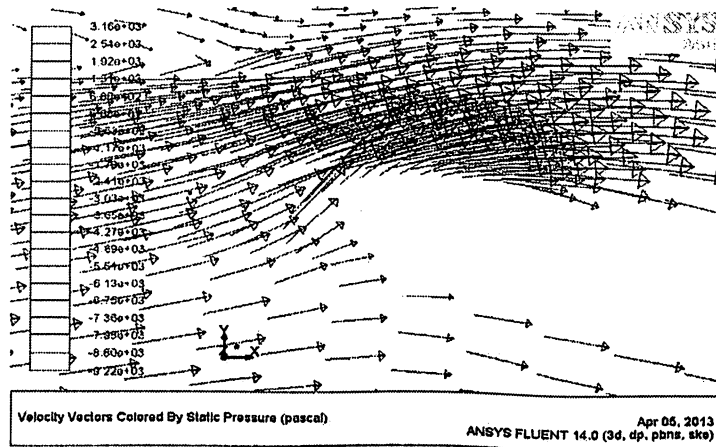


Figure 60: circulation at 10 deg

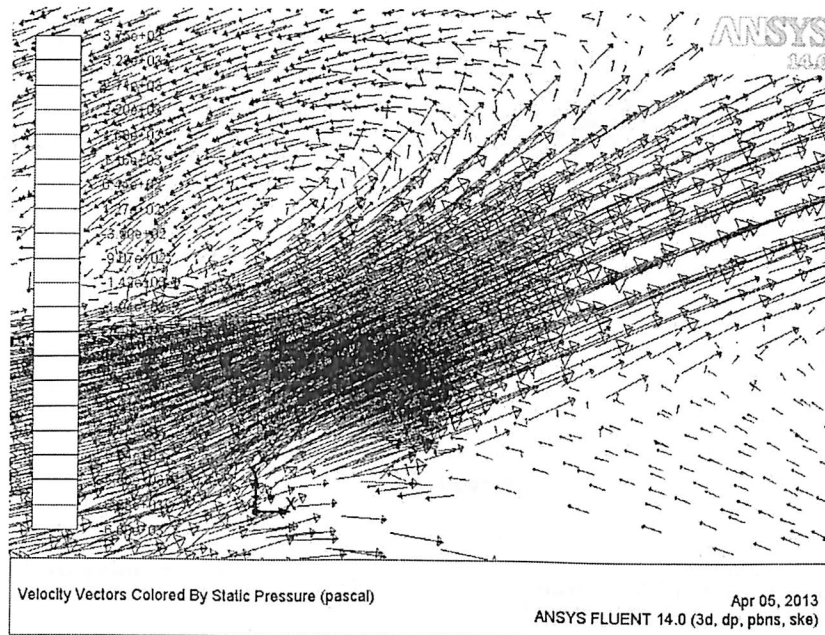


Figure 61: counter circulation at 15 deg

Slats are leading edge devices used to enhance lift of an airfoil. It was believed by many aerodynamicists including Ludwig Prandtl that “slats work by inducing a high energy stream to the flow of the main airfoil thus re-energizing its boundary layer and delaying stall. Practically the velocity at the L.E is abated at the main aerofoil because of the circulation effect produced by the slat thus abating pressure peaks of main airfoil.

The figure below shows the re-energizing of air flow on the upper surface of the aerofoil due to the circulation effect on the slat for a five element airfoil. The flow is re attached to the upper surface of the airfoil as the counter clockwise circulation is fed through a designed slot to the airfoil’s upper surface.

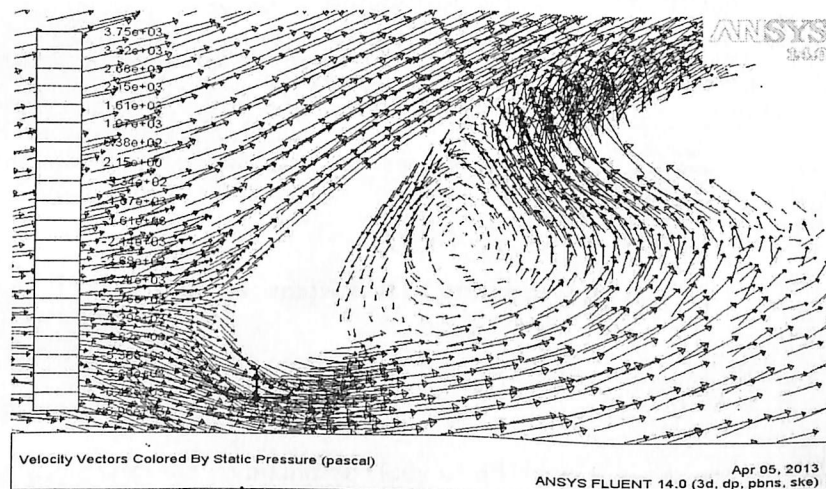
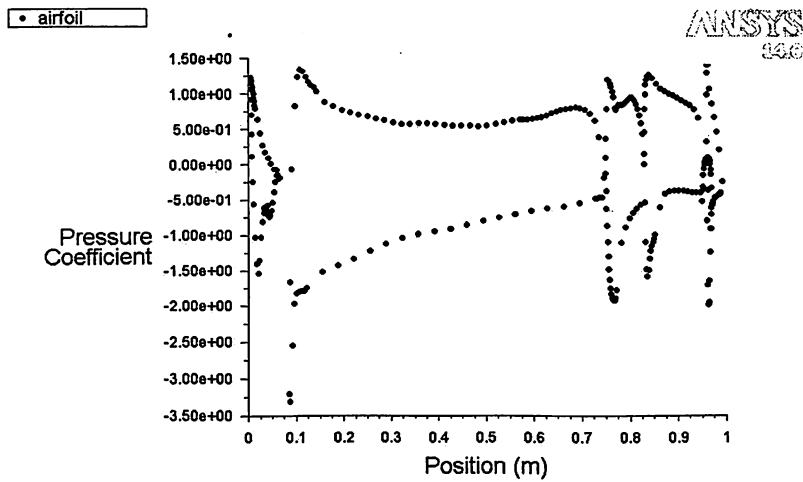
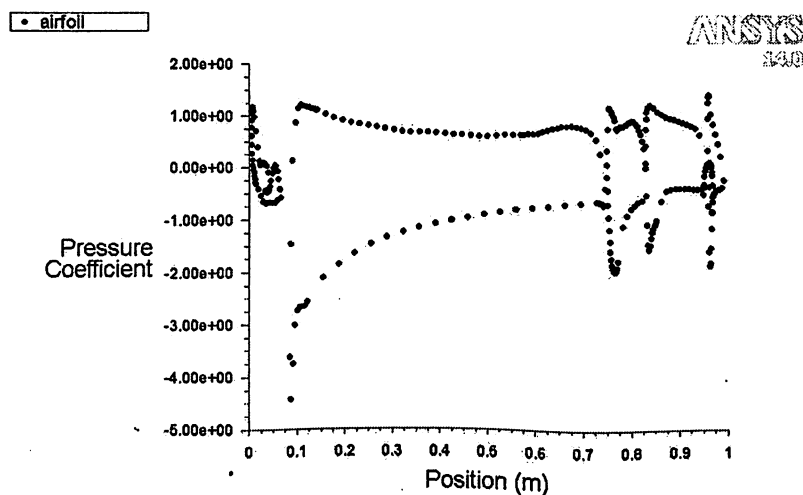


Figure 62: slat effect of 5 element airfoil



Pressure Coefficient
 ANSYS FLUENT 14.0 (3d, dp, pbns, ske) Apr 26, 2013

Figure 63: coefficient of pressure at 0 deg AoA



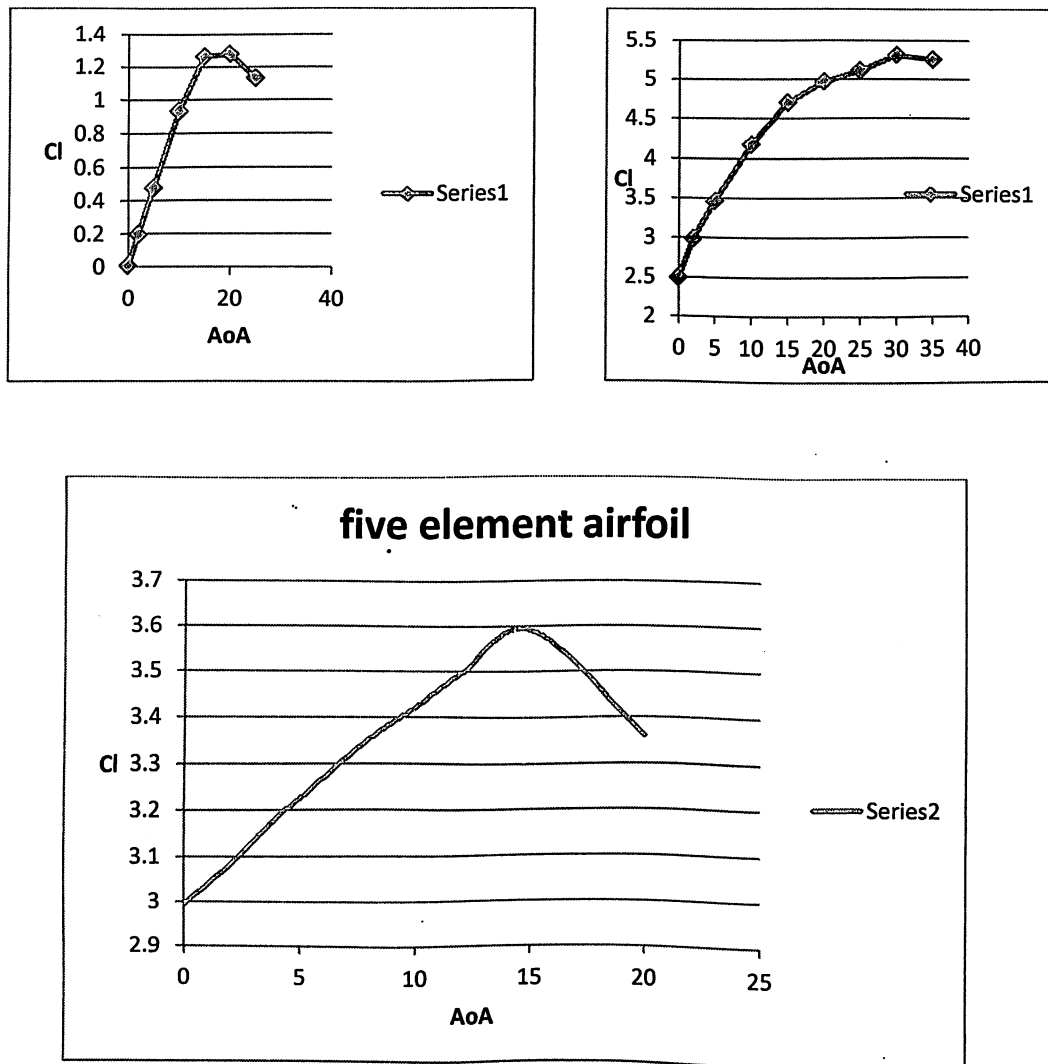
Pressure Coefficient
 ANSYS FLUENT 14.0 (3d, dp, pbns, ske) Apr 26, 2013

Figure 64: coefficient of pressure at 15 deg AoA

5.4. Comparison

This section deals with the comparative study of all the three geometries. The figure below shows the comparison of coefficient of lift of all three configurations. From the fig it becomes vivid that the value of coefficient of lift can be increased by the use of high lift devices.

The three element airfoil gives the highest lift coefficient as compared to the other two geometries whereas the five-element aerofoil gives the highest lift coefficient at any angle of attack. All the three configurations tend to stall at the TE due to the re-circulation of flow. Though the flow separation was alleviated by the use of high lift devices, the recirculation still persisted at higher angle of attack. To abate this effect at higher angles the use of boundary layer control is done.



Graph 4: comparison between various lift coefficient curve

Basic Airfoil :

- maximum coefficient of lift : 1.28
- Stalling angle : 20 deg

Three Element Airfoil :

- maximum coefficient of lift : 5.306
- Stalling angle : 30 deg

Five Element Airfoil :

- maximum coefficient of lift : 3.59
- Stalling angle : 15 deg

CHAPTER 6

FUTURE CONSIDERATION

The analysis of five element aerofoil concludes that though the camber and the plan-form of the aerofoil increases but the increased effective thickness due to downward motion of the deflected flap increase the pressure drag and thus decreases the efficiency of the high lift device. The answer to the above mentioned problem is the use of morphing concept. Two configurations are being produced in this report which can be taken for future work.

6.1. Case 1: 5 element aerofoil at 5 degree angle of attack^[6]

The following figure shows the streamlines over the aerofoil. The streamlines shows that the separation is occurring at the leading edge of the fourth and the fifth element. Thus if the gap between third and fourth element as well as fourth and the fifth element is reduced or covered, than the flow will remain attached for the much longer length of the elements. Thus the separation point will be delayed and the pressure drag can be reduced to considerable level. This is morphing technique which is currently under observation.

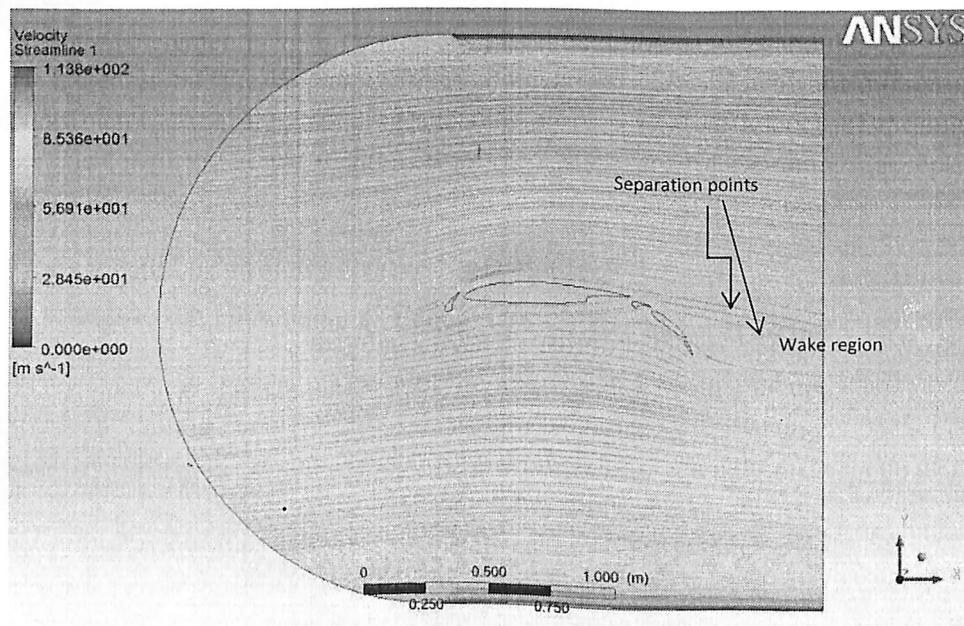


Figure 65: streamline at 5 deg for five element

Another method is to provide vortex generators at the separation points so that circulation can be produced and the separation is delayed.

6.2. Case 2: 5 element aerofoil at 15 degree angle of attack

Since this is the stalling angle, the flow separates from the leading edge of second element. Due to circulation provided by the gap between third and second element, the flow again gets attached but gets de-attached immediately at the leading edge. Same phenomenon occurs at fourth element and thus a large amount of pressure drag is added to the total drag which reduces the efficiency of the aerofoil. To delay separation point, the gap between first and second, second and third, third and fourth can be reduced one by one thus creating the possible combinations of configurations. Another method is to create vortex generators at the separation points, the reason being mentioned above.

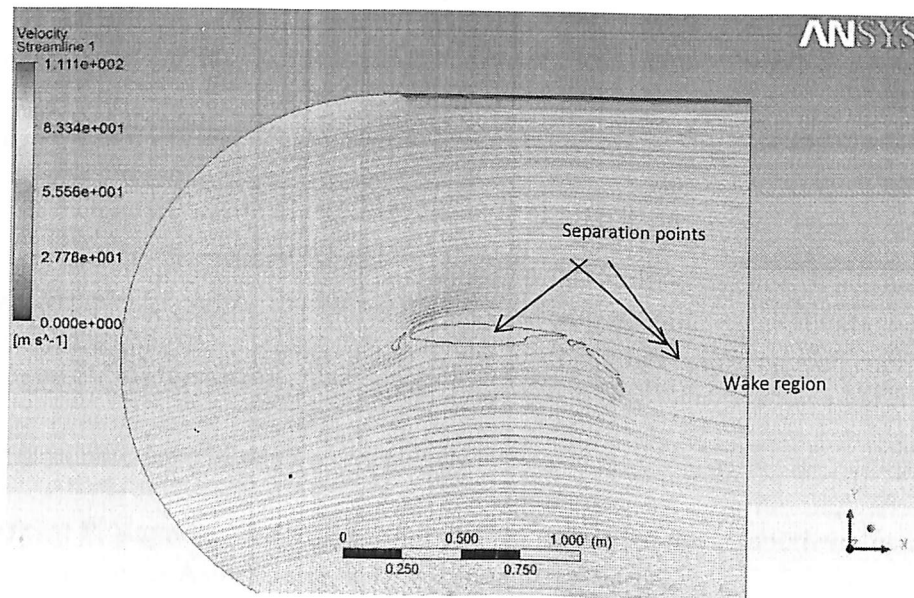


Figure 66: streamline at 15 deg AoA for five element airfoil

REFERENCES

1. **T.J Chung** (2002). *Computational Fluid Dynamics*. United States: Cambridge University press.
2. **L.J Clancy** (2006). *Aerodynamics*. India: Sterling Book House, Mumbai.
3. **John D. Anderson, Jr.**(1995).*Computational Fluid Dynamics*. Singapore: McGraw-Hill, Inc.
4. **Kashyap Krishna Kumaarr** (2011). *2D Numerical Study of Airfoil about a Multi-Element Airfoil*. Brunel University.
5. **Karthik Sundarraj** (2011). *Experimental & Numerical Study of Airfoils with Modified Trailing Edges*. Brunel University.
6. **Terrence A. Weisshaar**. *Morphing Aircraft Technology – New Shapes for Aircraft Design*. USA: Purdue University.
7. **John D. Anderson, Jr.**, "Introduction to flight", McGraw-Hill, New York, 1989
8. Ansys Reference Manual
9. **David P. Raymer**, "Aircraft Design: A Conceptual Design", American Institute of Aeronautics & Astronautics, Inc., Washington DC, 1992
10. **John D. Anderson, Jr.**, "Fundamental of Aerodynamics", McGraw-Hill, New York, 1991
11. Google images
12. **E.L Houghton, P.W Carpenter**, "Aerodynamics", University of Warwick
13. **A.D Young**, "The Aerodynamic Characteristics of Flaps"

Website References:

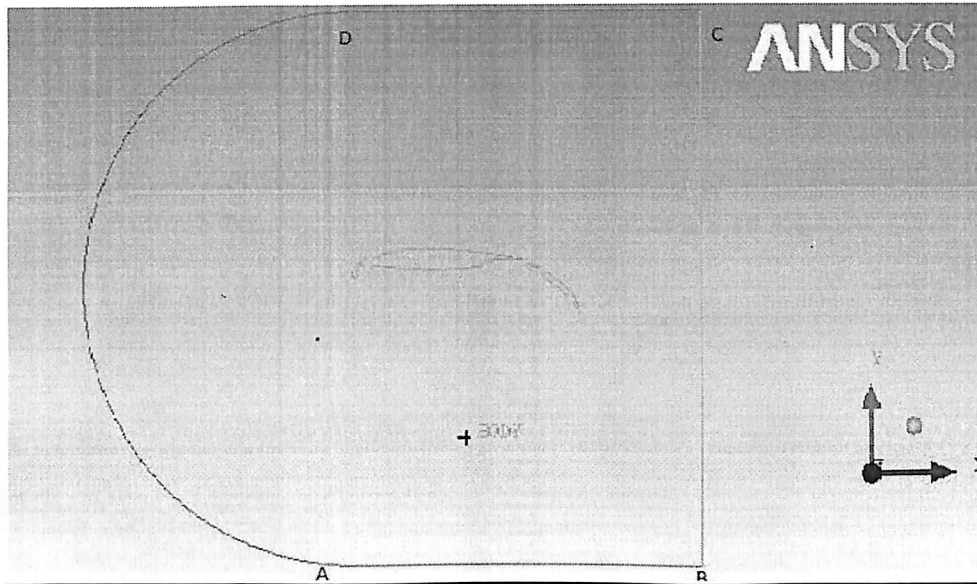
14. *Turbulence model*. Available: <http://www.wiki/standard k-epsilon model.html>. Last accessed 23rd feb 2013
15. *Leading edge slats*. Available: http://en.wikipedia.org/wiki/Leading-edge_slats. Last accessed 23rd mar 2013.
16. Van Dan, C.P. (february 2002). *The aerodynamic design of multi-element high-lift systems for transport airplanes*. Available:

<http://www.sciencedirect.com/science/article/pii/S0376042102000027>. Last accessed 3rd march 2013.

17. <http://www.aerospaceweb.org/question/aerodynamics/q0194.shtml>
18. <http://www.sciencedirect.com/science/article/pii/S0376042102000027>
19. <http://www.warbirdsresourcegroup.org/MRC/fw190convert2.html>
20. http://commons.wikimedia.org/wiki/File:Plain_flap_diagram.svg
21. <http://forums.jetcareers.com/threads/cessna-152-flaps.90904/>
22. <http://www.secretprojects.co.uk/forum/index.php?topic=2701.15>
23. <http://www.datwiki.net>
24. <http://www.pprune.org/tech-log/239334-krueger-flaps.html>
25. <https://data.epo.org/publication-server/html>
26. <http://www.pprune.org/tech-log/423330-le-flaps-slats-position-747-400-a.html>

APPENDIX

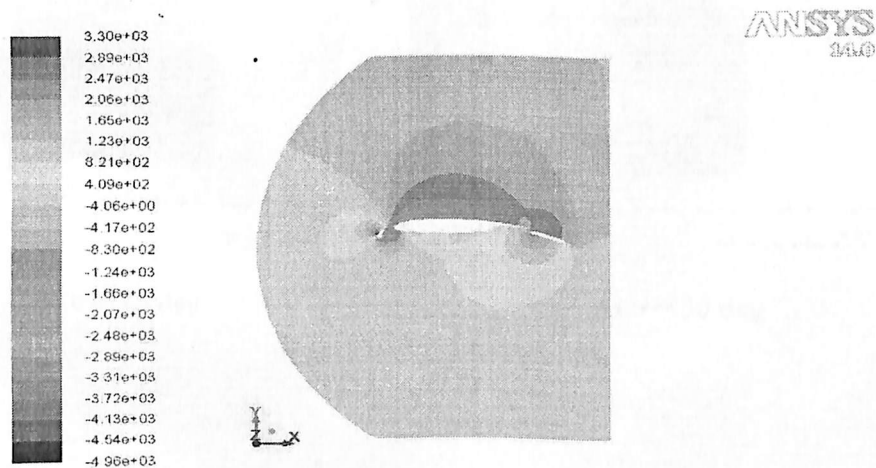
CHAPTER 4:



boundary depiction for five element airfoil

CHAPTER 5:

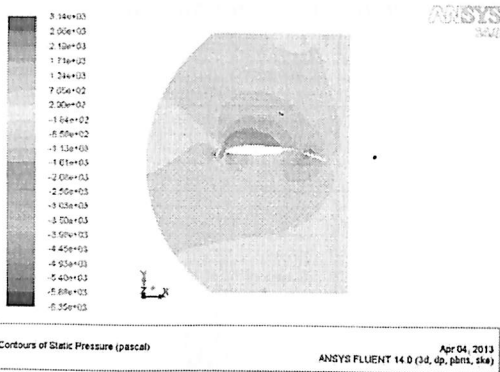
Pressure contour for three element airfoil:



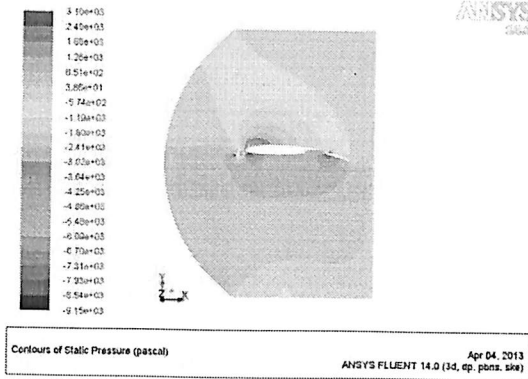
Contours of Static Pressure (pascal)

Apr 04, 2013
ANSYS FLUENT 14.0 (3d, dp, pbns, ske)

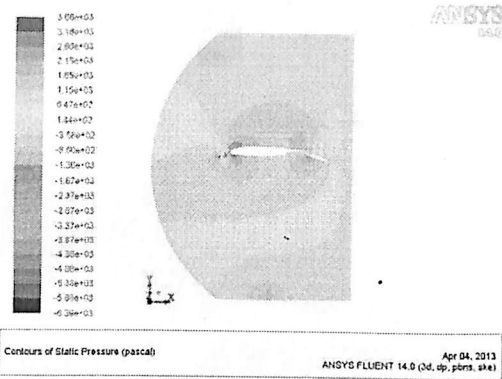
At $\alpha = 0$ deg



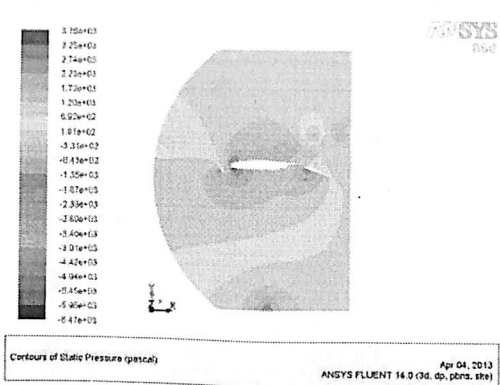
At $\alpha = 5$ deg



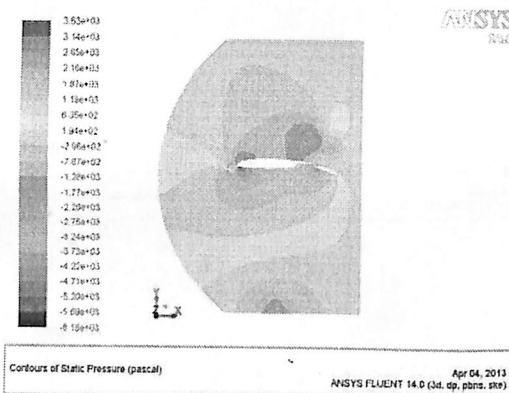
At $\alpha = 10$ deg



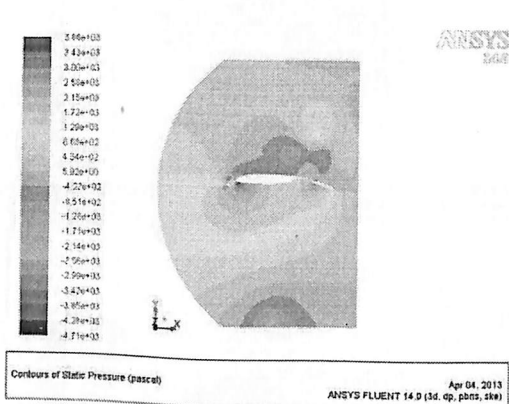
At $\alpha = 15$ deg



At $\alpha = 20$ deg

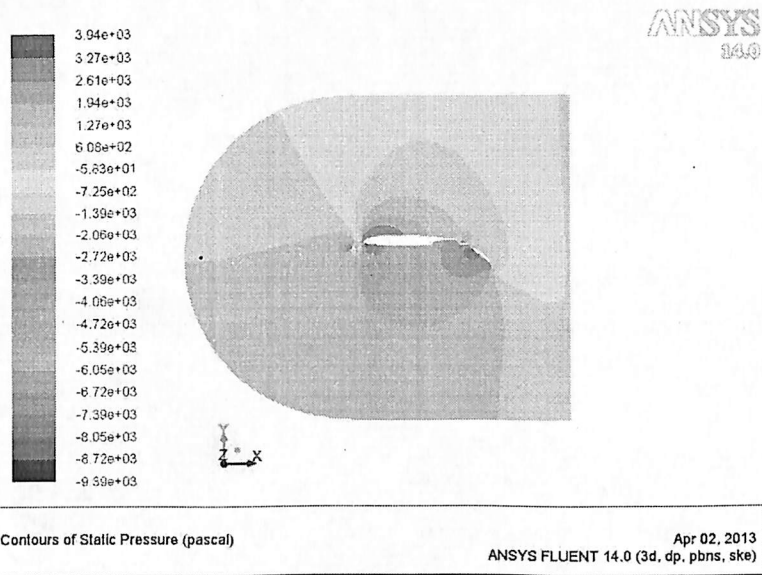


At $\alpha = 25$ deg

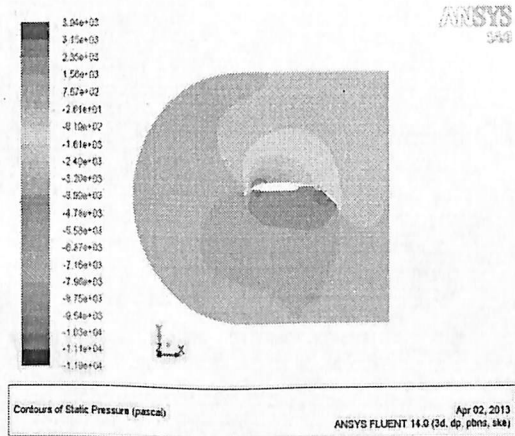
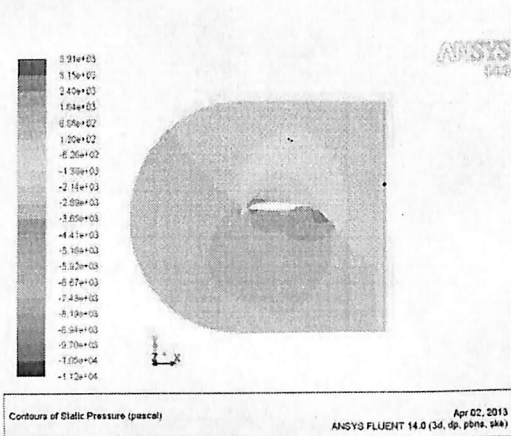


At $\alpha = 30$ deg

Pressure contour for five element airfoil:

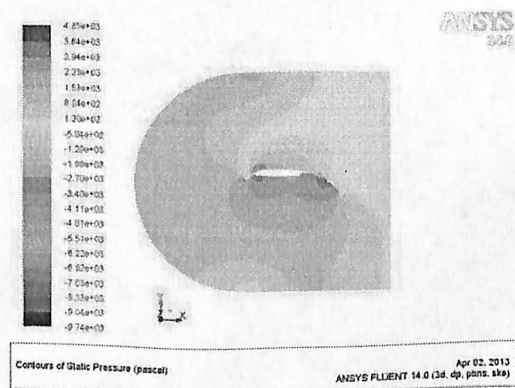
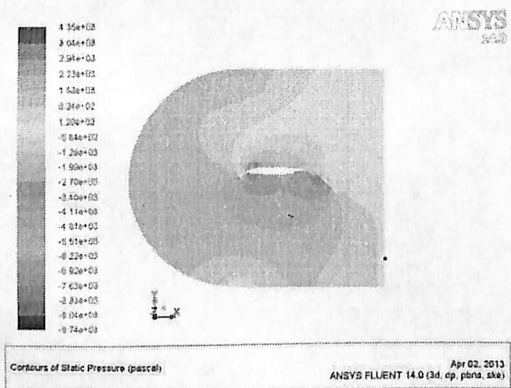


At $\alpha = 0$ deg



At $\alpha = 5$ deg

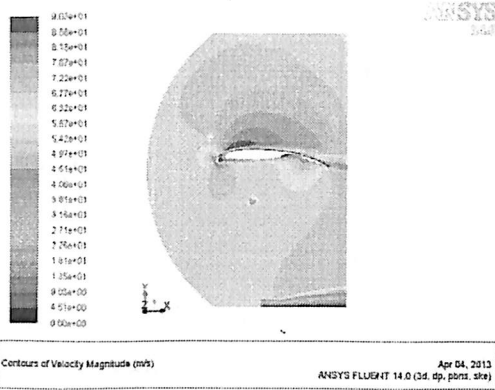
At $\alpha = 10$ deg



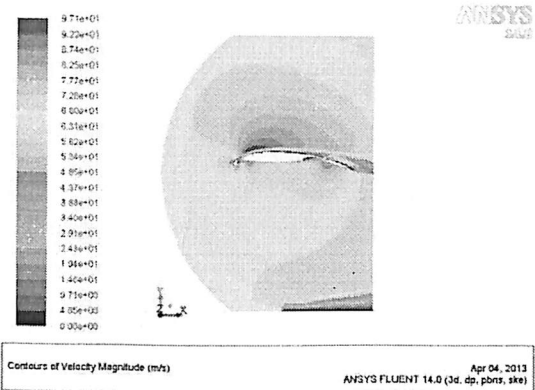
At $\alpha = 15$ deg

At $\alpha = 20$ deg

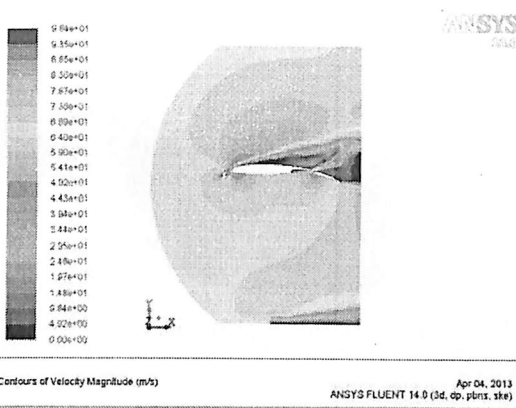
Velocity contour for three element:



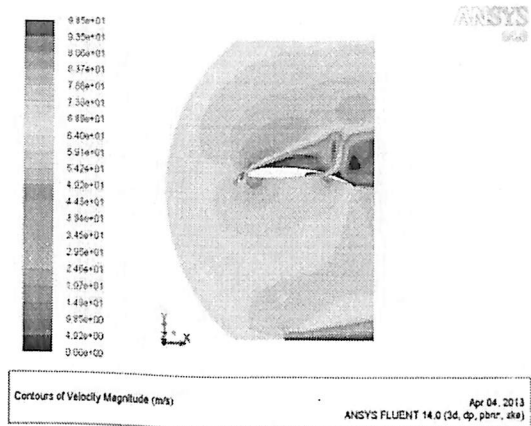
At $\alpha = 0$ deg



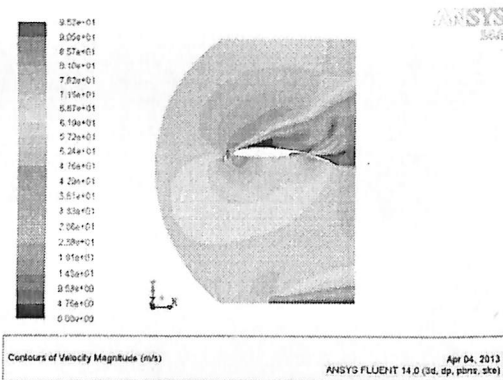
At $\alpha = 5$ deg



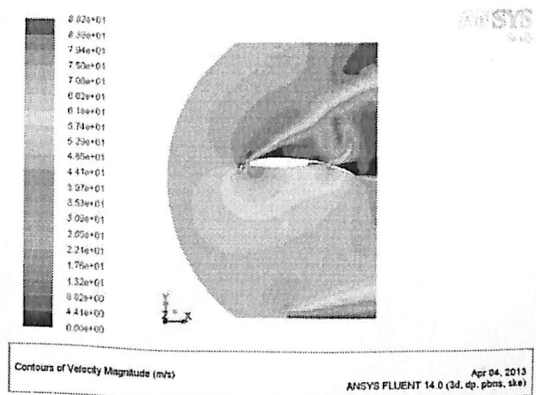
At $\alpha = 15$ deg



At $\alpha = 20$ deg

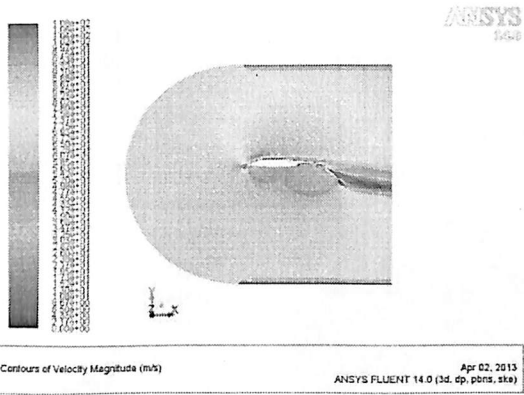


At $\alpha = 25$ deg

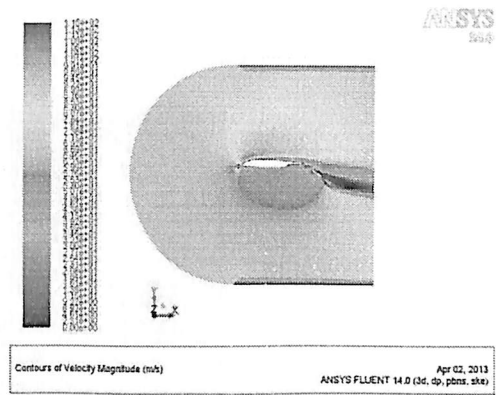


At $\alpha = 30$ deg

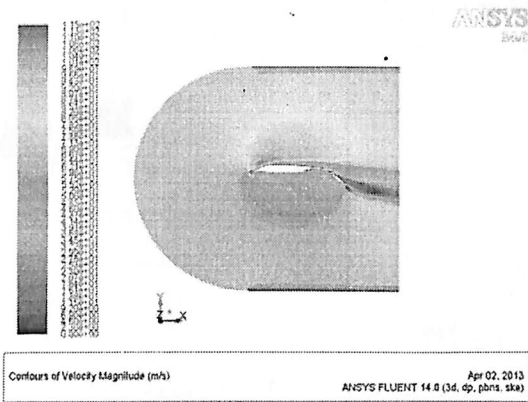
Velocity contour for five element:



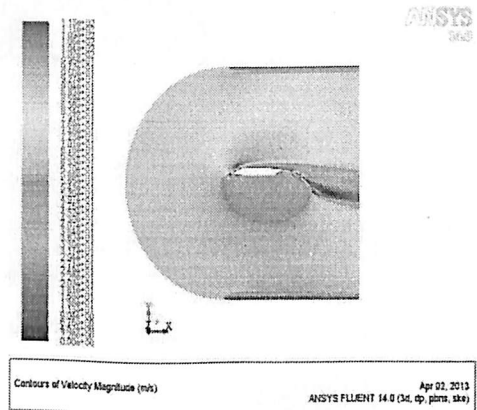
At $\alpha = 0$ deg



At $\alpha = 5$ deg

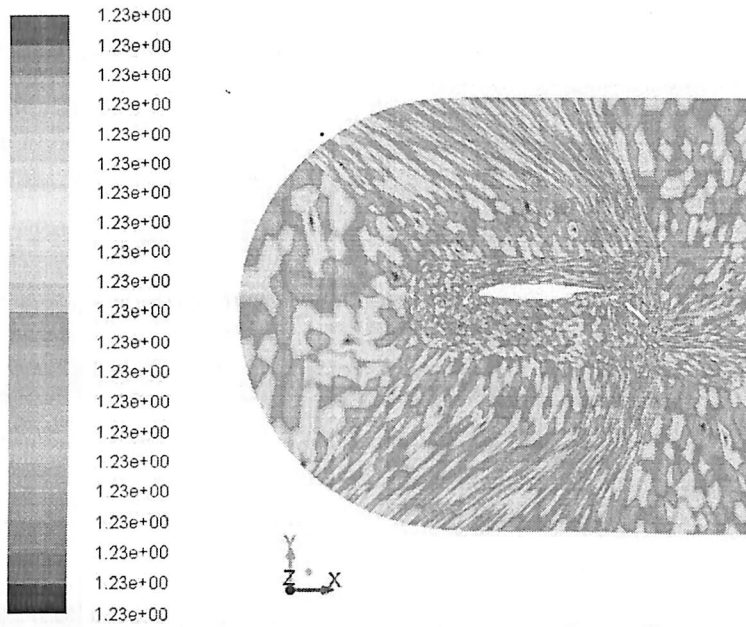


At $\alpha = 10$ deg



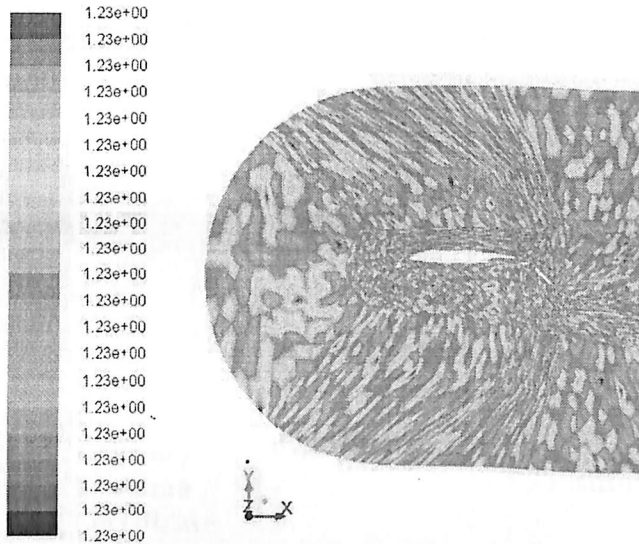
At $\alpha = 15$ deg

Density contour for five element:



Contours of Density (kg/m3) Apr 26, 2013
ANSYS FLUENT 14.0 (3d, dp, pbns, ske)

At $\alpha = 0$ deg



Contours of Density (kg/m3) Apr 26, 2013
ANSYS FLUENT 14.0 (3d, dp, pbns, ske)

At $\alpha = 15$ deg

RESUMES

Aakanksha Tiwari

Address for Correspondence:

University of Petroleum & Energy Studies
Energy Acres, P.O. Bidholi via Prem Nagar
Dehradun-248007(Uttarakhand), India

Mobile: +91 94109 60493

Email: aakankshatiwari08@gmail.com

CAREER OBJECTIVE

To strengthen and work with implementing the concepts learnt while continuously improving my skills and contributing quality ideas in the field of Aviation.

CURRENT ACADEMIC PROGRESSION: B. TECH. AEROSPACE ENGINEERING SEMESTER WISE SGPA

Semester I	Semester II	Semester III	Semester IV	Semester V	Semester VI	Semester VII
2.76	2.74	2.21	2.65	3.43	3.02	3.13

ACADEMIC BACKGROUND

Year(s)	Qualification - Degree / Diploma / Certificate	Board/University	College / Institute/ University	Percentage / CGPA
2009-2013	B. Tech. (Aerospace Engineering)	University of Petroleum and Energy Studies	College of Engineering Studies	2.86/4

2009	Senior Secondary	Central Board of Secondary Education, New Delhi	Aryaman Vikram Birla Institute Of Learning, Haldwani	80.0
2007	Higher Secondary	Central Board of Secondary Education, New Delhi	Rajeev Gandhi Navodaya Vidyalaya, Ramnagar	78.0

TRAINING AND PROJECTS UNDERTAKEN

Summer Internship Project:

Duration: 2 months

Company: Goodrich Aerospace, Bangalore.

Project Title: Development of Incoming Quality Plans of Received parts

Description: Development of Incoming Quality plans of received parts from Advanced Software solutions namely **TeamCenter** supporting Engineering Drawings were extracted to inspect and assimilate the production quality. Monitoring and keeping records using Hybrid Microsoft Office Tools were the prime objective of the company to reduce inspection time & provide delivery prior/according to the customer schedule.

Other Projects & Industrial Exposure

- **June 15, 2011 - July 29, 2011: Diploma in Mechanical CAD (CATIA V5 & AutoCAD) from CADD Centre, Dehradun**

Projects:

- **September 2012- April 2013: Project on "Study & Analysis on High Lift Devices And High Lift Devices Morphing For Multi Flight Regime" under the supervision of Prof. Karthik Sundarraj.**
Project comprises of Designing of **Multi-Element airfoil** – single element, Three-element and Five- element Airfoil are designed in **CATIA-V5** and imported to **Ansys14.0** for Computational Fluid Dynamics Analysis. Moreover, the advanced Aerospace technology like **Morphing Technique** is also studied and implemented.

- **September 2011 – April 2012: Project on Tandem Rotors under guidance of Mr. Sudhir Joshi**

Designing, Stabilization and Fabrication of Tandem Rotor wing Aircraft inspired from Boeing Chinook. Study of different parameters controlling Main two rotors of the rotary wing aircraft and performance analysis were performed.

ACADEMIC ACHIEVEMENTS

- Participated in Science Olympiad in year 2008 and secured **4th position** in the school.

CO-CURRICULAR ACTIVITIES

- Member of **Disciplinary Committee**.
- Member of American Society of Mechanical Engineers Student Section
- Attended the Seminar on Non Destructive Testing Techniques held at University in November 2010
- Attended the Aerobotic (Aeromodelling Workshop) held at University in June 2010.
- Attended Autonomous Robotics Workshop (eTRix) held at University in November 2009.
- **House Captain** and **Prefect** in school

EXTRA-CURRICULAR ACTIVITIES

- Participated in Robotics competition held at University.
- Attended various camps and rallies during school.
- Participated in various dance and music competition.

COMPUTER SKILLS

- **Analysis Software** : Ls-Dyna, Ansys 14.0
- **Design Software** : SolidWorks2008-10, AutoCAD and CATIA V5 R17
- **Programming Languages** : C, C++, Visual Basic, D.B.M.S. and S.Q.L.
- **Application Software** : M.S. Office (Excel & Word)
- **Operating Systems** : Windows/Vista/XP6

PERSONAL DETAILS

Date of Birth : 08/06/1992
 Father's Name : Mr. D.C. Tiwari
 Mother's Name : Mrs. Pushpa Tiwari

Category : General
Gender : Female
Nationality : Indian
Home Town : Haldwani
Permanent Address : C/O Mr. B.D. Joshi, Ekta Vihar, Phase-II, Gas Godam Road,
Kusumkhera, Haldwani, Uttarakhand-263139
Phone No. : 05946-261853, +91 89239 23433

Languages Known	Read (Beginner/Proficient/ Expert)	Write (Beginner/Proficient/ Expert)	Speak (Beginner/Proficient/ Expert)
English	Proficient	Proficient	Proficient
Hindi	Proficient	Proficient	Proficient

Mobility : Willing to locate anywhere in India and overseas.

I hereby declare that the details above are correct and true to the best of my knowledge.

Aakanksha Tiwari

Abhilasha Shah

Address for Correspondence:

University of Petroleum and Energy Studies

Energy Acres PO Bidholi via Prem Nagar

Dehradun-248007(Uttarakhand), India

Phone : +91 7409498669

Email : abhilasha.shah15@yahoo.in

CAREER OBJECTIVE

To be a part of the challenging team which strives for the better growth of the organization and which explores my potential and provides me with the opportunity to enhance my talent with an intention to be an asset to the company

ACADEMIC BACKGROUND

Year(s)	Qualification – Degree / Diploma / Certificate	Board/University	College / Institute/ University	Percentage / CGPA
2009-2013	B.Tech (Aerospace Engineering)	University of Petroleum & Energy Studies	College of Engineering Studies	3.03/4
2009	All India Senior Secondary School Examination	CBSE	Mohan Lal Sah Bal Vidya Mandir, Nainital	74.20
2007	All India Secondary School Examination	ICSE	Saint Mary's Convent, Nainital	84

TRAININGS & PROJECTS UNDERTAKEN

Summer Internship Project

Duration: 2 Month

Company: Mahindra Aerospace, Bangalore

Project Title: Aircraft Fuselage Load Analysis

Description: This project provides load distribution on the fixed wing aircraft fuselage. The critical loads on the fuselage are obtained after force balancing on the basis of shear force, bending moment, thrust and torque generated for different flight and landing conditions.

Other Projects & Industrial Exposure:

Completed Minor project on "Fabrication of tandem rotor helicopter"

Completed Major project on "Study and Analysis of High Lift Devices & High Lift Devices Morphing for Multi Flight Regime"

Two Month Training In CFD (star CCM+) at Flexilon, Bangalore

Training in ANSYS at Cad Arena, Dehradun

Industrial Tour To MAHINRA AEROSPACE, HAL, GOODRICH(Bangalore),

ACADEMIC ACHIEVEMENTS

- ✓ Got an award for securing highest marks in higher secondary in my community (2007)

CO-CURRICULAR ACTIVITIES

- ✓ Participated in PSI (placement selection improvement programme) held at university of petroleum and energy studies.
- ✓ Treasurer of the cultural India society under the universal solidarity moment conducted in the school for social welfare
- ✓ participated in Robotics Workshop conducted by IIT Mumbai held in university campus
- ✓ Been a member of ASME(American Society of Mechanical Engineers) and the colligative member of SAE India
- ✓ Participated in the disciplinary committee of "Urjaa 10"
- ✓ Aerobotic'10, aero modeling and fabrication workshop held at university of petroleum and energy studies

EXTRA CURRICULAR ACTIVITIES

- ✓ Participated in the national athletic meet as a high jumper held in Haridwar in the year 2006.
- ✓ Actively participated in debates and sports in school level.
- ✓ Participated in various sports activities in school as well as college level and was a member of the sports society in the college for 2 years.

COMPUTER SKILLS

Package : MS – Office, Auto-CAD, CATIA,CFD, ANSYS, Solid Works.

Operating System : Windows 98-2003, XP, Vista, Windows 7

PERSONAL DETAILS

Date of Birth (DD-MM-YYYY) : 15-08-1991

Father's Name : Mr. Akhilesh Kumar Shah

Mother's Name : Mrs. Sangeeta Shah

Category : General

Gender : Female

Nationality : Indian

Home Town : Nainital

Permanent Address : Ganga Sadan, Sudershan Hotel Compound,
Tallital - Nainital , Uttarakhand

Permanent Phone No. : +91 7409498669

Languages Known	Read (Beginner/Proficient/ Expert)	Write (Beginner/Proficient/ Expert)	Speak (Beginner/Proficient/ Expert)
English	Proficient	Proficient	Proficient
Hindi	Proficient	Proficient	Proficient

Mobility : Willing To Relocate Anywhere In India And Overseas

I declare that the details above are correct and true to the best of my knowledge.

Abhilasha Shah

Deepali Joshi

Address for Correspondence:

University of Petroleum and Energy Studies

Energy Acres PO Bidholi via Prem Nagar

Dehradun-248007(Uttarakhand), India

Phone : +91 9634183922

Email : deepalijoshi886@yahoo.com

CAREER OBJECTIVE

To acquire Aerospace Engineering position in a respectable organization and use my technical skills and hardwork for the betterment of the organization and also improve my knowledge by gaining experience.

ACADEMIC BACKGROUND

Year(s)	Qualification - Degree / Diploma / Certificate	Board/University	College / Institute/ University	Percentage / CGPA
2009-2013	B.Tech (Aerospace Engineering)	University of Petroleum & Energy Studies	College of Engineering Studies	2.6
2009	All India Senior Secondary School Examination	C.B.S.E.	Aryman Vikram Birla Institute Of Learning, Haldwani	70.1
2007	Higher Secondary	I.C.S.E.	Saint Mary's Convent, Nainital	76.33

TRAININGS & PROJECTS UNDERTAKEN

Summer Internship Project

Duration: 35

Days

Company: Air India , New Delhi

Project Title: V2500 A1 Engine, in Jet Engine Overhaul Complex of A320, in Air India.

Description: The project dealt with the detailed study of the engine and its sub assemblies, methods to assemble and disassemble the modules of the engine.

Other Projects & Industrial Exposure:

- ✓ Participated In Robotics workshop conducted by ThinkLABS SINE IIT Bombay at UPES to build autonomous robots using electronic components.
- ✓ Report on Geocentrism and Heliocentrism under Dr. Parag Mantri.
- ✓ Participated in Aero Modeling Workshop organized by UPES in 2010.
- ✓ Diploma in Computational Fluid dynamics (CFD) from Techzilon Training Solutions (Flexilon), Bangalore.
- ✓ Minor project on Design and Mechanism of Tandem Rotors.
- ✓ One month training in ANSYS at CAD AERENA, Dehradun.
- ✓ Major project on Numerical Analysis On Multielement Airfoil (In Progress).

ACADEMIC/EXTRA-CURRICULAR ACHIEVEMENTS

- ✓ Participated in inter school basketball matches.
- ✓ Participated and secured 2nd position in inter house throws competition.
- ✓ Attended Robotics workshop at UPES, DEHRADUN Conducted By IIT BOMBAY Team.
- ✓ Attended Aero Modeling workshop at UPES ,DEHRADUN.

CO-CURRICULAR ACTIVITIES

- ✓ Member of the Colligate Club of Society of Automotive Engineers (SAE) to discuss ideas and projects of automotive sector.
- ✓ Committee Member of the Aerospace Club.
- ✓ Student Member of American Society of Mechanical Engineers (ASME).
- ✓ Member of YUVA (organization for under privileged children).

COMPUTER SKILLS

- ✓ **Package** : MS – Office, Solid Works, C/C++, Java, SQL
- ✓ **Software** : Computational Fluid Dynamics(CFD), Ansys.
- ✓ **Operating System** : Windows 98-2003, XP, Vista, Windows 7

PERSONAL DETAILS

Date of Birth : 18-02-1992
Father's Name : Mr. Mahesh Chandra Joshi
Mother's Name : Mrs. Mamta Joshi
Category : General
Gender : Female
Nationality : Indian
Home Town : Nainital
Permanent Address : Alma Lodge, No. 7, Mallital, Nainital, Uttrakhand - 263 001
Permanent Phone No. : +91 96341 83922, +91 97585 09074

Languages Known	Read (Beginner/Proficient/ Expert).	Write (Beginner/Proficient/ Expert)	Speak (Beginner/Proficient/ Expert)
Hindi	Proficient	Proficient	Proficient
English	Proficient	Proficient	Proficient

Mobility : Willing To Relocate Anywhere In India And Overseas

I declare that the details above are correct and true to the best of my knowledge.

Deepali Joshi